

**RHEOLOGY AND ELECTROSPINNING OF NEAT AND LAPONITE-
FILLED POLY(ETHYLENE OXIDE) SOLUTIONS**

by

Vikram Kumar Daga

A thesis submitted to the Faculty of the University of Delaware in partial fulfillment of the requirements for the degree of Master of Chemical Engineering

Winter 2006

Copyright 2006 Vikram Kumar Daga
All Rights Reserved

UMI Number: 1435916

Copyright 2006 by
Daga, Vikram Kumar

All rights reserved.

UMI[®]

UMI Microform 1435916

Copyright 2007 by ProQuest Information and Learning Company.
All rights reserved. This microform edition is protected against
unauthorized copying under Title 17, United States Code.

ProQuest Information and Learning Company
300 North Zeeb Road
P.O. Box 1346
Ann Arbor, MI 48106-1346

RHEOLOGY AND ELECTROSPINNING OF NEAT AND LAPONITE-FILLED POLY(ETHYLENE OXIDE) SOLUTIONS

by

Vikram Kumar Daga

Approved: _____
Norman J. Wagner, Ph.D.
Professor in charge of thesis on behalf of the Advisory Committee

Approved: _____
Mark A. Barteau, Ph.D.
Chair of the Department of Chemical Engineering

Approved: _____
Eric W. Kaler, Ph.D.
Dean of the College of Engineering

Approved: _____
Conrado M. Gempesaw II, Ph.D.
Vice Provost for Academic and International Programs

ACKNOWLEDGMENTS

My knowledge has undergone a step change through the graduate program at Department of Chemical Engineering, University of Delaware. I thank the University and, in particular, the department for its inputs and help in bringing about this enhancement.

I thank my advisor, Prof. Norman Wagner and co-advisor, Prof. John Rabolt for guidance and support through my masters. I would also like to express my gratitude to the students of the Wagner and Kaler research groups and my friends who have been helping with discussions, training on instruments and suggestions in addition to making life enjoyable through good company.

There are several people outside the department who have helped me in research. Help from Prof. Henning Winter, University of Massachusetts on IRIS software and from the graduate students of the Rabolt and Pochan research groups, Materials Science and Engineering, with experiments and discussions is greatly acknowledged. Assistance from Jessica Penetar, as a part of her undergraduate research, in experimental phase behavior characterization is acknowledged.

TABLE OF CONTENTS

| | |
|----------------------|---|
| LIST OF TABLES..... | vi |
| LIST OF FIGURES..... | vii |
| ABSTRACT..... | xi |
| Chapter | |
| 1 | INTRODUCTION..... 1 |
| | 1.1 Motivation..... 1 |
| | 1.2 Description and present status of electrospinning..... 5 |
| | 1.3 Objectives..... 9 |
| | 1.4 Experimental..... 9 |
| | References..... 12 |
| 2 | RHEOLOGY OF NEAT AND LAPONITE-FILLED POLY(ETHYLENE OXIDE)-WATER SOLUTIONS..... 14 |
| | 2.1 Introduction..... 14 |
| | 2.2 Ageing and fixing the sample prehistory..... 18 |
| | 2.3 Rheology of PEO-water solutions..... 24 |
| | 2.3.1 Viscosity and concentration regimes..... 26 |
| | 2.3.2 Time-temperature superposition..... 29 |
| | 2.3.3 Time-concentration superposition..... 35 |
| | 2.3.4 Relaxation spectrum..... 42 |
| | 2.4 Rheology of PEO-water-laponite solutions..... 43 |
| | 2.4.1 Effect of laponite on the viscosity..... 43 |
| | 2.4.2 Time-temperature superposition..... 47 |
| | 2.4.3 First time-concentration superposition..... 48 |
| | 2.4.4 Complete time-concentration superposition..... 56 |
| | 2.5 Discussion..... 58 |
| | 2.6 Conclusions..... 63 |
| | References..... 65 |
| 3 | ELECTROSPINNING OF NEAT AND LAPONITE-FILLED POLY(ETHYLENE OXIDE)-WATER SOLUTIONS..... 69 |

| | | |
|---|---|-----|
| | 3.1 Introduction..... | 69 |
| | 3.2 Results..... | 72 |
| | 3.3 Discussion..... | 81 |
| | Appendix 3.1..... | 89 |
| | References..... | 95 |
| 4 | CONCLUSIONS AND FUTURE WORK..... | 99 |
| | 4.1 Conclusions..... | 99 |
| | 4.2 Other preliminary investigation: formation of pits..... | 101 |
| | 4.2.1 Polymer-solvent-nonsolvent phase diagram..... | 102 |
| | 4.2.2 Model for the formation of pits..... | 114 |
| | 4.3 Future work..... | 117 |
| | Appendix 4.1..... | 118 |
| | References..... | 121 |

LIST OF TABLES

| | | |
|-----------|--|----|
| Table 2.1 | PW solutions prepared for rheological characterization..... | 25 |
| Table 2.2 | Horizontal TTSP shift factors for PW10, PW11 and PW12..... | 33 |
| Table 2.3 | Shift factors for TCSP of PW solutions..... | 39 |
| Table 2.4 | Discrete relaxation spectra of PW TCSP master curve..... | 42 |
| Table 2.5 | PWL mixtures prepared for rheological characterization..... | 44 |
| Table 2.6 | Horizontal TTSP shift factors and activation energy of flow for PWL mixtures..... | 51 |
| Table 2.7 | Shift factors for the TCSP (=TCSP ₁) of PWL mixtures on their respective PW base solutions (the required rheology of PW3 for TCSP of Group 1 mixtures was predicted from the PW TCSP master curve shown in Figure 2.10 with shift factors (equations 2.6 and 2.7) extrapolated to the concentration of PW3)..... | 54 |
| Table 3.1 | Diameter and viscosity of neat and laponite-filled poly(ethylene oxide) fibers..... | 75 |

LIST OF FIGURES

| | | |
|-------------|--|----|
| Figure 1.1 | Electrospinning set up..... | 8 |
| Figure 2.1 | Thixotropy of a 2.67 wt. % laponite dispersion over 45 days..... | 20 |
| Figure 2.2 | Amplitude sweep of a 2.67 wt. % laponite dispersion three days after preparation shows a maximum in G'' | 21 |
| Figure 2.3 | Change in viscosity of PWL6 at 25 °C with time (ascending and descending shear rates are represented by filled and empty symbols respectively)..... | 23 |
| Figure 2.4 | Steady-shear viscosity and validation of Cox-Merz rule for PW solutions at 25 °C (symbols - steady shear viscosity vs. shear rate, lines - complex viscosity vs. angular frequency)..... | 27 |
| Figure 2.5 | Concentration regimes of PW solutions as defined by the zero-shear viscosity at 25°C..... | 28 |
| Figure 2.6 | Dynamic moduli of PW12 at 4, 11, 18 and 25 °C..... | 30 |
| Figure 2.7 | TTSP master curve of PW12 referenced to 25 °C..... | 31 |
| Figure 2.8 | Horizontal shift factors, a_T , for TTSP of PW10, PW11 and PW12..... | 34 |
| Figure 2.9 | Dynamic moduli of PW solutions in the concentrated regime: PW5 to PW12 (PW10, PW11 and PW12 from their TTSP master curves) at 25°C..... | 36 |
| Figure 2.10 | TCSP master curve of the PW solutions referenced to 5.5 wt. % PEO (PW10) at 25°C..... | 37 |
| Figure 2.11 | Horizontal and vertical TCSP shift factors for PW5 to PW12 and their comparison with the scaling provided for polymer solutions in the literature (Baumgärtel and Willenbacher, 1996)..... | 40 |

| | | |
|-------------|--|----|
| Figure 2.12 | TCSP shifted PW curves by employing the shift factors given by gaussian scaling with concentration of the polymer..... | 41 |
| Figure 2.13 | Concentration map of neat and laponite filled aqueous PEO solutions prepared for electrospinning: circles, triangles and squares represent the PEO solutions, laponite dispersions and laponite-filled PEO solutions respectively. Solutions that lie along an arrow represent members of a group..... | 45 |
| Figure 2.14 | Steady-shear viscosity and validation of Cox-Merz rule for PWL mixtures at 25 °C (Symbols - viscosity vs. shear rate, lines - complex viscosity vs. angular frequency. The dashed line for the case of PWL5 implies a deviation from the Cox-Merz rule.)..... | 46 |
| Figure 2.15 | Dynamic moduli of PWL1 at 4, 11, 18, 25 and 32 °C..... | 49 |
| Figure 2.16 | TTSP master curve of PWL1, TTSP master curve of PWL5 and the calculated PW3 curve all referenced to 25 °C..... | 50 |
| Figure 2.17 | Groupwise TCSP (= TCSP ₁) master curves of PWL mixtures at 25 °C referenced to PW base solution in each group..... | 53 |
| Figure 2.18 | TCSP shift factors for groupwise shifting (= TCSP ₁) of PWL TTSP master curves at 25 °C on the respective PW base solutions..... | 55 |
| Figure 2.19 | Complete TCSP (= TCSP ₂) master curve of PWL mixtures at 25 °C referenced to Group 4 (or PW10)..... | 57 |
| Figure 2.20 | Phase split of PWL5 and PWL6 into solution and gel phases. Tie lines are shown connecting the composition of the overall mixtures and the two phases formed..... | 62 |
| Figure 3.1 | SEM micrographs of neat and laponite containing aqueous poly(ethylene oxide) solutions..... | 74 |
| Figure 3.2 | Dependence of the diameter of electrospun fibers of neat polymer solutions with the zero shear viscosity of the spun solutions: (-■-) PW solutions (present work) with electric field, E= 1.54 kV/cm (◆) PW solutions at E= 0.7 kV/cm (Fong <i>et al.</i> , 1999a), (- - -) the diameter correlation obtained for polyesters at E=0.75 kV/cm (McKee <i>et al.</i> , 2004)..... | 76 |

| | | |
|-------------|---|-----|
| Figure 3.3 | Diameter of electrospun fibers of laponite-filled aqueous poly(ethylene oxide) solutions compared to that for PW solutions..... | 77 |
| Figure 3.4 | Diameter distribution of electrospun fibers belonging to groups 1 and 3 (The line+symbol representation of PW3 and PWL1 is to indicate the formation of beads on their electrospun fibers.)..... | 79 |
| Figure 3.5 | Diameter distribution of electrospun fibers belonging to groups 2, 4 and 5..... | 80 |
| Figure 3.6 | Correlation of electrospinning data using dimensional analysis (Helgeson and Wagner, 2005) for neat PEO solutions presented in this (■) and other work (Fong <i>et al.</i> , 1999) (●), and for fibers spun from polyester solutions ¹ (▲). Half-filled points represent fibers in which significant beading was reported..... | 83 |
| Figure 3.7 | Evidence of splaying for the case of PWL6 fibers..... | 88 |
| Figure 3.8 | All SEM images of PWL1 fibers..... | 89 |
| Figure 3.9 | All SEM images of PWL2 fibers..... | 90 |
| Figure 3.10 | All SEM images of PWL3 fibers..... | 91 |
| Figure 3.11 | All SEM images of PWL4 fibers..... | 91 |
| Figure 3.12 | All SEM images of PWL5 fibers..... | 92 |
| Figure 3.13 | All SEM images of PWL6 fibers..... | 93 |
| Figure 3.14 | All SEM images of PWL8 fibers..... | 94 |
| Figure 4.1 | Phase diagrams for different parameter values obtained using a single known initial guess, (f): Dotted curve, $\chi_{12} = -0.3$, $\chi_{13} = 1$, $\chi_{23} = 0.2$, $m_2 = 5$, $m_3 = 1000$, Solid outer curve: $\chi_{12} = 0.03$, $\chi_{13} = 1$, $\chi_{23} = 0.2$, $m_2 = 5$, $m_3 = 10000$, Solid inner curve: $\chi_{12} = 0.03$, $\chi_{13} = 1$, $\chi_{23} = 0.2$, $m_2 = 5$, $m_3 = 1000$, Dash-dot curve: $\chi_{12} = 0.3$, $\chi_{13} = 1$, $\chi_{23} = 0.2$, $m_2 = 5$, $m_3 = 1000$ | 111 |

| | | |
|------------|--|-----|
| Figure 4.2 | Phase diagram of water – THF – PS (190000 g/mol). Black thick line: calculated binodal for $\chi_{12}=0.927$, $\chi_{13}=3.2$ and $\chi_{23}=0.2$. Black filled circles: concentration of the polymer rich phase as predicted, black empty circles: concentration of the polymer lean phase as predicted, lines connecting black circles: tie lines. Diamond, star and inverted triangles represent experimental data points. Diamonds: distinct phase separation with gel-like bottom phase, star: phase separation with cloudy bottom phase and a clear upper phase, inverted triangle: no phase separation. Dashed lined represent constant concentration lines with a distance between two such consecutive lines equivalent to a difference of 0.2 volume fraction..... | 113 |
| Figure 4.3 | Schematic diagram of an element of the moving jet..... | 115 |
| Figure 4.4 | Temperature of the jet as it moves starting from the needle tip..... | 116 |
| Figure 4.5 | Water content in the jet as it moves starting from the needle tip..... | 116 |

ABSTRACT

Aqueous solutions composed of dispersed nanoparticles and entangled polymers are shown to exhibit a common viscoelasticity over a range of particle and polymer concentrations. Time-temperature superposition and time-concentration superposition are applied to generate master curves for the linear viscoelasticity of neat and laponite RD-filled viscoelastic solutions of poly(ethylene oxide) in water. The shift factors were correlated in terms of temperature and concentration and explained qualitatively in terms of the molecular interactions in concentrated and entangled polymer solutions and polymer-nanoclay solutions. The addition of laponite is more effective in modifying the solution rheology than the addition of an equivalent weight of polymer. Ageing studies show that, unlike the polymer solutions which are stable, the addition of laponite leads to ageing on the timescale of days.

In parallel with the rheology, electrospinning is reported for the same systems to explore the effects of change in the rheology of polymer and polymer-nanoclay formulations. A correlation between fiber diameter and the spinning solution's zero-shear viscosity is observed and compared to previous work reported by (McKee *et al.*, 2004). The addition of laponite nanoclay to the PEO solutions, which results in rheologically simple solutions, leads to different fiber morphologies for the same shear viscosity in contradiction with earlier reports for titania particles (Drew *et al.*, 2003). The research identifies additional physicochemical properties that are important in setting electrospun fiber morphology.

Chapter 1

INTRODUCTION

1.1 Motivation

Traditionally conventional polymeric fibers ranging in size from a few microns to about 500 microns are produced in industry through extrusion and drawing of polymer melts or their concentrated solutions. Through evaporation of solvent in the case of dry spinning or cooling of the polymer melt in the case of melt spinning solidification within the polymeric thread leads to fibers with diameters in micron range (Ondarcuhu and Joachim, 1998). Although the use of conventional polymeric fibers are numerous, there exists a smaller size range of polymer fibers which could have potential use in a variety of future products and processes where conventional fibers show poor or no performance (Haberstroh *et al.*, 2003; Kim *et al.*, 2004; Reneker, 2004; S.-Gibson *et al.*, 2002). Thus, in the past two decades, considerable research emphasis has been made on the production of polymer fibers of size between a few nanometers to a few microns which, due to their size ranging to a few nanometers are often denoted as “nanofibers”. Since nanofibers cannot be produced by conventional spinning methods, research in the area of nanofiber production technologies is required. Much of the current research in this area is directed towards understanding these processes and better control over the morphology of the nanofibers formed. The methods available to make nanofibers are:

- a) Drawing
- b) Self assembly
- c) Phase separation
- d) Template synthesis
- e) Fiber diameter reduction by chemical treatment
- f) Electrospinning

To appreciate the advantages of electrospinning, our primary focus, we first briefly discuss these methods and thus better understand why electrospinning is more advantageous in several ways.

As noted above, normal drawing of fibers is limited in size to smallest diameters of a few microns. However, with a special case of low molecular weight polymers, it was shown that under carefully controlled experimental conditions fibers of about 20 to 60 nm in diameter can be obtained (Ondarcuhu and Joachim, 1998). However, this method works only when the low molecular weight polymer solution is used at the threshold of solidification, and hence, the design of such a solution for different polymers would involve a tedious trial and error procedure and the process would require a very precise temperature and concentration control.

Self assembly has been used to produce nanofibers (Liu *et al.*, 1999; Whitesides and Grzybowski, 2002). In one method, nanofibers of a polymer were produced from block copolymers which were dissolved in a suitable solvent and then a

phase separation was induced to cause the different blocks to organize in a core-shell structure. The self assembled structure thus produced was treated with a solvent which selectively dissolved away one of the blocks leaving behind the other as nanofibers (Liu *et al.*, 1999).

Similarly, phase separation of polymer solutions could also be used to make nanofibers. It is known that during the phase separation of a polymeric system, if the polymer chain length and concentration is sufficient, the polymer rich phase initiates with the formation of viscoelastic polymer network from which the solvent squeezes out over time (Tanaka, 1997; Taniguchi and Onuki, 1996). The time elapsed after the initiation of phase separation controls the size of the fibrils in the network. In one case, by a procedure involving thermally induced gelation, solvent exchange and freeze-drying, biodegradable polymer matrices were made with fibrils of the matrix ranging in size from 50 to 500 nm in diameter (Ma and Zhang, 1998).

Template synthesis is the name given to methods in which a flowable material is forced through or on a rigid structure. The material attains the shape of the geometry used. In one such method, nanoporous membranes were used as templates (Martin, 1996). When a polymer solution was forced through the membrane, it flowed through the nanopores of the membrane and thereby attained nanoscale diameters. The nanometer jets that emerged from the other side of the membrane were treated with a solidifying solution to avoid coalescence of the polymer jets.

Fiber diameter reduction was used to reduce the size of fibers of copolymers of poly(lactic acid) and poly(glycolic acid) (PLGA; 50:50 wt%) by chemical treatment with NaOH, washing with water, sterilizing by UV light and then soaking overnight in ethanol (Haberstroh *et al.*, 2003). This method is specific to the polymer used and would require a careful selection of chemical agents to etch the various polymers.

As can be noticed, the methods discussed above for producing nanofibers suffer a common disadvantage that multiple steps are involved in a complex process. Drawing requires a careful control of concentration near the solidification conditions and works only with low molecular weight polymers. Methods based on self assembly and phase separation are governed by complex polymer-solvent thermodynamics, which in turn is affected by the local temperature and concentration, which are difficult to control. It is also clear that for these methods to work, a careful choice of solvent, temperature and concentration conditions would be required. In addition, certain other follow up treatments are required to finally obtain nanofibers. The method of template synthesis is less taxing as compared to self assembly and phase separation, but it still requires an additional step of meticulous construction of nanoporous membranes.

Electrospinning is the only method that can be used to produce nanofibers simply, directly and in a fast manner from polymer solutions and melts. The polymer nanofibers are produced directly as an end result of a simple process based upon easily controllable operating parameters such as spinning voltage and working distance.

There are several advantages of electrospinning over the other methods. Firstly, a wide variety of both synthetic and biopolymers can be electrospun at a variety of polymer concentration and temperatures in the same way. Secondly, electrospinning is versatile enough and nanoparticles can be incorporated within the nanofiber matrix easily (Drew *et al.*, 2003, Ye *et al.*, 2004, Krikorian *et al.*, 2004 and Salalha *et al.*, 2004). This would be difficult to achieve by self-assembly and phase separation as those processes depend upon the thermodynamics and therefore, it might be possible that a particle rich second phase forms instead of particles being incorporated within the phase separating fibrils. However, electrospinning only requires dispersion of the particles into the polymer solution as the rapid process is less likely to allow phase separation of particles. A variety of materials could thus be added to the fibers to impart or enhance the properties of the fiber produced. Thus, electrospinning offers an efficient and yet a simple way to trap the nanoparticles in a one dimensional array embedded in the polymer of choice. Thirdly, electrospinning can be used to make fibers even with a few milligrams of a polymer. This makes electrospinning an ideal process for making nanofibers with novel polymeric materials often produced in small quantities on a laboratory scale for research purposes.

1.2 Description and present status of electrospinning

As shown in Figure 1.1, the electrospinning set up is simple in design and easy to operate. It consists of a high voltage supply connected to the needle of a syringe containing a polymer solution and an earthed collector (metallic substrate) at some distance (working distance) from the needle tip. The set up used for the present work was arranged in a vertical manner with the syringe on the top and flat aluminum

foil as the collector at some distance below the needle tip of the syringe. The piston of the syringe is pushed by a syringe pump connected to a motor that drives the pump at a set flow rate and therefore squeezes out the polymer solution at a desired flow rate. When no electricity is provided, the polymer solution coming out of the needle forms a pendant droplet which breaks off under its own weight and falls by the action of gravity on the collector. For electrospinning to carry out, a spinning voltage *i.e.*, an electric potential difference between the needle tip and the collector and a charge on polymer solution is required. When the needle tip is connected to a positive potential and the aluminum foil (collector) is earthed, at a low spinning voltage between the needle tip and the collector, the pendant droplet attains a conical shape (Taylor cone) due to the balance between the surface tension, gravity and electrostatic forces acting on it (Yarin *et al.* , 2001). With an increase in the spinning voltage, a fine jet issues from the tip of the cone and travels towards the collector and collects on it in the form of a mat made of fibers.

Electrospinning process depends upon the operating conditions and the rheological and electrical properties of the solution (Fong and Reneker, 1999). Modeling of the electrospinning trajectory has met with partial success in capturing the diameter of electrospinning fibers (Shin *et al.*, 2001, Feng, 2002). It is of interest to quantify relationships connecting the resultant fiber mat properties, such as fiber diameter and morphology, to the solution's rheology, electrical properties, surface tension and the process variables. For example, it was recently found that the final diameter of polyester fibers correlates with the spinning solution's zero-shear viscosity (McKee *et al.*, 2004). It is unknown, however, if such correlations hold for other

polymer-solvent systems, or whether the shear viscosity is sufficient to truly correlate final fiber diameter.

Recently, nanoparticles have been incorporated into the spinning solutions to yield composite fiber mats with potentially enhanced or new physical properties (Drew *et al.*, 2003, Ye *et al.*, 2004, Krikorian *et al.*, 2004 and Salalha *et al.*, 2004). Electrospinning investigations of aqueous poly(ethylene oxide) (PEO) solutions by Drew *et al.* (2003) suggest that the addition of titanium oxide particles also enables electrospinning at lower polymer concentrations than normally possible. Particle addition leads to similar fiber diameters when the spinning solutions have comparable shear viscosities. Here again, whether this observation is general and whether similar quantitative relationships hold between fiber morphology and size and spinning solution properties in the presence of nanoparticles has not been established.

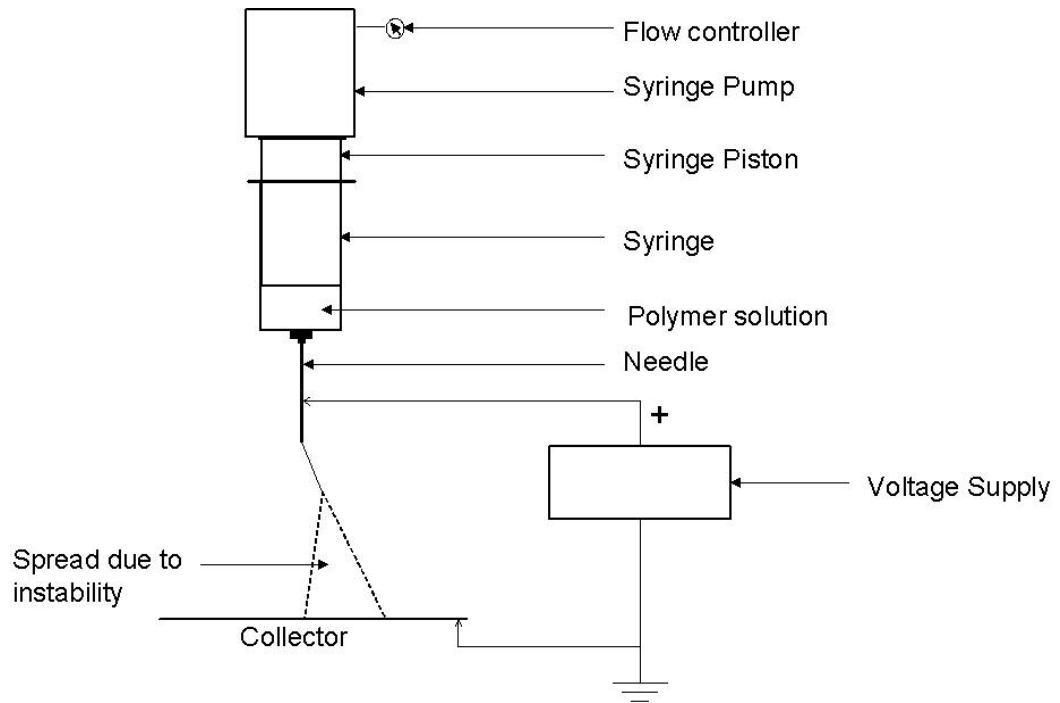


Figure 1.1: Electrospinning set up

1.3 Objectives

The goals of the work reported here are to determine if the correlation between zero shear viscosity and electrospun fiber diameter and morphology also holds for an aqueous polymer solution, and whether this can be extended to the electrospinning of solutions containing dispersed nanoparticles. In contrast to the polyester solutions examined by McKee *et al.* (2004), here we study viscoelastic, aqueous solutions of PEO (Devanand and Selser, 1991; Hammouda *et al.*, 2002; Hammouda *et al.*, 2004; Ho *et al.*, 2003). In addition, the solvent used here (water) is less volatile than the 70/30 w/w mixture of chloroform/dimethyl formamide used by McKee *et al.* (2004), which may also be a factor in setting fiber morphology. The rheological simplicity of the model system of aqueous PEO-laponite has been established (Chapter 2) and exploited to examine the influence of the addition of nanoclay on the electrospun fiber properties (Chapter 3). In addition, a method to determine the critical polymer concentration of a spinning solution above which beading is suppressed has been established.

1.4 Experimental

PEO (Scientific Polymer Products, Inc.) with reported nominal $M_w=9 \times 10^5$ g/mol, laponite RD (Southern Clay Products) and deionized water with a resistivity of $18.3 \text{ M}\Omega\text{-cm}$ were used as supplied to make the solutions. PEO (6.62 and 8.0 wt. %) was added to deionized water in plastic bottles and sealed. The bottles were shaken vigorously by hand immediately after addition of water to PEO to completely disperse the PEO. Dispersing PEO increases the surface area of dissolution and therefore causes a faster dissolution of PEO in water. Three days were allowed for the

complete dissolution of PEO in water during which the solutions were placed on rotating mixer for gentle mixing. The aqueous PEO solutions (PW solutions) of lower concentrations were prepared by diluting either of the two stocks with an additional amount of deionized water, after which, the diluted samples were mixed for a day. Laponite (1.5 and 2.2 wt. %) was added to deionized water and shaken vigorously for a few minutes and then sonicated for ~30 minutes using a probe sonicator with simultaneous mixing using a magnetic stirrer bar. Because laponite dispersions age rapidly due to the tendency of laponite particles to organize in aqueous medium into a structure (Dijkstra *et al.*, 1995; Willenbacher, 1996), these dispersions were used within two hours of sonication to prepare the PWL mixtures as discussed below.

Addition of solid laponite powder into aqueous PEO solutions or solid PEO into laponite dispersions causes local gelation upon contact and impedes further dispersion of the solid added. Therefore, the PWL mixtures of desired concentrations were prepared from stock solutions of PEO and laponite dispersions by mixing 6.62 wt. % PEO solution with 1.5 wt. % laponite dispersion and mixing 8 wt. % PEO solution with 2.2 wt. % laponite dispersion in different weight ratios to obtain ternary mixtures.

The PWL samples thus prepared were vigorously shaken by hand and mixed on a rotating mixer for ~24 h prior to rheological measurement. The PWL mixtures were optically clearer than neat PW solutions but some of the mixtures with higher laponite concentration showed evidence of some colorless gel-like agglomerates that settled with time. These agglomerates are characteristic of the PWL

system (Mongondry *et al.*, 2004) and were fully redispersed by a spatula by mixing for 5 to 10 minutes prior to rheological measurement and electrospinning experiments.

The shear rheology was measured using concentric cylinder geometry (CC27) on a MCR500 (Paar Physica) with a solvent trap to avoid evaporation and peltier temperature control ($\pm 0.03^\circ\text{C}$). Amplitude sweeps were performed to limit the frequency sweep measurements in the linear viscoelastic regime. The reported data was obtained for frequencies from 0 to 100 rad/s performed in controlled strain mode with a strain amplitude of 10 %. The data was processed using the manual shifting mode of IRIS software package version 8.04 (Winter and Mours, 2004) to perform superpositions (TTSP, TCSP) and spectrum calculations.

Electrospinning experiments were performed using a device described previously (Megelski *et al.*, 2002). A DC voltage of 20 kV, a collector to tip distance of 13 cm and a flow rate of 3 ml/h was used for all experiments. Fiber mats were collected on aluminum substrate (foil) and SEM (JEOL JSM 6335F) digital micrographs were obtained and analyzed using Adobe Photoshop software to obtain the fiber diameter distributions.

REFERENCES

- Devanand K and Selser JC (1991) Asymptotic-Behavior and Long-Range Interactions in Aqueous-Solutions of Poly(Ethylene Oxide). *Macromolecules* **24**(22): 5943-5947
- Dijkstra M, Hansen JP and Madden PA (1995) Gelation of a clay colloid suspension. *Physical Review Letters* **75**(11): 2236-2239.
- Drew C, Wang XY, Samuelson LA and Kumar J (2003) The effect of viscosity and filler on electrospun fiber morphology. *Journal of Macromolecular Science-Pure and Applied Chemistry* **A40**(12): 1415-1422.
- Haberstroh KM, Thapa A, Miller DC and Webster TJ (2003). Bio-inspired, nano-structured polymers for use in soft tissue replacement applications. 2003 Summer Bioengineering Conference, June 25-29, Sonesta Beach Resort in Key Biscayne, Florida.
- Hammouda B, Ho D and Kline S (2002) SANS from poly(ethylene oxide)/water systems. *Macromolecules* **35**(22): 8578-8585.
- Hammouda B, Ho DL and Kline S (2004) Insight into clustering in poly(ethylene oxide) solutions. *Macromolecules* **37**(18): 6932-6937.
- Ho DL, Hammouda B and Kline SR (2003) Clustering of poly(ethylene oxide) in water revisited. *Journal of Polymer Science Part B-Polymer Physics* **41**(1): 135-138.
- Kim GT, Shin JH, Lee JS, Ahn YC, Hwang YJ, Jeong KH, Lee JK and Sung CM (2004). Development of the electrospun nanofiber media for filtration application: effect of moisture. *Proceedings - World Filtration Congress, 9th, New Orleans, LA, United States, Apr. 18-24, 2004*
- Liu G, Ding J, Qiao L, Guo A, Dymov BP, Gleeson JT, Hashimoto T and Saijo K (1999) Polystyrene-block-poly(2-cinnamoyl ethyl methacrylate) nanofibers - Preparation, characterization and liquid crystalline properties. *Chemistry-A European Journal* **5**(9): 2740-2749.

- Ma PX and Zhang R (1998) Synthetic nano-scale fibrous extracellular matrix. *Journal of Biomedical Materials Research* **46**(1): 60-72.
- Martin CR (1996) Membrane-based synthesis of nanomaterials. *Chem. Mater.* **8**: 1739-1746.
- Megelski S, Stephens JS, Chase DB and Rabolt JF (2002) Micro- and nanostructured surface morphology on electrospun polymer fibers. *Macromolecules* **35**(22): 8456-8466.
- Mongondry P, Nicolai T and Tassin JF (2004) Influence of pyrophosphate or polyethylene oxide on the aggregation and gelation of aqueous laponite dispersions. *Journal of Colloid and Interface Science* **275**(1): 191-196.
- Ondarcuhu T and Joachim C (1998) Drawing of single nanofibre over hundreds of microns. *Europhysics Letters* **42**(2): 215-220.
- Reneker DH (2004). Nanofibers, electrospinning and filtration. *Proceedings - World Filtration Congress, 9th, New Orleans, LA, United States, Apr. 18-24, 2004.*
- S.-Gibson H, Gibson P, Wadsworth L, Hemphill S and Vontorcik J (2002) Effect of filter deformation on the filtration and air flow for elastomeric nonwoven media. *Advances in Filtration and Separation Technology* **15**: 525-537.
- Tanaka H (1997) Viscoelastic model of phase separation. *Physical Review E* **56**: 4451-4462.
- Taniguchi T and Onuki A (1996) Network domain structure in viscoelastic phase separation. *Physical Review Letters* **77**: 4910-4913.
- Whitesides GM and Grzybowski B (2002) Self-assembly at all scales. *Science* **295**: 2418-2421.
- Willenbacher N (1996) Unusual thixotropic properties of aqueous dispersions of Laponite RD. *Journal of Colloid and Interface Science* **182**(2): 501-510.
- Yarin AL, Koombhongse S and Reneker DH (2001) Taylor cone and jetting from liquid droplets in electrospinning of nanofibers. *Journal of Applied Physics* **90**(9): 4836-4846.
- Ye, H. H.; Lam, H.; Titchenal, N.; Gogotsi, Y.; Ko, F. *Applied Physics Letters* 2004, **85**, 1775-1777

Chapter 2

RHEOLOGY OF NEAT AND LAPONITE-FILLED POLY(ETHYLENE OXIDE)-WATER SOLUTIONS

2.1 Introduction

Understanding the important parameters that govern the formation of electrospun nanofibers is of interest. In general the electrical properties and rheological properties of the polymeric fluid strongly affect the process. In this chapter, the rheology of model systems, neat and laponite-filled aqueous PEO solutions has been studied. It is discussed how the rheology of these systems can be reduced to master curves which reveals the similarity between the two systems in terms of their microstructure. The method used also provides an example of how the rheology of ternary systems may be characterized as a function of temperature and concentrations.

Polymer-clay nanocomposites exhibiting superior properties find applications in various commercial products in the agricultural (Greenblatt *et al.*, 2004; Theng, 1970), pharmaceutical (Greenblatt *et al.*, 2004; Wong, 2004), electrochemical (Aranda, 2003; Doeff and Reed, 1998; Feller and Bruzard, 2004), photochemical (Majumdar, 2003) and personal care (Sengupta *et al.*, 2002; Smith *et al.*, 1989) industries. The final material properties of such composites are often highly dependent on their processing history due to the strong coupling between the

nanocomposite's microstructure and rheology. Hence, it is of importance to establish the rheological effects associated with the addition of nanoparticles to polymers and polymer solutions.

For example, one application attracting recent research interest is the electrospinning of polymeric materials to produce nanoscale fibers (Casper *et al.*, 2004; Huang *et al.*, 2003; Jayaraman *et al.*, 2004; Megelski *et al.*, 2002). Colloidal particles have been incorporated within the electrospun fibers for such purposes as to enhance the mechanical properties of the electrospun fibers (Krikorian *et al.*, 2004) and to generate high specific surface area catalytic particles (Drew *et al.*, 2003). The rheology of the spinning solution is known to affect the fiber diameter (McKee *et al.*, 2004). Consequently, the rational design and control of the electrospinning process requires knowledge of the rheological properties of the spinning solution and its dependence on polymer and particle concentrations.

Polymer processing benefits from the use of time-temperature superposition (TTSP), whereby the linear viscoelasticity of polymers can often be reduced to a master curve (Baumgärtel and Willenbacher, 1996; Ferry, 1980) over a range of temperatures and deformation frequencies. Similarly, polymer solutions within the concentrated regime have been shown to exhibit time-concentration superposition (TCSP) (Baumgärtel and Willenbacher, 1996; Ferry, 1980; Schausberger and Ahrer, 1995). In the latter, concentration effects on the entanglement density and dominant relaxation time can be reduced to an underlying master curve. This reduction reflects the common, underlying mechanisms

responsible for the viscoelasticity. In addition to the obvious savings in data management, reduction to an underlying, universal, viscoelastic spectrum is helpful both for measuring the rheology in a larger experimental window and for the prediction of the viscoelasticity at state points not actually measured. Likewise, the rheology of weakly attracting colloidal suspensions at different volume fractions or interaction energies, within a certain range, can be superimposed to reflect the commonality in the underlying viscoelasticity (Trappe and Weitz, 2000).

The addition of nanoparticles to polymers and polymer solutions should significantly modify the viscoelasticity of the polymer or polymer solution if the particles strongly interact with the polymer. However, even relatively weakly interacting nanoparticles can have significant and nontrivial effects on the polymer's rheology because of their high surface to volume ratio and similar size scales with the polymer (Mackay *et al.*, 2003). As it is becoming increasingly common to add nanoparticles into polymers and polymer solutions to either enhance or impart desired properties to the resulting mixture, a systematic approach that could facilitate rheological measurements, their correlation and possible prediction is desirable.

The ternary mixture with laponite nanoclay dispersed in aqueous solutions of poly(ethylene oxide) (PEO), henceforth referred to as PWL mixture, is a model polymer-nanoclay dispersion that has received sufficient attention to make it both of academic and practical interest. PWL mixtures, with or without the presence of counterions, have been studied extensively at a wide range of PEO concentration through rheology, SANS and molecular modeling. At concentrations greater than 2 wt.

%, aqueous laponite dispersions form a thixotropic gel with time (Willenbacher, 1996). Monte Carlo simulations (Dijkstra *et al.*, 1995) of laponite gels suggest a “house of cards” structure driven by electrostatic attraction between oppositely charged edges and faces of the laponite discs (van Olphen, 1977). Many other structural models have been proposed to explain the structure and properties of laponite gels (Schmidt *et al.*, 2002). The introduction of water soluble polymers is known to retard or inhibit the gelation kinetics (Mongondry *et al.*, 2004; Sardinha and Bhatia, 2002a; Sardinha and Bhatia, 2002b). The structure formation with time causes a significant change in rheology over days (Sardinha and Bhatia, 2002a; Sardinha and Bhatia, 2002b), such that ageing must be accounted for in any quantitative experimental study. Phase behavior studies and rheology of PWL system delineate the boundary within which PWL mixtures shear thicken reversibly to form ‘shake gels’ (Feller *et al.*, 2004; Pozzo and Walker, 2004; Zebrowski *et al.*, 2003). Flow-birefringence studies revealed that upon shear the laponite discs orient along the flow direction (Schmidt *et al.*, 2000; Schmidt *et al.*, 2002).

SANS investigations show that PEO adsorbs to and can bridge between laponite discs, leading to the formation of a polymer-nanoparticle network in solution (Feller *et al.*, 2004; Lal and Auvray, 2001; Nelson and Cosgrove, 2004; Pozzo and Walker, 2004; Schmidt *et al.*, 2000). Therefore, it can be expected that the addition of laponite particles to semi-dilute and concentrated PEO solutions will contribute additional structure to the solution polymer-colloid interactions that will affect the solution’s viscoelasticity. This change could result in an increase in the effective entanglement density through PEO-laponite bridging interactions. However, laponite

particles could also remove PEO chains from the entanglement network if adsorption occurs without significant bridging. This idea is also supported by the variety of molecular configurations that result from PEO-laponite interactions as was summarized by Pozzo and Walker (2004) in their pictorial diagrams of the molecular microstructures possible. Among the various structures shown, in some the polymer chains effectively bind together the various laponite discs to form gels whereas in other cases the polymer chains are adsorbed on discs in such a way that they do not bind the laponite discs and thus resulting in sol phases which effectively would amount to removal of some PEO chains from the bulk and therefore reduce the bulk entanglement density. Consequently, it is not known a priori whether such ternary mixtures will exhibit a simple enough rheological behavior to be represented in a universal manner by an underlying viscoelastic master curve. Here, we explore whether this is possible by performing rheological investigations on a series of model PEO-laponite aqueous solutions covering a relevant and interesting range of compositions and temperatures.

2.2 Ageing and fixing the sample prehistory

Limited ageing studies were performed to define and limit the sample prehistory in our experiments. In the following discussion “day 1” refers to the first day of the rheological measurement, *i.e.* the day of preparation of laponite dispersion, the fourth day after initial mixing of PEO and water to form PW solution and a day after initial mixing of the laponite dispersion and PW stock solution to prepare PWL mixture.

The shear viscosity and the frequency sweep of a 5 wt. % PEO solution was observed to be identical over a period of 40 days and therefore, did not show evidence of ageing.

The shear rate sweeps measured over 45 days on a 2.7 wt. % laponite dispersion in water are shown in Figure 2.1, each curve measured on a freshly loaded sample. Just after preparation, this dispersion showed a low, nearly Newtonian viscosity which can be seen as the rheology on day 1 in Figure 2.1. Within three days, however, the low shear viscosity is replaced by an effective yield stress, which continued to increase slowly with time. As shown in Figure 2.2, this dispersion showed a maximum in the loss modulus, G'' at high strains in the amplitude sweep measurement indicating a development of complex structure as was also observed by Willenbacher (Willenbacher 1996). This viscoelasticity is due to specific colloid-colloid interactions and should be distinguished from that arising from colloid-polymer interactions, discussed shortly.

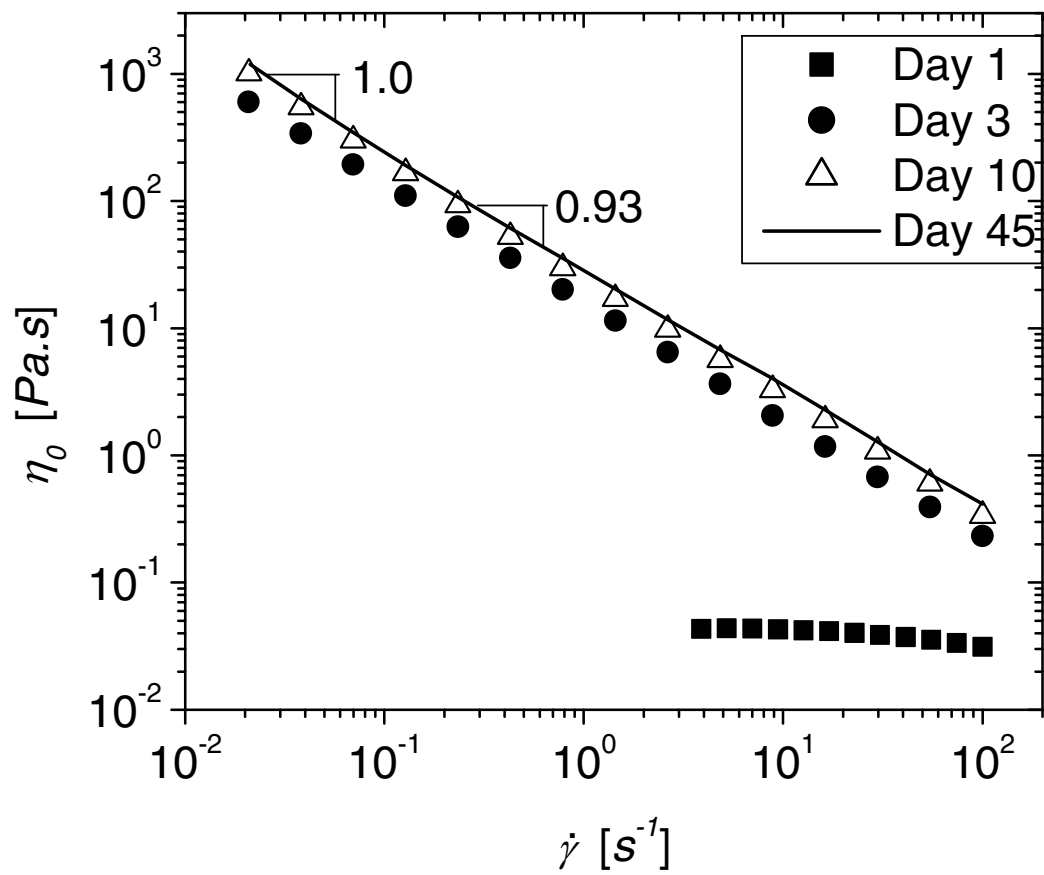


Figure 2.1: Thixotropy of a 2.67 wt. % laponite dispersion over 45 days.

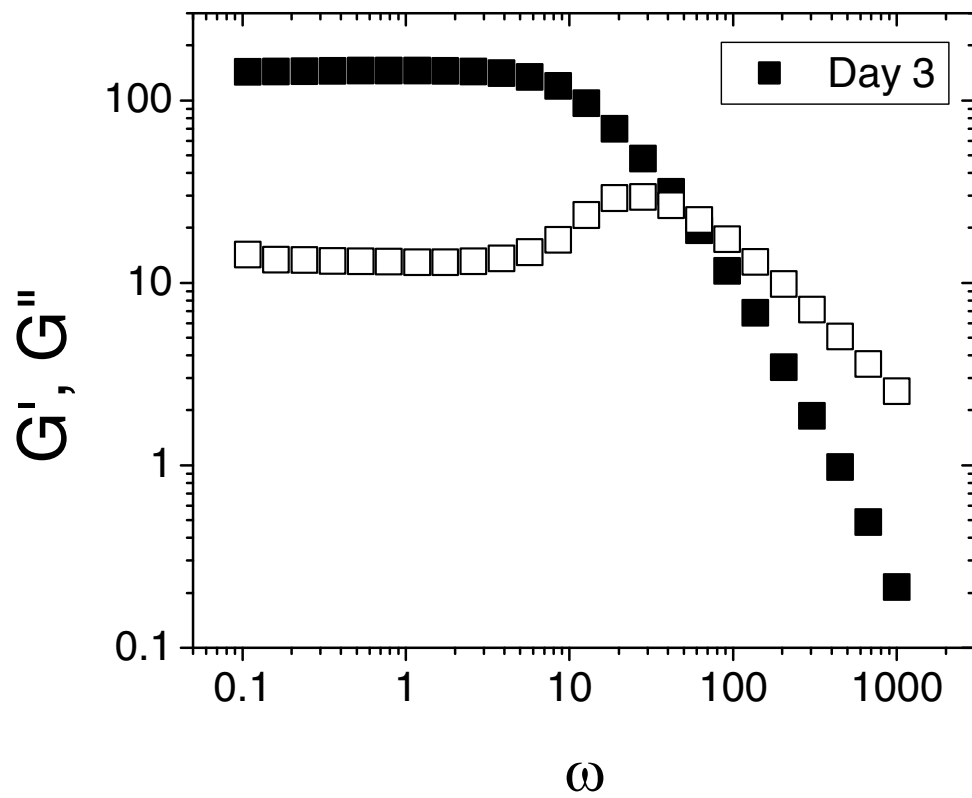


Figure 2.2: Amplitude sweep of a 2.67 wt. % laponite dispersion three days after preparation shows a maximum in G'' .

A stock of PWL mixture with PEO wt. % = 3.69, laponite wt. % = 1.18 was prepared following the same protocols as described earlier for other PWL mixtures and viscosity measurements performed in ascending (up to 500 s^{-1}) and descending sweeps as shown in Figure 2.3. The viscosity was observed to be substantially lower upon descending from high shear rates, which indicates partial shear redispersion of the structure. Even though the total solid content in the shown PWL solution is greater than the laponite dispersion shown in Figure 2.1, the latter shows a more rapid increase in the zero shear viscosity validating the retardation effect of PEO on the gelation kinetics of laponite dispersions (Sardinha and Bhatia 2002a; Sardinha and Bhatia 2002b).

Ageing studies were carried out to find out how the systems change with time so that necessary care could be taken to avoid ageing effects on the measured rheology and the electrospinning carried out. Except for ageing studies, where we deliberately sought information on how the system changes with time, all the other reported measurements were carried out with presheared PWL mixtures within 1 to 4 days after preparation. The measured rheology for samples prepared according to this protocol were found to be reproducible and consequently, differences in the observed rheology are a consequence of the differences in composition and not due to sample ageing.

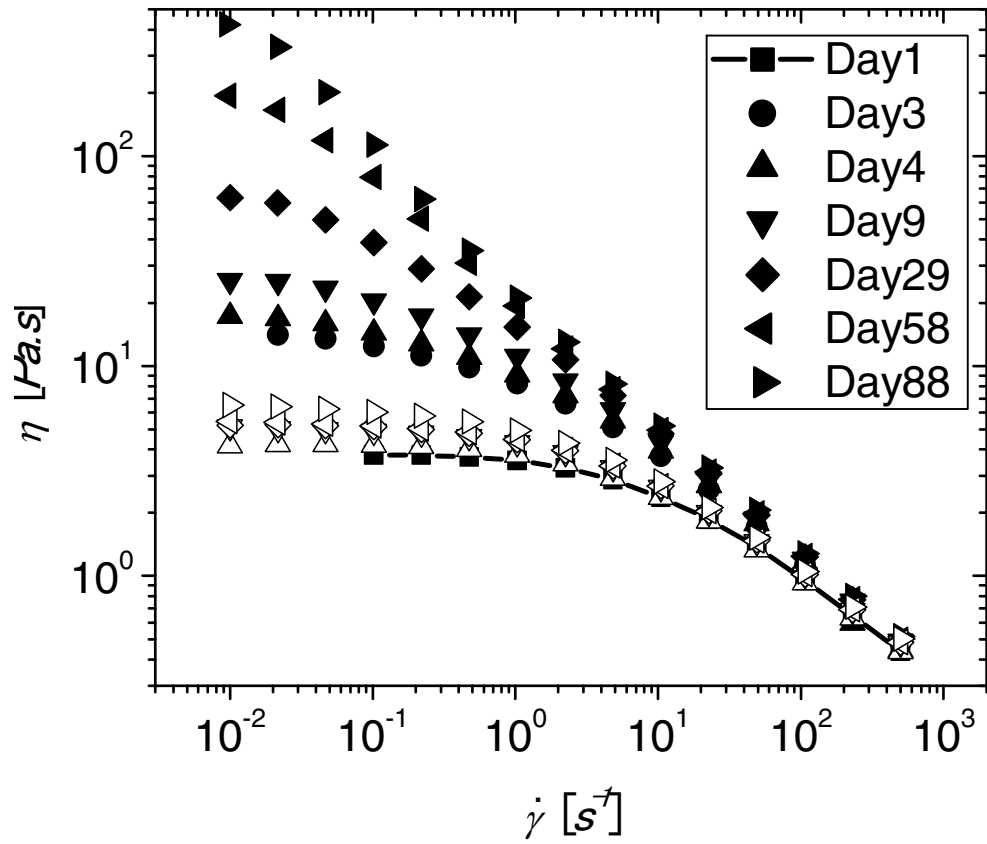


Figure 2.3: Change in viscosity of PWL6 at 25 °C with time (ascending and descending shear rates are represented by filled and empty symbols respectively).

2.3 Rheology of PEO-water solutions

PW solutions of 12 different concentrations, as indicated in Table 2.1, were prepared for the rheological characterization. The samples were designed to span the semi-dilute to concentrated regimes so as to be of practical importance as well as to explore the suitability of the two different concentration regimes for TTSP and TCSP. For PEO-water system, the Mark-Houwink-Sakurada equation for PEO of $M_w=1 \times 10^5$ g/mol is given as (Polymer Handbook, 4th ed., 1999),

$$[\eta] = 0.0449 M_w^{0.67} \quad (2.1)$$

Using expression 2.1, for PEO of $M_w=9 \times 10^5$ g/mol (used here), the concentrations, c^* and c^{**} , are given approximately as,

$$c^* = \frac{1}{[\eta]} = 0.02 \text{ g/ml} \quad c^{**} \approx c^* = 0.0183$$

The density of PEO and water are both close to 1 g/ml, so these values correspond to:

$$c^* = 0.02 \text{ wt} \% \quad c^{**} = 0.0183 \text{ wt} \% \quad (2.2)$$

Table 2.1: PW solutions prepared for rheological characterization.

| Solution | PEO <i>wt. %</i> |
|----------|---------------------|
| PW1 | 2.24 |
| PW2 | 2.37 |
| PW3 | 2.52 |
| PW4 | 3.10 |
| PW5 | 3.74 |
| PW6 | 3.85 |
| PW7 | 4.00 |
| PW8 | 4.50 |
| PW9 | 5.00 |
| PW10 | 5.50 |
| PW11 | 6.00 |
| PW12 | 6.50 |

2.3.1 Viscosity and concentration regimes

The measured shear viscosities, η , of the PW solutions are shown in Figure 2.4, where a pseudo-newtonian plateau at low $\dot{\gamma}$ is followed by significant shear thinning. Also shown in Figure 2.4 is the complex viscosity, η^* , vs. angular frequency, ω , which overlap with the viscosity curve in the low frequency limit, thereby validating the extended Cox-Merz rule for the PW solutions both in semi-dilute and concentrated regimes.

In Figure 2.5, the zero shear viscosity, η_0 , is plotted as a function of PEO concentration of PEO, c . The data corresponds quantitatively with previously published data for the same system measured by Fong *et al.* (1999) in the low concentration range. Here we have performed measurements at higher concentrations as well. The change in slope of $d(\ln \eta_0)/d(\ln c)$ vs. c on a log-log plot from 2.4 to 5.0 occurs at a concentration of about 3.2 wt. % PEO. Based on the aforementioned calculations, we identify this as the transition from the semi-dilute to concentrated entangled regime. The difference with the calculated value of c^{**} (expression 2.2) is likely to be due to the large molecular weight polydispersity (= 3.5) in the PEO. The zero shear viscosity is given by,

$$\eta_0 = (0.0013 \pm 0.0009)c^{(5.0 \pm 0.4)} \quad (2.3)$$

in the concentrated regime, where η_0 is in *Pa.s* and c is in wt. %.

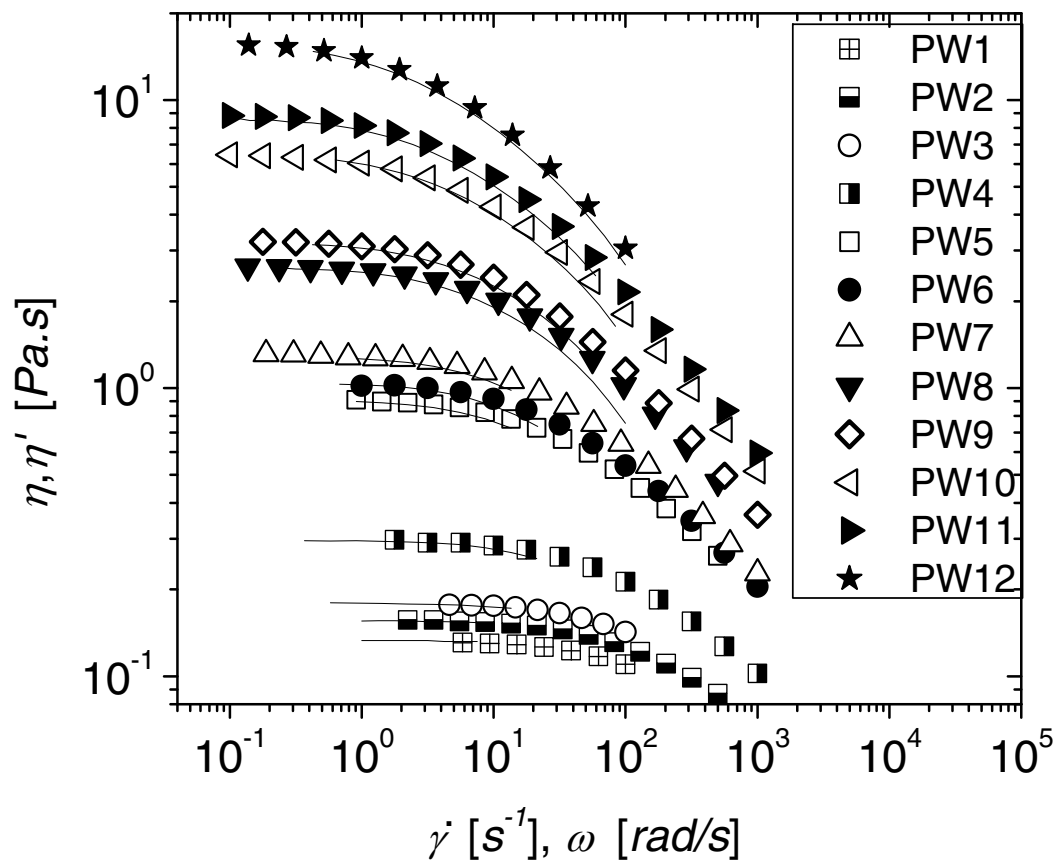


Figure 2.4: Steady-shear viscosity and validation of Cox-Merz rule for PW solutions at 25 °C (symbols - steady shear viscosity vs. shear rate, lines - complex viscosity vs. angular frequency).

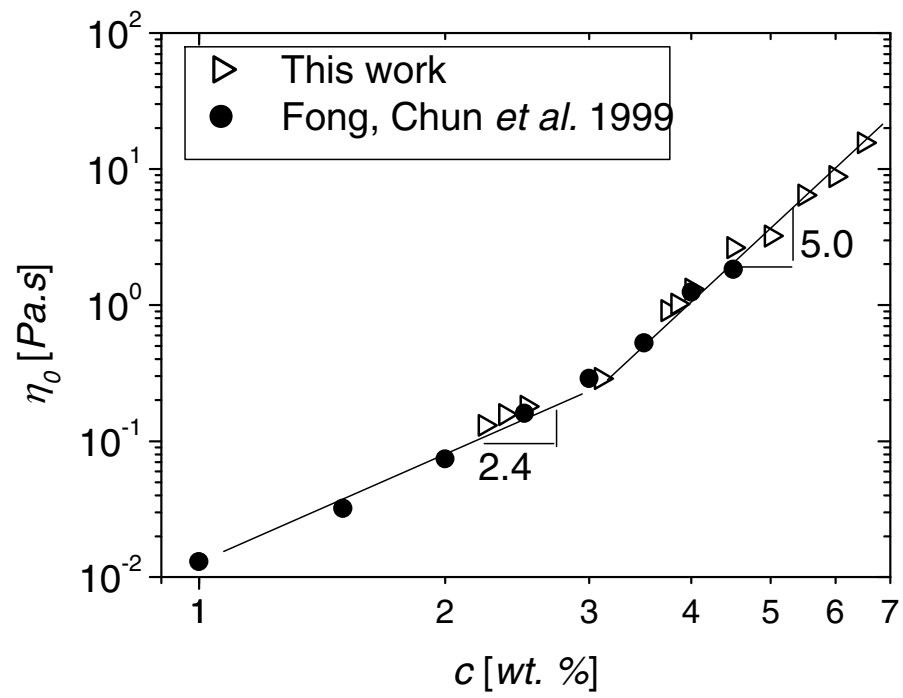


Figure 2.5: Concentration regimes of PW solutions as defined by the zero-shear viscosity at 25 °C.

2.3.2 Time-temperature superposition

As discussed by Baumgärtel and Willenbacher (1996), superposition should be possible with the rheology of polymer solutions in the concentrated regime, namely PW5 to PW12. All of these samples exhibited a maxwellian frequency sweep response with appreciable storage modulus. Figure 2.6 shows the frequency sweeps for PW12 measured at four temperatures, namely 4, 11, 18 and 25 °C. In the legends the name of sample is followed by the letter T (for temperature) and the measurement temperature in degrees Celsius. Figure 2.7 shows the same data after time-temperature superposition (TTSP) referenced to 25 °C. As anticipated, only horizontal (time) shifting was required as the vertical shift factors given as,

$$b_T = T_{ref} \rho_{ref} / T \rho \quad (2.4)$$

are expected to be unity for such a limited temperature range. As PW12 superimposes well it is a thermorheologically simple fluid over this limited temperature range. The master curve in Figure 2.7 is denoted by the same symbol as used to denote the reference curve in Figure 2.6 as a reminder that the master curve is only an extension of the reference curve in a larger experimental (in this case frequency) window. Similarly, all the other master curves discussed later are represented by the symbols used for the reference curve during superposition. Shifting a low temperature data onto a higher temperature data extends the latter into high frequency domain as can be seen by comparing Figures 2.6 and 2.7. TTSP was also performed for samples, PW10 and PW11, with similar results as seen for PW12.

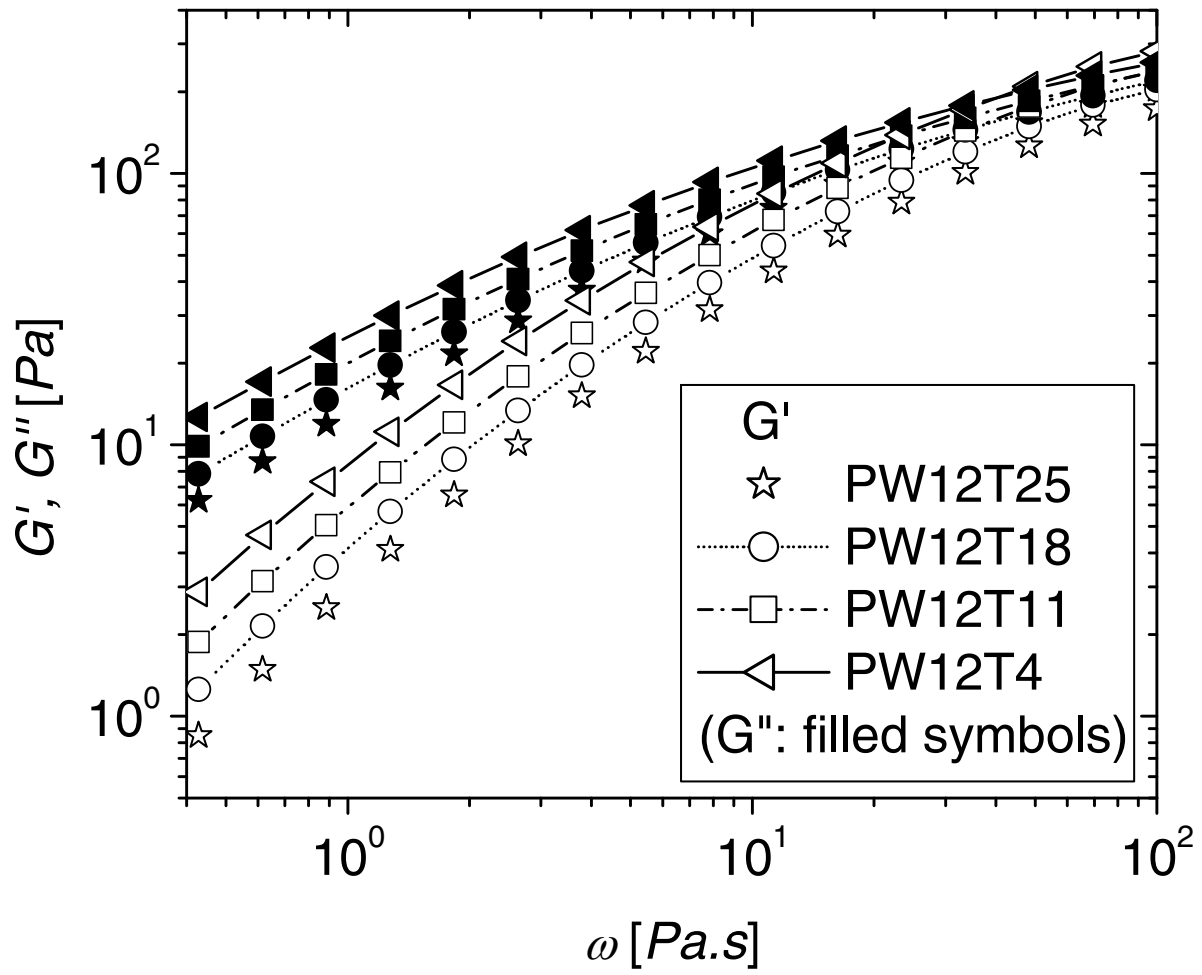


Figure 2.6: Dynamic moduli of PW12 at 4, 11, 18 and 25 °C.

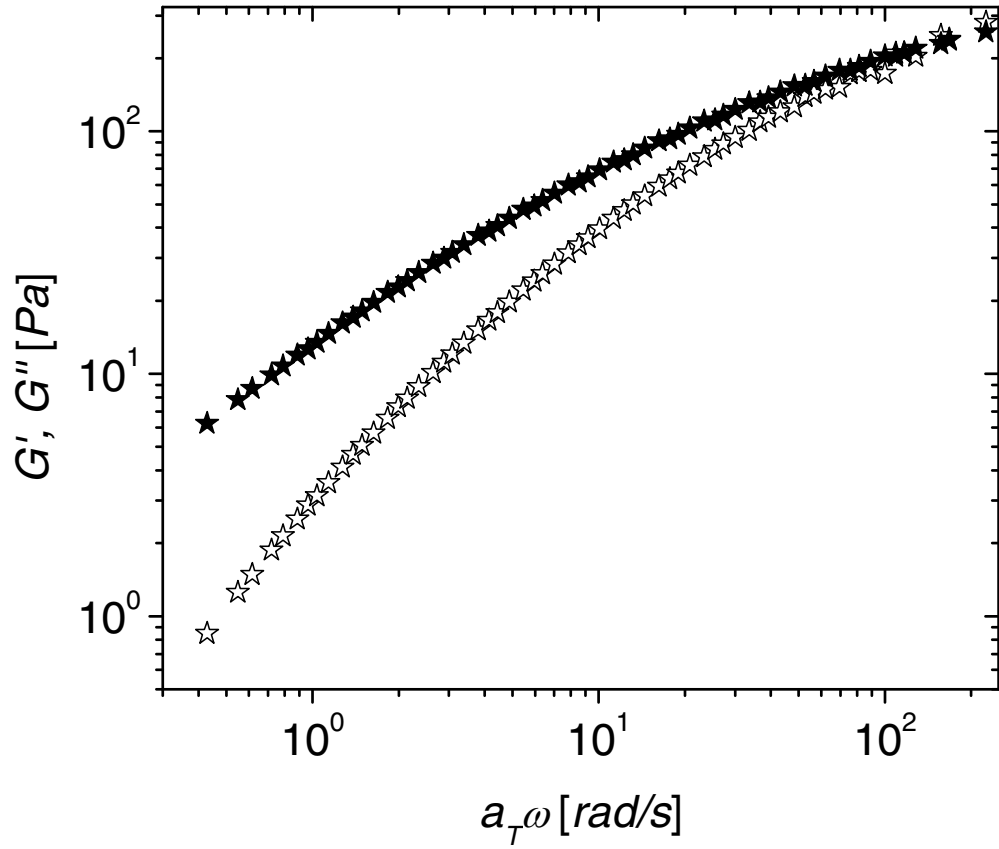


Figure 2.7: TTSP master curve of PW12 referenced to 25 °C.

The shift factors resulting from the TTSP of PW10, PW11 and PW12 are listed in Table 2.2 and plotted in Figure 2.8. To gain insight into the molecular processes contributing to the viscosity and to predict the rheology at any temperature within the range of measurement temperatures, it is of interest to correlate the shift factors, a_T , with temperature. The glass transition temperature, T_g , of the PW solutions were estimated by the Gordon-Taylor equation using the Simha-Boyer rule (Hancock and Zografis, 1994) with the following values for the individual T_g and density, ρ : $T_{g,PEO}=218$ K, $T_{g,water}=135$ K, $\rho_{PEO}=1.1$ g/cm³ and $\rho_{water}=1$ g/cm³. All the measurement temperatures employed were greater than (T_g+100) K of any solution and therefore the TTSP shift factors are expected to follow the Arrhenius equation,

$$a_T = \exp \left[\frac{-\Delta H}{R} \left(\frac{1}{T} - \frac{1}{T_{ref}} \right) \right] \quad (2.5)$$

which is validated by the exponential fit in Figure 2.8. The activation enthalpy for flow did not depend upon the concentration and was found to be,

$$-\Delta H = (26.4 \pm 0.8) \text{ kJ/mol}$$

which is larger than that of the solvent, water (17 kJ/mol) (Welty *et al.*, 1984) and therefore, consistent with the fact that the viscoelasticity is dominated by polymer-polymer interactions.

Table 2.2: Horizontal TTSP shift factors for PW10, PW11 and PW12.

| Solution | T (°C) | a_T |
|----------|--------|-------|
| PW10 | 25 | 1 |
| PW10 | 20 | 1.2 |
| PW10 | 15 | 1.46 |
| PW10 | 10 | 1.79 |
| PW11 | 25 | 1 |
| PW11 | 18 | 1.3 |
| PW11 | 11 | 1.71 |
| PW11 | 4 | 2.32 |
| PW12 | 25 | 1 |
| PW12 | 18 | 1.28 |
| PW12 | 11 | 1.68 |
| PW12 | 4 | 2.26 |

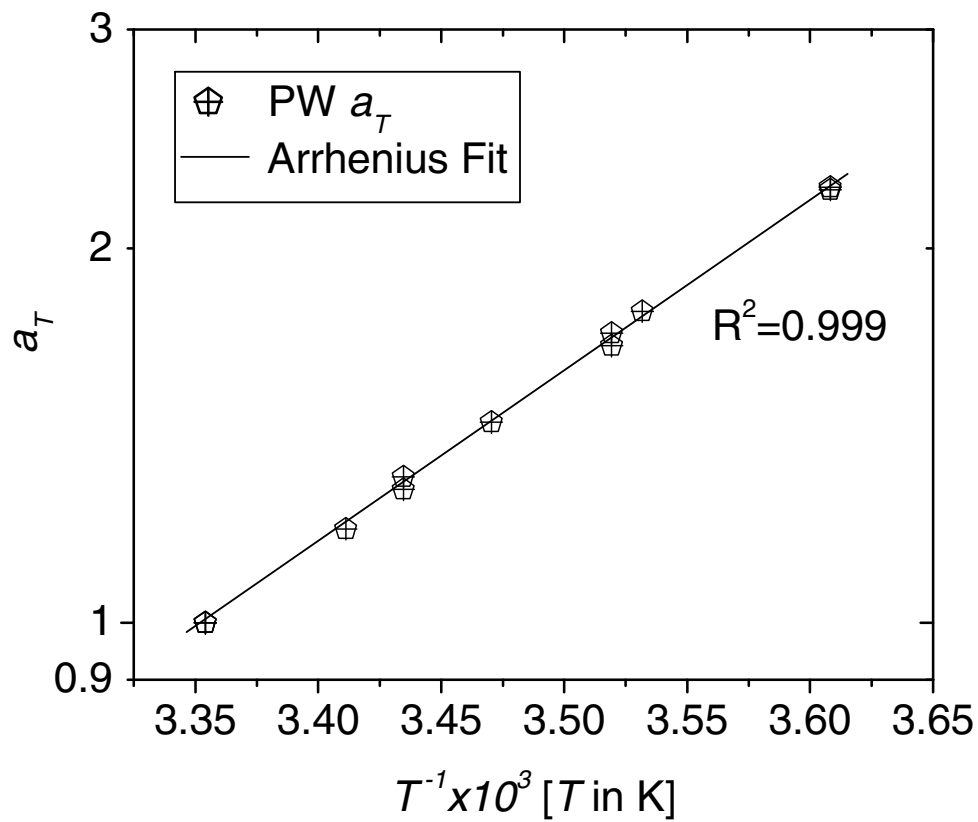


Figure 2.8: Horizontal shift factors, a_T , for TTSP of PW10, PW11 and PW12.

2.3.3 Time-concentration superposition

In Figure 2.9 the dynamic moduli of PW solutions in the concentrated regime, namely, PW5, PW6, ..., PW9 measured at 25 °C are shown along with the TTSP master curves for samples PW10, PW11 and PW12. The PW solutions belonging to the semi-dilute concentration regime, namely, PW1, PW2, PW3 and PW4, do not show any appreciable elasticity and therefore, were not considered further. As is apparent from Figure 2.9, for PW solutions that belonged to the concentrated regime, the curves at different concentrations of PEO have the same Maxwellian shape and therefore, are shifted horizontally and vertically to create concentration master curve referenced to the 5.5 wt. % PW solution, (*i.e.* PW10, at 25 °C) as shown in Figure 2.10. Here vertical shifting is also required because the vertical shift factors depend upon the concentration (Baumgärtel and Willenbacher, 1996; Ferry, 1980).

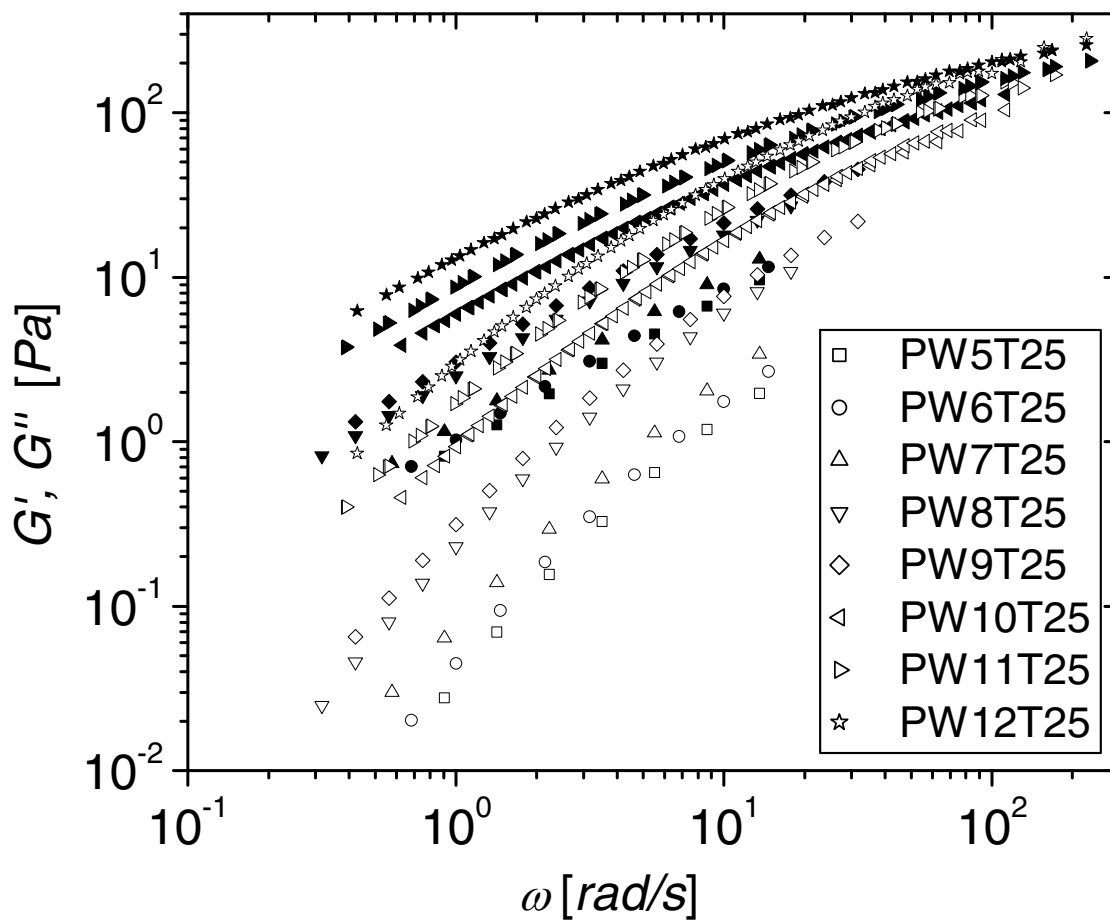


Figure 2.9: Dynamic moduli of PW solutions in the concentrated regime: PW5 to PW12 (PW10, PW11 and PW12 from their TTSP master curves) at 25 °C.

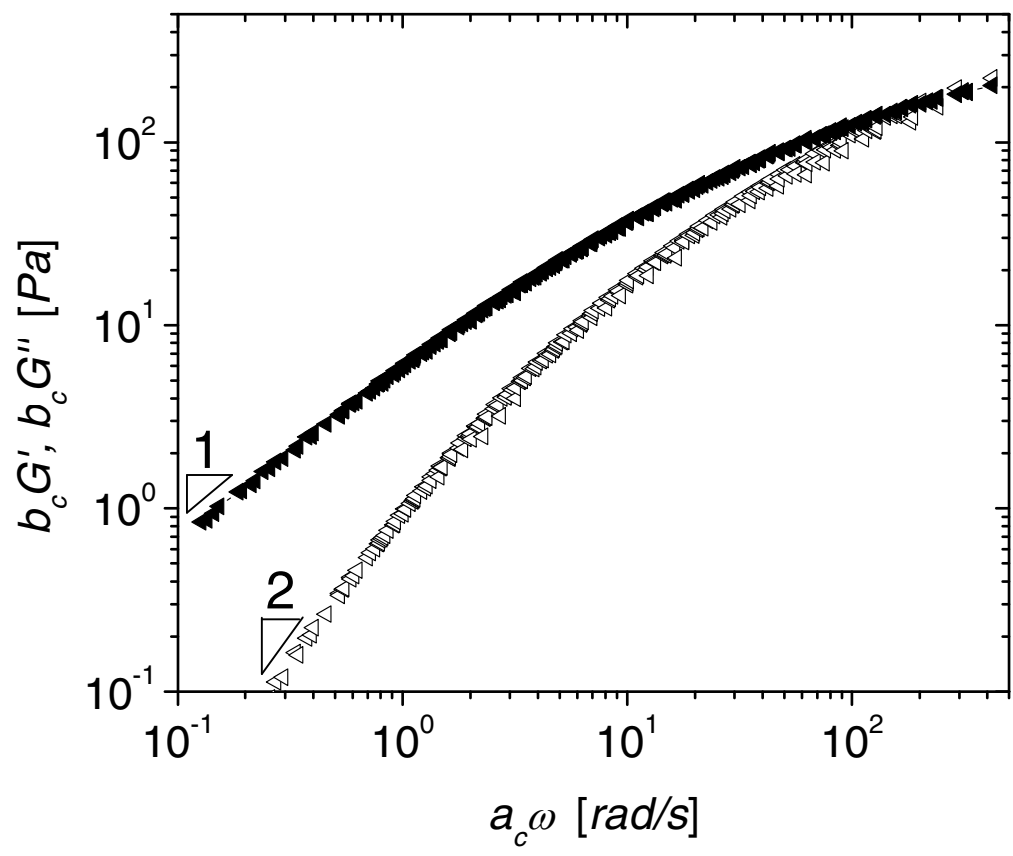


Figure 2.10: TCSP master curve of the PW solutions referenced to 5.5 wt. % PEO (PW10) at 25 °C.

The shift factors resulting from the TCSP of PW5 to PW12 data are shown in Table 2.3 and plotted in Figure 2.11. Also shown for comparison are the shift factors calculated using the scalings expected for ideal Gaussian chains as reported by Baumgärtel and Willenbacher (1996) ($a_c \propto c^{3.5}$, $b_c \propto c^{-2.2}$). Our TCSP shift factors, a_c and b_c , also follow power law correlations with concentration given as,

$$a_c = (6.7 \times 10^{-4} \pm 2.6 \times 10^{-4})c^{(4.2 \pm 0.2)} \quad (2.6)$$

$$b_c = (3.25 \pm 0.38)c^{(-0.72 \pm 0.08)} \quad (2.7)$$

where c is in wt. %. This difference in scaling can be rationalized in terms of solvent quality effects, as will be discussed shortly.

It is interesting to explore the results of shifting if the shift factors were assumed to follow the scaling for gaussian chains as found by Baumgärtel and Willenbacher (1996), *i.e.* $a_c = Ac^{3.5}$ and $b_c = Bc^{-2.2}$. For this, the value of shift factors for reference curves were chosen as unity and the prefactors, A and B were found by putting $c = 5.5$ wt. %. With the prefactors known, the shift factors were calculated for different concentrations. After the shifting was carried out using the calculated shift factors, the curves did not superimpose in any frequency window as shown in Figure 2.12 which suggests that PEO chains in water are not simple gaussian chains. Also shown are the $\tan \delta$ curves which also do not superimpose. An explanation of why the PEO solutions do not follow the scaling expected for idealized gaussian polymer chains in theta solvents will be presented in section 2.5.

Table 2.3: Shift factors for TCSP of PW solutions.

| Solution | a_c | b_c |
|----------|-------|-------|
| PW3 | 0.03* | 1.68* |
| PW5 | 0.168 | 1.26 |
| PW6 | 0.186 | 1.2 |
| PW7 | 0.234 | 1.17 |
| PW8 | 0.457 | 1.15 |
| PW9 | 0.525 | 1.07 |
| PW10 | 1 | 1 |
| PW11 | 1.41 | 0.912 |
| PW12 | 1.86 | 0.794 |

(* values were found by correlating a_c and b_c with concentration)

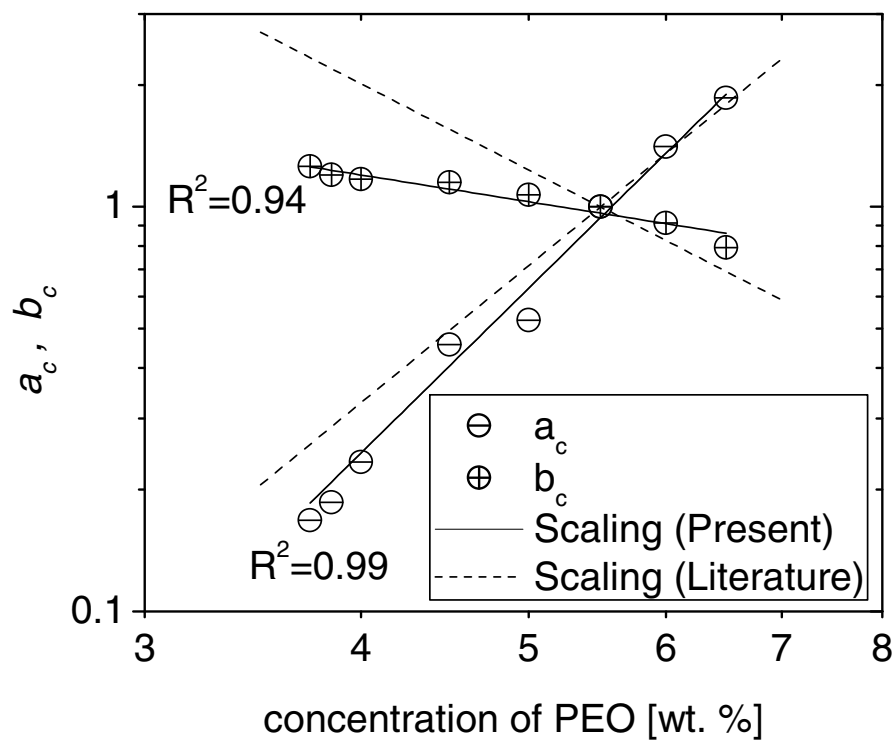


Figure 2.11: Horizontal and vertical TCSP shift factors for PW5 to PW12 and their comparison with the scaling provided for polymer solutions in the literature (Baumgärtel and Willenbacher, 1996).

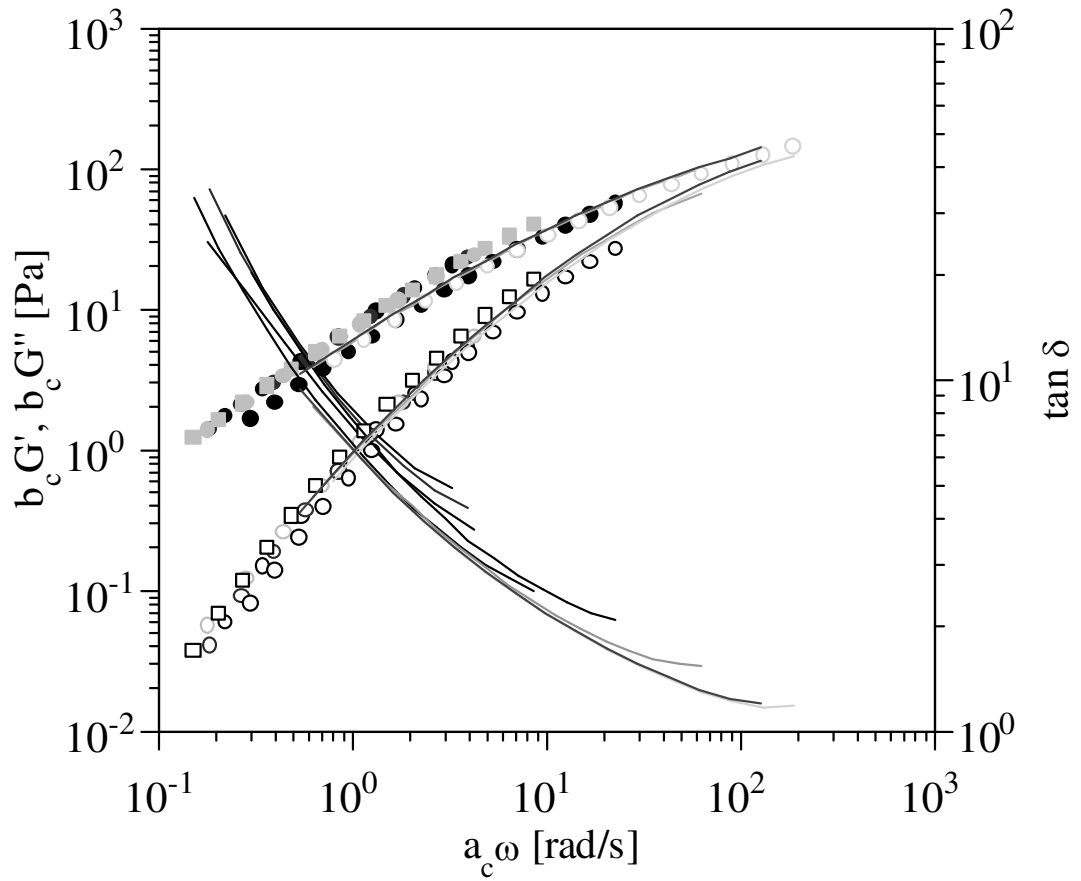


Figure 2.12: TCSP shifted PW curves by employing the shift factors given by gaussian scaling with concentration of the polymer.

2.3.4 Relaxation spectrum

For completeness, the discrete relaxation spectrum of the PW master curve shown in Figure 2.10 is tabulated in Table 2.4, where 6 (N) modes were found to accurately represent the master curve. Using the spectra, the master curve G' and G'' data as a function of ω can be found using the relations,

$$G'(\omega) = \sum_{i=1}^N \frac{g_i \lambda_i^2 \omega^2}{1 + \lambda_i^2 \omega^2} \quad G''(\omega) = \sum_{i=1}^N \frac{g_i \lambda_i \omega}{1 + \lambda_i^2 \omega^2} \quad (2.8)$$

Table 2.4: Discrete relaxation spectra of PW TCSP master curve.

| Relaxation strength g_i [Pa] | Relaxation time λ_i [s] |
|-----------------------------------|------------------------------------|
| 7380 | 6.41×10^{-3} |
| 142 | 3.13×10^{-2} |
| 52.1 | 1.17×10^{-1} |
| 13.8 | 3.71×10^{-1} |
| 3.33 | 1.43×10^0 |

2.4 Rheology of PEO-water-laponite solutions

The concentrations of PWL mixtures (PWL1 to PWL9) prepared for rheological characterization and their mixing times on the vibrating mixer prior to testing are listed in Table 2.5. The concentrations of ternary mixtures were designed to investigate the effects of adding laponite to originally neat PW solutions (PW base solutions) of different concentrations. As shown in Table 2.5, five different groups were formed with each group containing a PW base solution and corresponding PWL mixtures with the PEO to water ratio ($100P/(P+W)$) equal to the PW base solution. Thus, successive mixtures in each group can be compared to the corresponding neat PW base solution in the group to determine the effects of laponite addition upon the rheology of PW solutions. Figure 2.13 shows on a triangular plot, the concentration of binaries mixed to form the ternaries of desired concentrations. As expected by the lever-arm rule, the concentration of the ternary PWL mixture formed by mixing the two binaries, PW solution and laponite dispersion lies on the straight line (shown as dotted lines) connecting the binaries. The five arrows shown start at the PW base solution in each of the five groups and connects the PWL samples belonging to each of the five groups.

2.4.1 Effect of laponite on the viscosity

The shear thinning response of the PWL mixtures is shown in Figure 2.14 along with the corresponding dynamic viscosity $\eta^*(\omega)$, which are in reasonable agreement except for PWL5 shown in dashed line. PWL5 contained the highest concentration of laponite and indicates the beginning of the failure of Cox-Merz rule at high laponite concentrations.

Table 2.5: PWL mixtures prepared for rheological characterization.

| Ternary mixture | PW base solution | Group | P% | L% | W % | 100xP/(P+W) | 100xL/(L+P) | Mixing time [day] |
|-----------------|------------------|-------|------|------|-------|-------------|-------------|-------------------|
| PWL1 | PW3 | 1 | 2.49 | 0.94 | 96.57 | 2.51 | 27.31 | 2 |
| PWL2 | PW5 | 2 | 3.71 | 0.66 | 95.63 | 3.73 | 15.09 | 1 |
| PWL3 | PW8 | 3 | 4.48 | 0.49 | 95.04 | 4.50 | 9.79 | 1 |
| PWL4 | PW10 | 4 | 5.49 | 0.26 | 94.26 | 5.50 | 4.48 | 2 |
| PWL5 | PW3 | 1 | 2.48 | 1.52 | 96.00 | 2.52 | 38.00 | 2 |
| PWL6 | PW5 | 2 | 3.69 | 1.18 | 95.12 | 3.74 | 24.28 | 1 |
| PWL7 | PW8 | 3 | 4.45 | 0.97 | 94.57 | 4.50 | 17.96 | 3 |
| PWL8 | PW10 | 4 | 5.46 | 0.7 | 93.84 | 5.50 | 11.33 | 4 |
| PWL9 | PW12 | 5 | 6.47 | 0.42 | 93.10 | 6.50 | 6.10 | 2 |

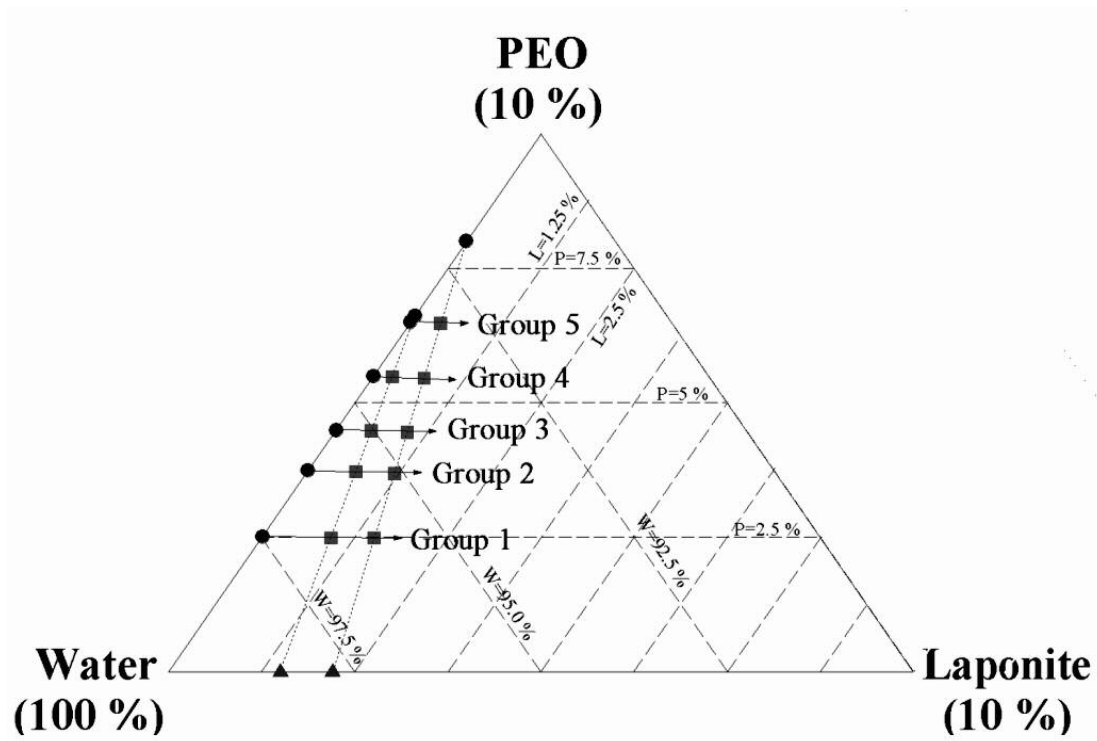


Figure 2.13: Concentration map of neat and laponite filled aqueous PEO solutions prepared for electrospinning: circles, triangles and squares represent the PEO solutions, laponite dispersions and laponite-filled PEO solutions respectively. Solutions that lie along an arrow represent members of a group.

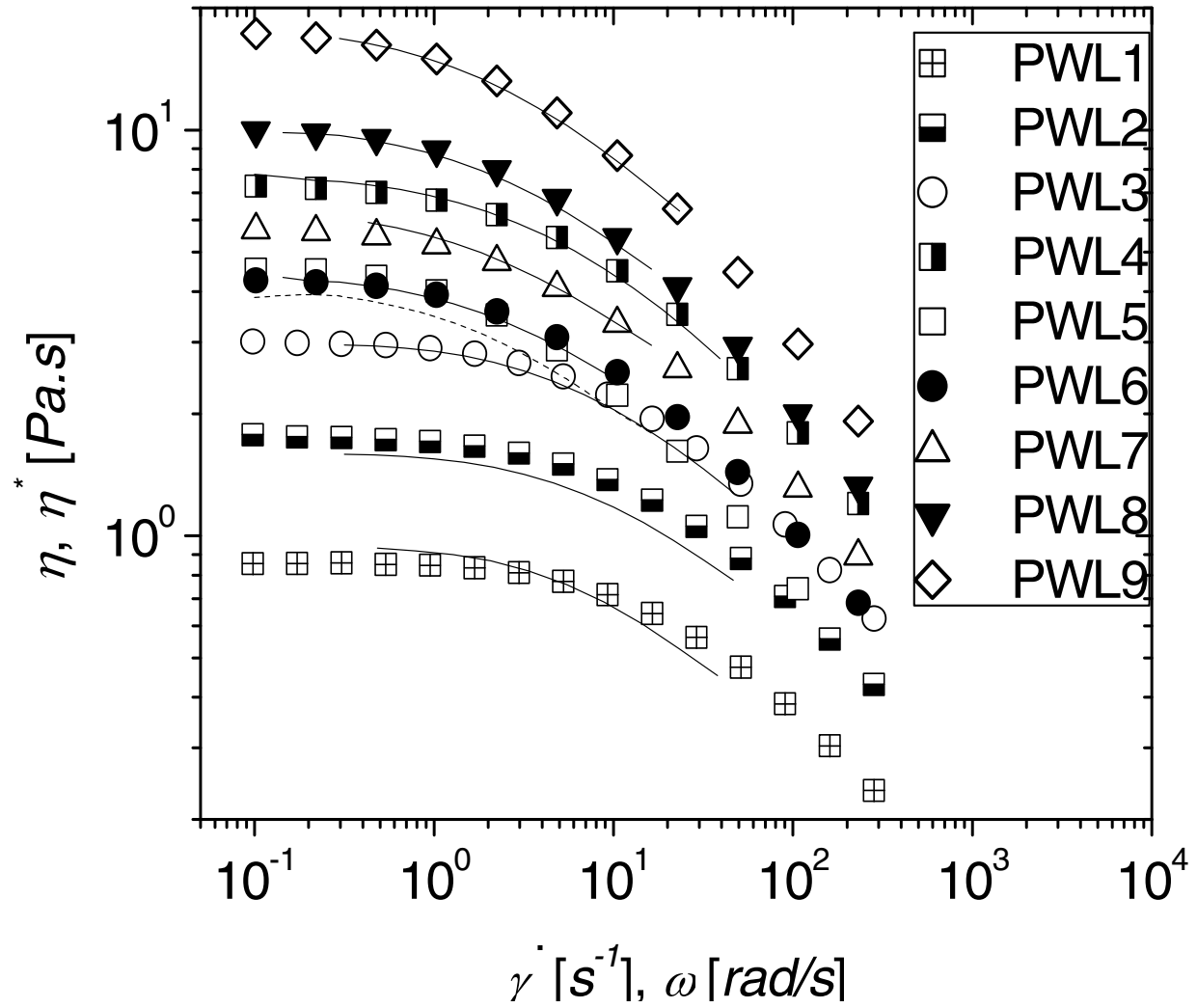


Figure 2.14: Steady-shear viscosity and validation of Cox-Merz rule for PWL mixtures at 25 °C (Symbols - viscosity vs. shear rate, lines - complex viscosity vs. angular frequency. The dashed line for the case of PWL5 implies a deviation from the Cox-Merz rule.).

As expected of the PWL mixtures containing PEO in excess, the shear viscosity is qualitatively similar to the PW solutions but quantitative comparison of data in Figure 2.4 and Figure 2.14, shows that at the same solids loading, the viscosity is larger for higher laponite concentrations.

2.4.2 Time-temperature superposition

The frequency sweep measurements were performed for laponite-filled systems at five different temperatures each, namely, 4, 11, 18, 25 and 32 °C. Upon TTSP of the data referenced to 25 °C the data superimposed well showing that the PWL mixtures are thermorheologically simple, at least, in this limited temperature range. Once again, no vertical shifting was required for TTSP because of the narrow temperature range. As an example, the dynamic shear moduli of PWL1 are shown at five different temperatures in Figure 2.15. It is remarkable to note that unlike its corresponding base solution, PW3, the PWL1 mixture with less than 1 wt. % laponite showed a substantial elasticity and a Maxwellian behavior. Shown in Figure 2.16 is the TTSP master curve of PWL1 referenced to 25 °C, the TTSP master curve of PWL5 referenced to 25 °C, and the curve for PW3 predicted from the PW master curve shown in Figure 2.10 using the shift factor correlations, 2.6 and 2.7. This is a hypothetical prediction by extrapolation from the PW master curve made for purposes of comparison; sample PW3 does not exhibit this viscoelasticity in experiment as it falls in the semi-dilute regime.

Listed in Table 2.6 are the TTSP shift factors (master curves not shown for brevity), a_T , for samples PWL1 to PWL9 along with the activation energy for flow,

obtained by fitting a_T vs. T data of PWL mixtures to Arrhenius equation (equation 2.5). The fitted values can be used to predict a_T , and hence the rheology of PWL1 to PWL9 in the range of 4 to 32 °C.

2.4.3 First time-concentration superposition

As shown in Figure 2.16 for group 1, the viscoelastic spectra for samples in the same group have a similar shape but are displaced as the laponite content is increased. Therefore, the curves of PWL mixtures in a group were superimposed onto curves for the respective PW base solutions belonging to that particular group. Figure 2.17 shows the five pairs of G' and G'' master curves, one for each group. This shifting is referred to as TCSP₁ henceforth and the shift factors referred to as, a_{cl} and b_{cl} , are listed in Table 2.7. As within each group the PEO-water concentration is fixed, this first TCSP (TCSP₁) accounts for the changes associated with the addition of laponite to a base PW solution. Comparisons of master curves between groups compares samples with different concentrations of polymer.

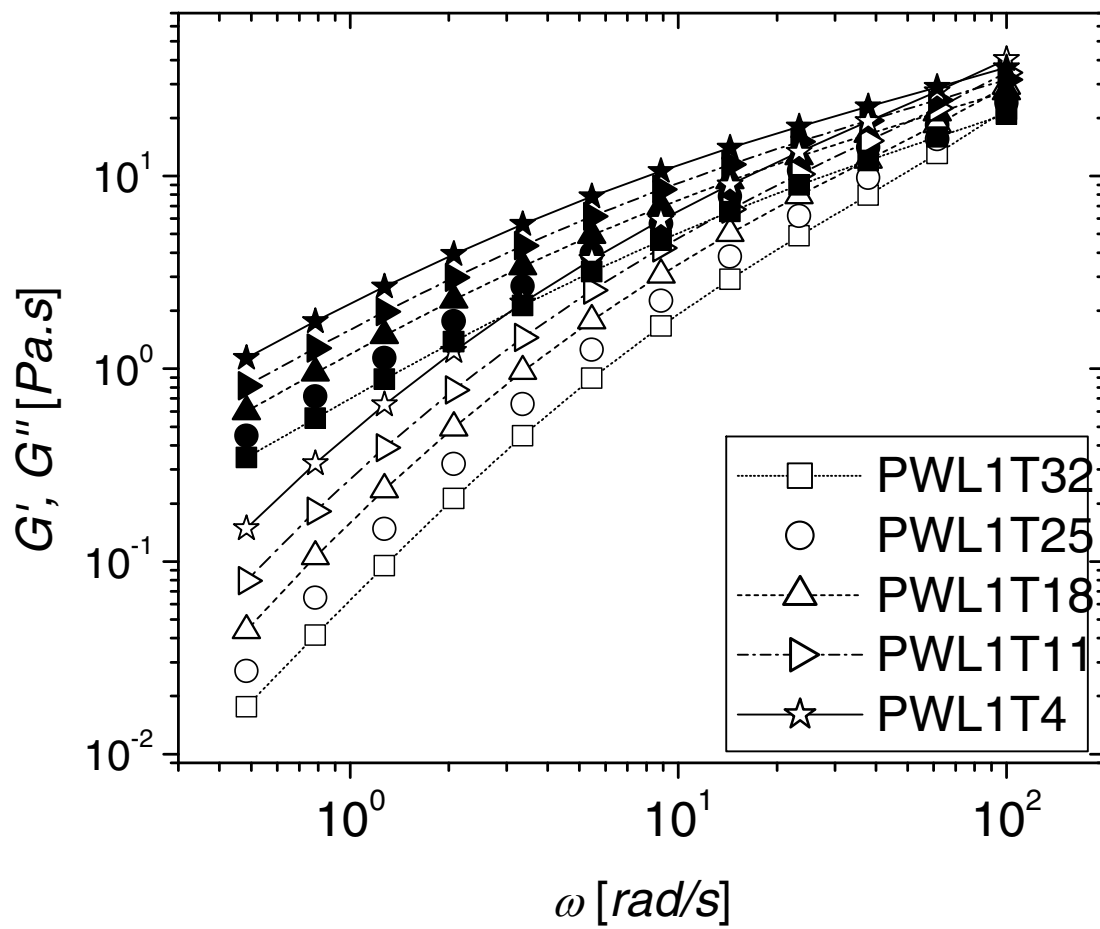


Figure 2.15: Dynamic moduli of PWL1 at 4, 11, 18, 25 and 32 °C.

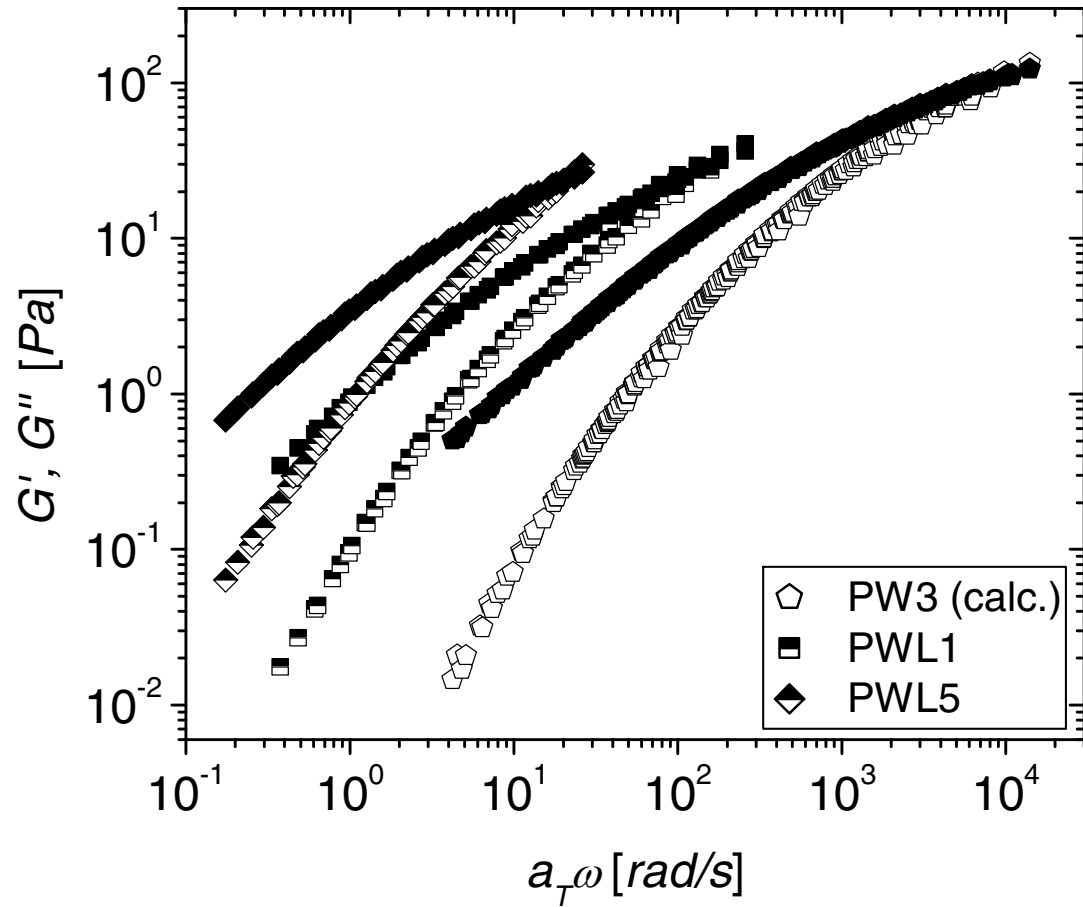


Figure 2.16: TTSP master curve of PWL1, TTSP master curve of PWL5 and the calculated PW3 curve all referenced to 25 °C.

Table 2.6: Horizontal TTSP shift factors and activation energy of flow for PWL mixtures.

| | 32 °C | 25 °C | 18 °C | 11 °C | 4 °C | $-\Delta H$ [kJ/mol] |
|------|-------|-------|-------|-------|------|-------------------------|
| PWL1 | 0.778 | 1 | 1.32 | 1.81 | 2.57 | 30.0 |
| PWL2 | 0.768 | 1 | 1.33 | 1.81 | 2.54 | 30.0 |
| PWL3 | 0.772 | 1 | 1.32 | 1.78 | 2.48 | 29.3 |
| PWL4 | 0.771 | 1 | 1.34 | 1.77 | 2.41 | 28.6 |
| PWL5 | 0.843 | 1 | 1.24 | 1.61 | 2.18 | 23.9 |
| PWL6 | 0.793 | 1 | 1.29 | 1.73 | 2.37 | 27.5 |
| PWL7 | 0.801 | 1 | 1.3 | 1.74 | 2.42 | 27.8 |
| PWL8 | 0.787 | 1 | 1.29 | 1.72 | 2.34 | 27.4 |
| PWL9 | 0.796 | 1 | 1.28 | 1.67 | 2.24 | 26.0 |

Upon further inspection, and as shown in Figure 2.18, it is apparent that the shift factors, a_{cl} and b_{cl} , are strong functions of the percentage of laponite in the mixture on a water free basis tabulated as $100L/(L+P)$ in Table 2.5. The shift factor, a_{cl} , was found to conform to a piecewise exponential function (expression 2.9), whereas the shift factor, b_{cl} , was described well by a single exponential function (expression 2.10).

$$a_{cl} = \begin{cases} (1.04 \pm 0.05) \exp \left[(0.036 \pm 0.007) \left(\frac{100L}{(L+P)} \right) \right], & 0 \leq \frac{100L}{(L+P)} < 10 \\ (0.42 \pm 0.08) \exp \left[(0.139 \pm 0.005) \left(\frac{100L}{(L+P)} \right) \right], & \frac{100L}{(L+P)} \geq 10 \end{cases} \quad (2.9)$$

$$b_{cl} = (1.09 \pm 0.10) \exp \left[(0.022 \pm 0.004) \left(\frac{100L}{(L+P)} \right) \right] \quad (2.10)$$

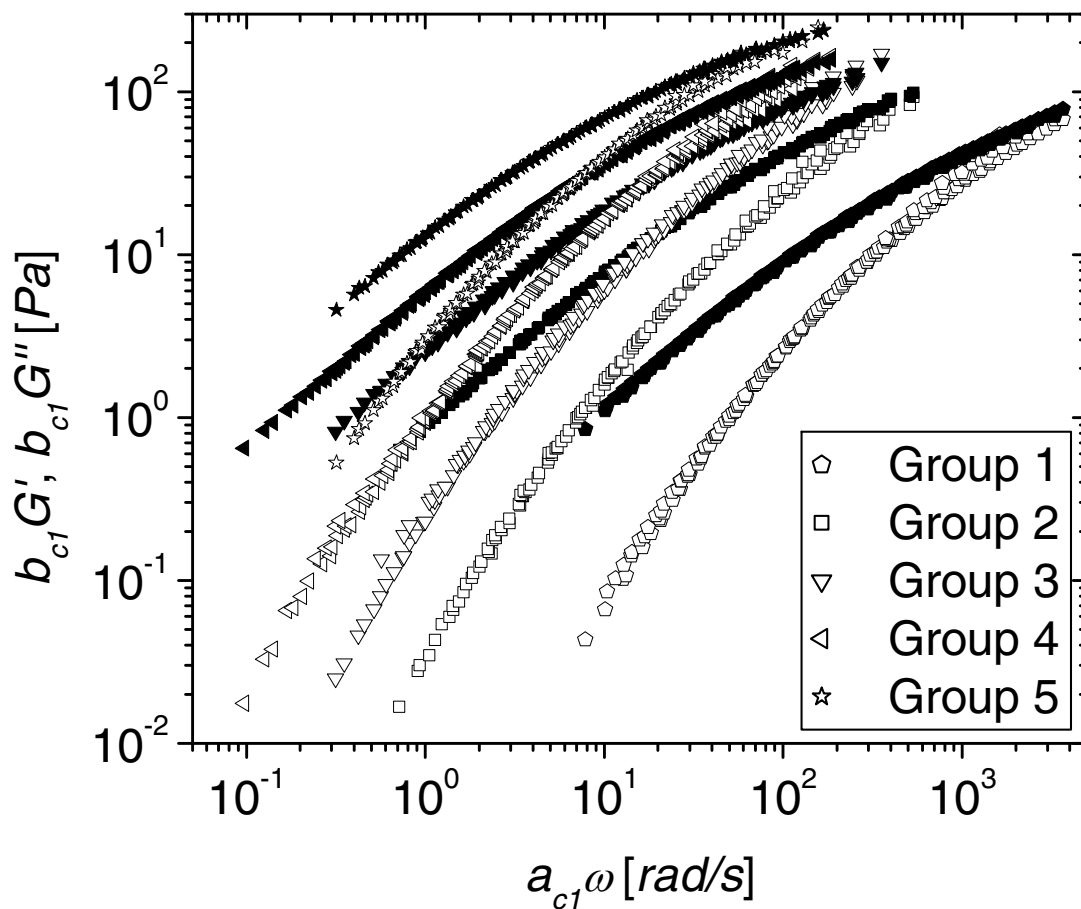


Figure 2.17: Groupwise TCSP (= TCSP₁) master curves of PWL mixtures at 25 °C referenced to PW base solution in each group.

Table 2.7: Shift factors for the TCSP (=TCSP₁) of PWL mixtures on their respective PW base solutions (the required rheology of PW3 for TCSP of Group 1 mixtures was predicted from the PW TCSP master curve shown in Figure 2.10 with shift factors (equations 2.6 and 2.7) extrapolated to the concentration of PW3).

| | | a_{cl} | b_{cl} |
|---------|------|----------|----------|
| Group 1 | PW3 | 1 | 1 |
| | PWL1 | 20.9 | 2.45 |
| | PWL5 | 81.3 | 2.24 |
| Group 2 | PW5 | 1 | 1 |
| | PWL2 | 2.95 | 1.62 |
| | PWL6 | 9.95 | 2.01 |
| Group 3 | PW8 | 1 | 1 |
| | PWL3 | 1.45 | 1.32 |
| | PWL7 | 4.37 | 1.74 |
| Group 4 | PW10 | 1 | 1 |
| | PWL4 | 1.26 | 1.07 |
| | PWL8 | 1.95 | 1.23 |
| Group 5 | PW12 | 1 | 1 |
| | PWL9 | 1.35 | 1.15 |

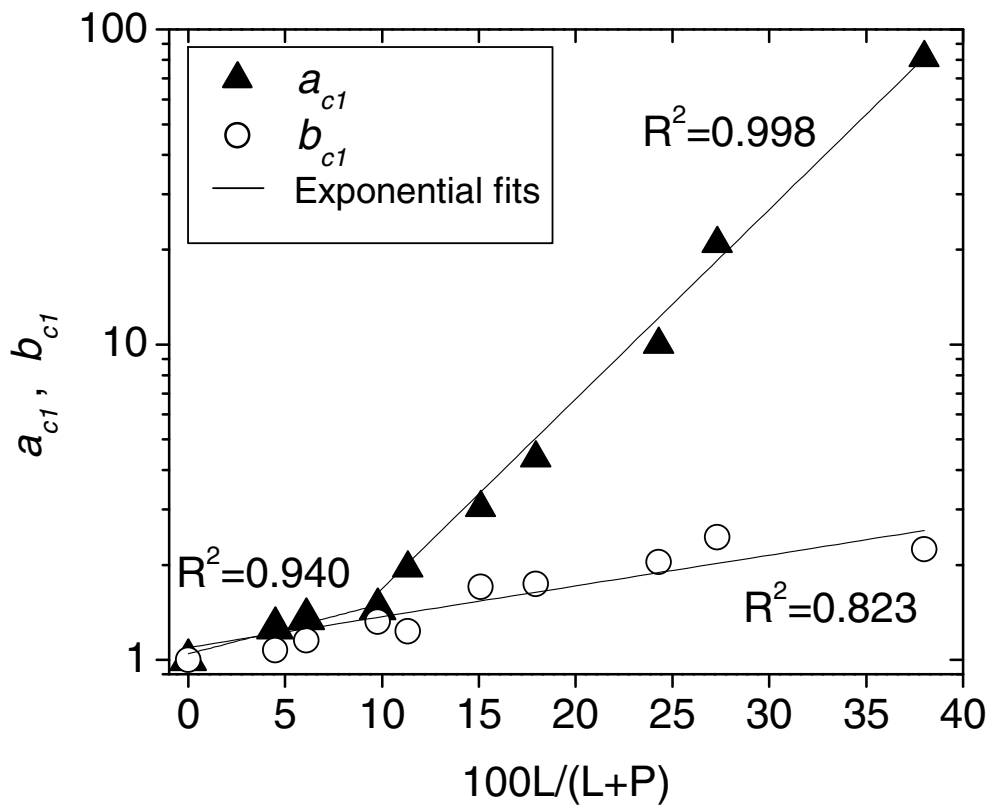


Figure 2.18: TCSP shift factors for groupwise shifting (= TCSP₁) of PWL TTSP master curves at 25 °C on the respective PW base solutions.

2.4.4 Complete time-concentration superposition

The master curves formed by shifting the various laponite concentrations onto the base PW solutions (*i.e.* the results of TCSP₁) are observed to successfully TCSP. This TCSP is shown in Figure 2.19 and denoted by TCSP₂. The group 4 master curve was chosen as reference for TCSP₂. This is equivalent to shifting the curves for base solutions, PW3, PW6, PW8 and PW12 onto PW10 chosen as reference. Therefore, the shift factors, a_{c2} and b_{c2} , for TCSP₂ should be identical to the shift factors that result from the TCSP of PW solutions as listed in Table 2.3. By the same reasoning, the relaxation spectrum of the PW TCSP master curve, listed in Table 2.4, is expected and was found to reproduce the PWL master curve obtained after TCSP₂, as is the case.

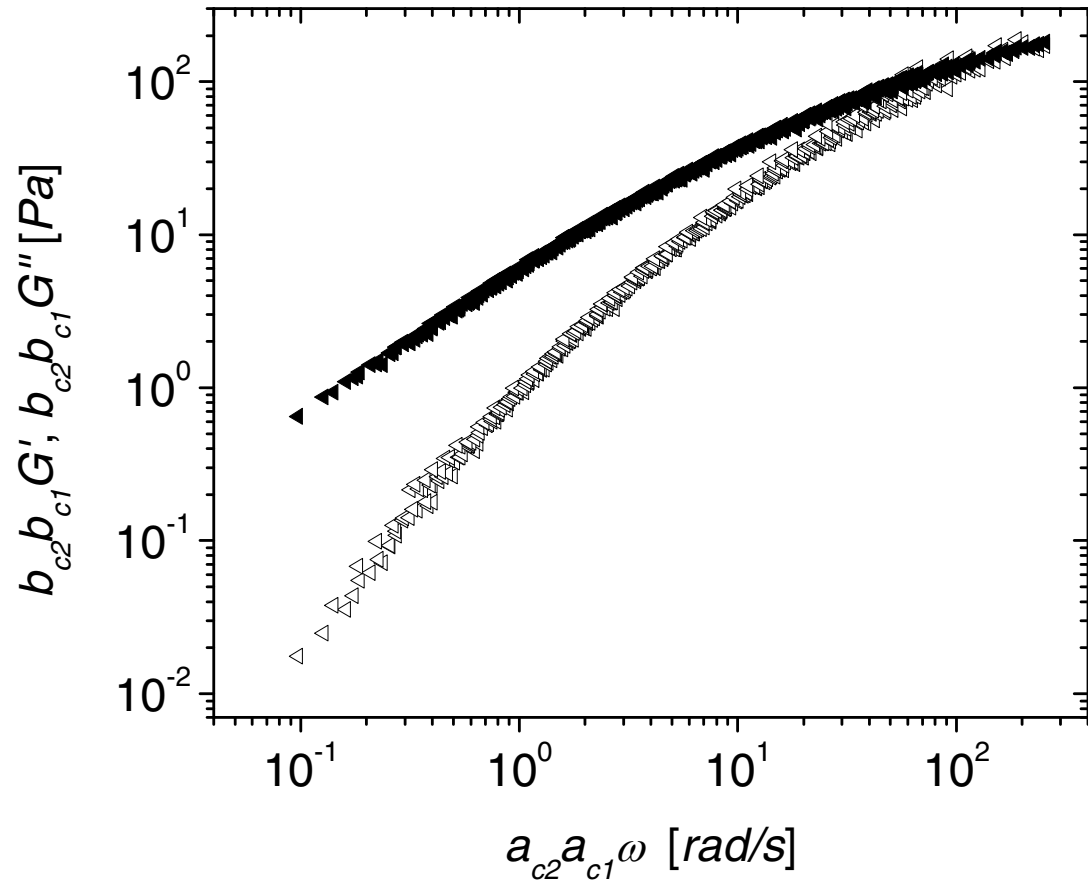


Figure 2.19: Complete TCSP (= TCSP₂) master curve of PWL mixtures at 25 °C referenced to Group 4 (or PW10).

2.5 Discussion

Reducing temperature reduces molecular motion and hence, increases the relaxation time of the entangled polymer chain; hence the corresponding increase in the values of the TTSP shift factors, a_T , of both neat and laponite filled PW solutions. Over this small temperature range, however, the density does not change significantly (Ferry, 1980) so vertical shifting is not required.

TCSP shift factors for the PW solutions, $a_{c1} \propto c^\alpha$ and $b_{c1} \propto c^\beta$, are related to the concentration dependence of the zero shear viscosity $\eta_0 \propto c^\phi$ by $\phi = \alpha - \beta$. This relation can be derived as follows. For a flowing system, in the limit of zero frequency, the following should hold:

$$\eta_0 = \lim_{\omega \rightarrow 0} \eta'(\omega)$$

$$\text{where, } \eta' = \frac{G''}{\omega}$$

$$\Rightarrow \eta_0 = \lim_{\omega \rightarrow 0} \left(\frac{G''}{\omega} \right) = \left[\frac{\left(\frac{G''_{shifted}}{b_c} \right)}{\frac{\omega_{shifted}}{a_c}} \right]$$

$$\text{or } \eta_0 \left(\frac{b_c}{a_c} \right) = \lim_{\omega_{shifted} \rightarrow 0} \left(\frac{G''_{shifted}}{\omega_{shifted}} \right) = \text{constant}$$

Therefore, $\eta_0 \left(\frac{b_c}{a_c} \right) = \text{constant}$ ($= \eta_0$ of PW10 which was chosen as the reference)

Also, this means that,

$$\eta_0 \propto \left(\frac{a_c}{b_c} \right) \Rightarrow \eta_0 \propto c^{4.92 \pm 0.28} \text{ (i.e. } \phi = \alpha - \beta) \quad (2.11)$$

This value of $\phi = \alpha - \beta = 4.92 \pm 0.28$ (from expressions 2.6 and 2.7) as found through frequency sweep measurements is in agreement with the measured value of $\phi = 5.0 \pm 0.4$ (expression 2.3) through viscosity measurements.

The concentration scaling of PW TCSP shift factors were found to be different from those proposed by Baumgärtel and Willenbacher (1996) for polystyrene-ethylbenzene systems. The scaling exponent of b_c is -0.72 instead of -2.2 which implies a weaker dependence of the plateau modulus upon the concentration of polymer for the PW solutions as compared to ideal solutions. This can be understood as an effect of solvent quality. Water is a good solvent for PEO at around 25 °C as previously shown through second virial coefficient and radius of gyration measurements at 30 °C (Devanand and Selser, 1991) and a favorable Flory-Huggins interaction parameter, $\chi = 0.12$ ($= -w/RT$) at 30 °C in the range between 5 to 40 wt. % PEO (2290 g/mol) solution in water (Kjellander and Florin, 1981). As the polymer concentration increases, the solvent quality should tend toward theta conditions. Hence, the swollen PEO chains in good solvent will reduce in coil size with increasing polymer concentration. Thus, adding PEO will not lead to the expected increase in chain overlap, and hence, one expects to observe a weaker concentration dependence of the plateau modulus (and hence the vertical shift factor b_c) as given by equation 2.7. The higher than expected scaling exponent for the relaxation time (a_c) can be rationalized through an increase in molecular friction with increasing polymer concentration due to specific polymer-polymer segment interactions mitigated by hydrogen bonding. Indeed hydrogen-bonded clusters have been reported for similar

PEO water solutions (Hammouda *et al.*, 2002; Hammouda *et al.*, 2004; Ho *et al.*, 2003).

Normally in the case of polymers the relaxation time and the plateau modulus both increase simultaneously. Adding laponite to the base PW solutions increased the relaxation time and yet *decreased* the plateau modulus. This counter-intuitive observation is a consequence of the specifics of the PEO-laponite interactions. The concentration variable, $100L/(L+P)$ was observed to correlate the $TCSP_1$ shift factors over the different polymer and laponite concentrations. This variable is closely related to the parameter, Γ_t , used earlier to characterize the phase behavior of PWL system (Pozzo and Walker, 2004). Assuming, the specific adsorption surface area provided by the laponite discs for PEO adsorption to be $s \text{ m}^2/\text{g}$, Γ_t^{-1} is given as,

$$\Gamma_t^{-1} = \frac{sL}{100P} \frac{\text{m}^2}{\text{mg}} \quad (2.12)$$

where, P and L denote the *wt. %* of PEO and laponite in a PWL mixture. For small laponite concentrations, as is the case here, the two parameters are nearly proportional. Therefore the trend in the shift factors, a_{c1} and b_{c1} , with the relative laponite concentration variable, $100L/(L+P)$, can be understood simply in terms of the surface area provided by laponite per unit mass of PEO present.

The increase in the shift factor, b_{c1} with $100L/(L+P)$ reflects the corresponding reduction in the plateau modulus apparent in Figure 2.16. A decrease in the plateau modulus with the addition of laponite particles to the PW base solutions

suggests that PEO adsorbs to the laponite and is consumed from the bulk where it caused entanglements, thus reducing the entanglement density. However, some polymer bridging must also occur because there is a net increase in the longest relaxation time as characterized by a_{cl} (Table 2.7 and Figure 2.18). To confirm this proposition, the gel and the solution phases of two representative PWL mixtures, PWL5 and PWL6, were separated by centrifugation at 1200 rpm for 15 minutes and the concentration and quantity of both the phases was measured by thermogravimetric analysis (TGA) as shown in Figure 2.20. The gel phase contains a higher concentration of both PEO and laponite, which is consistent with the aforementioned hypothesis. The amount of PEO removed from the network to form gel particles is a relatively small, however, as the gel phase is only about a fifth of the sample. This suggests that the removal of PEO chains from the entanglement network by adsorption onto laponite leads to a relatively small effect on the rheology as observed. The presence of some bridging adsorbed PEO chains on laponite in the solution phase increases the dominant relaxation time (and hence a_{cl}) as seen in Table 2.7 and Figure 2.18. Thus, in terms of Pozzo and Walker (2004), both gel and sol phases formed with the amount of gel phase about 20 % of the entire material.

Figure 2.18 demonstrates that above the value $100L/(L+P)\approx 10$ the addition of laponite greatly increases the longest relaxation time (a_{cl}) for the polymer solution. It has been reported that ~ 1 wt. % PEO is capable of saturating the laponite surface by adsorption, in a 2 wt. % aqueous dispersion of laponite (Lal and Auvray, 2000; Lal and Auvray, 2001).

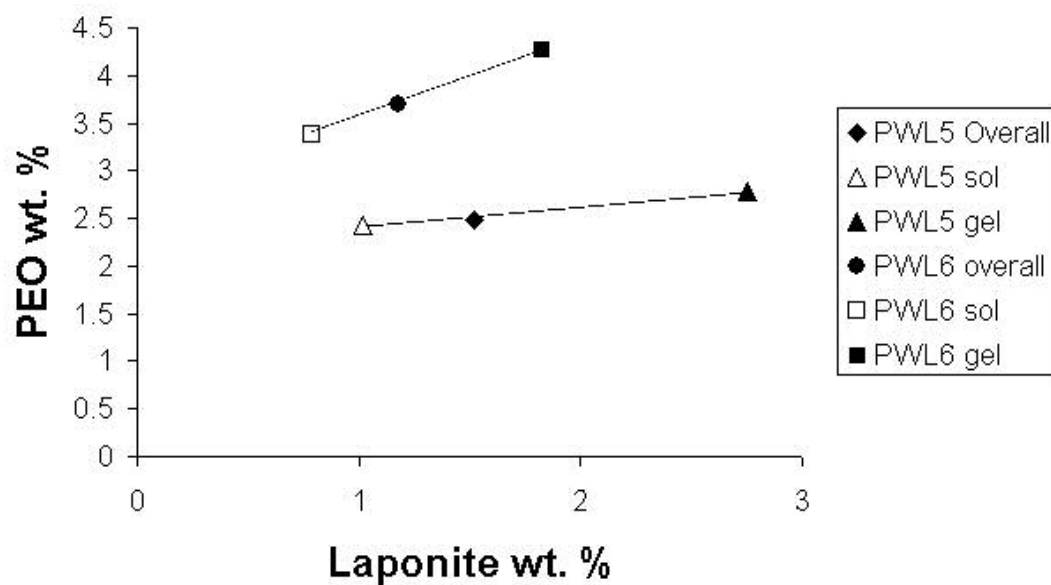


Figure 2.20: Phase split of PWL5 and PWL6 into solution and gel phases. Tie lines are shown connecting the composition of the overall mixtures and the two phases formed.

Therefore, laponite particles present in the PWL mixtures discussed in this work are expected to be saturated with adsorbed PEO. However, the likelihood of bridging relative to nonbridging polymer will depend upon the relative concentrations: *i.e.*, at low relative laponite concentrations there is less probability of a chain adsorbing to multiple laponite particles. Whereas, at higher laponite concentrations, polymer bridging is more likely and percolation of the bridge network is possible. Consequently, the change in behavior of the TCSPs with relative laponite concentration are interpreted to suggest changes in the structure of the adsorbed polymer layer and the likelihood of polymers contributing to bridges.

2.6 Conclusions

PEO-water solutions were observed to be thermorheologically simple in the concentrated solution regime over the temperature range of 4-32 °C. However, unlike previous measurements for nearly ideal chains in theta solvents, aqueous PEO solutions exhibit a weaker increase in plateau modulus and a stronger increase in relaxation time with increasing polymer concentration. The former is qualitatively understood as a consequence of the good solvent quality whereas the latter is attributed to specific hydrogen bonding interactions present in aqueous PEO solutions.

The addition of laponite to these solutions also yielded thermorheologically simple solutions (although ageing effects were observed), but with nontrivial concentration dependencies of the shift factors. Specifically, adding laponite was observed to decrease the plateau modulus while weakly increasing the relaxation time up to a critical relative concentration, whereupon the dominant

relaxation time was observed to diverge rapidly. This complex behavior is interpreted as a competition between PEO adsorption on laponite removing PEO from the entanglement network versus forming new bridging networks. Evidence of gel formation upon ageing within the solutions confirms this simple interpretation.

These results provide a practical framework for correlating rheological data on polymer-nanoparticle solutions and for predicting linear viscoelasticity of such solutions. They also illustrate the value in using a master curve analysis to derive microstructural insights from bulk rheological measurements.

REFERENCES

- Aranda P, Mosqueda Y, Perez-cappe E, Ruiz-hitzky, E (2003) Electrical characterization of poly(ethylene oxide)-clay nanocomposites prepared by microwave irradiation. *Journal of Polymer Science, Part B: Polymer Physics* 41(24): 3249-3263.
- Baumgärtel M and Willenbacher N (1996) The relaxation of concentrated polymer solutions. *Rheologica Acta* 35(2): 168-185.
- Casper CL, Stephens JS, Tassi NG, Chase DB and Rabolt JF (2004) Controlling surface morphology of electrospun polystyrene fibers: Effect of humidity and molecular weight in the electrospinning process. *Macromolecules* 37(2): 573-578.
- Devanand K and Selser JC (1991) Asymptotic-Behavior and Long-Range Interactions in Aqueous-Solutions of Poly(Ethylene Oxide). *Macromolecules* 24(22): 5943-5947.
- Dijkstra M, Hansen JP and Madden PA (1995) Gelation of a clay colloid suspension. *Physical Review Letters* 75(11): 2236-2239.
- Doeff MM and Reed JS (1998) Li ion conductors based on laponite/poly(ethylene oxide) composites. *Solid State Ionics* 115: 109-115.
- Drew C, Wang X, Samuelson LA and J. K (2003) The effect of viscosity and filler on electrospun fiber morphology. *Journal of macromolecular science* A40(12): 1415-1422.
- Feller JF, Bruzaud S and Grohens Y (2004) Influence of clay nanofiller on electrical and rheological properties of conductive polymer composite. *Materials Letters* 58(5): 739-745.
- Ferry JD, *Viscoelastic properties of polymers* 3 rd., John Wiley & Sons (1980): 641 pp.
- Fong H, Chun I and Reneker DH (1999) Beaded nanofibers formed during electrospinning. *Polymer* 40(16): 4585-4592.

- Greenblatt GD, Hughes L and Whitman DW (2004) Polymer-clay nanocomposite for extended release of active ingredient. Eur. Pat. Appl, EP 1470823, 13 pp.
- Hammouda B, Ho D and Kline S (2002) SANS from poly(ethylene oxide)/water systems. *Macromolecules* 35(22): 8578-8585.
- Hammouda B, Ho DL and Kline S (2004) Insight into clustering in poly(ethylene oxide) solutions. *Macromolecules* 37(18): 6932-6937.
- Hancock BC and Zografi G (1994) The relationship between the glass-transition temperature and the water-content of amorphous pharmaceutical solids. *Pharmaceutical Research* 11(4): 471-477.
- Ho DL, Hammouda B and Kline SR (2003) Clustering of poly(ethylene oxide) in water revisited. *Journal of Polymer Science Part B-Polymer Physics* 41(1): 135-138.
- Huang Z-M, Zhang Y-Z and Kotaki M (2003) A review on polymer nanofibers by electrospinning and their applications in nanocomposites. *Composites Science and Technology* 63(15): 2223-2253.
- Jayaraman K, Kotaki M, Zhang YZ, Mo XM and Ramakrishna S (2004) Recent advances in polymer nanofibers. *Journal of Nanoscience and Nanotechnology* 4(1-2): 52-65.
- Kjellander R and Florin E (1981) Water-Structure and Changes in Thermal-Stability of the System Poly(Ethylene Oxide)-Water. *Journal of the Chemical Society-Faraday Transactions I* 77: 2053-2077.
- Krikorian V, Casper C, Rabolt J and Pochan D (2004) Electrospinning of nanocomposite fibers based on poly(L-lactic acid) and organoclays. *Polymeric Materials Science and Engineering* 90(51).
- Lal J and Auvray L (2000) Interaction of polymer with clays. *Journal of Applied Crystallography* 3(3, Pt. 1): 673-676.
- Lal J and Auvray L (2001) Interaction of polymer with discotic clay particles. *Molecular Crystals and Liquid Crystals* 356: 503-515.
- Mackay ME, Dao TT, Tuteja A, Ho DL, Van Horn B, Kim HC and Hawker CJ (2003) Nanoscale effects leading to non-Einstein-like decrease in viscosity. *Nature Materials* 2(11): 762-766.

- Majumdar DB, Thomas N.; Schwark, Dwight W. (2003) Clay-polymer nanocomposite coatings for imaging application. *Applied Clay Science* 23(5-6): 265-273.
- McKee MG, Wilkes GL, Colby RH and Long TE (2004) Correlations of solution rheology with electrospun fiber formation of linear and branched polyesters. *Macromolecules* 37(5): 1760-1767.
- Megelski S, Stephens JS, Chase DB and Rabolt JF (2002) Micro- and nanostructured surface morphology on electrospun polymer fibers. *Macromolecules* 35(22): 8456-8466.
- Mongondry P, Nicolai T and Tassin JF (2004) Influence of pyrophosphate or polyethylene oxide on the aggregation and gelation of aqueous laponite dispersions. *Journal of Colloid and Interface Science* 275(1): 191-196.
- Nelson A and Cosgrove T (2004) A small-angle neutron scattering study of adsorbed poly(ethylene oxide) on laponite. *Langmuir* 20(6): 2298-2304.
- Pozzo DC and Walker LM (2004) Reversible shear gelation of polymer-clay dispersions. *Colloids and Surfaces a-Physicochemical and Engineering Aspects* 240(1-3): 187-198.
- Sardinha H and Bhatia SR (2002a). Controlling gel formation in clay dispersions via water-soluble polymer: viscoelasticity and kinetics of gel formation. Submitted to RheoFuture Thermo Haake Young Scientists Award 2002
- Sardinha H and Bhatia SR (2002b) Kinetics of gel formation in polymer-clay dispersions. *Abstracts of Papers of the American Chemical Society* 224: U526-U526.
- Schausberger A and Ahrer IV (1995) On the time-concentration superposition of the linear viscoelastic properties of plasticized polystyrene melts using the free-volume concept. *Macromolecular Chemistry and Physics* 196(7): 2161-2172.
- Schmidt G, Nakatani AI, Butler PD, Karim A and Han CC (2000) Shear orientation of viscoelastic polymer-clay solutions probed by flow birefringence and SANS. *Macromolecules* 33(20): 7219-7222.
- Schmidt G, Nakatani AI and Han CC (2002) Rheology and flow-birefringence from viscoelastic polymer-clay solutions. *Rheologica Acta* 41(1-2): 45-54.

- Sengupta AK, Spindler R, Darlington JW and (Amcol International Corporation U (2002) Multifunctional particulate additive for personal care and cosmetic compositions. PCT Int. Appl., WO 2002062310, 74 pp.
- Smith DN, Goodman H, Buse WR and (ECC International Ltd. U (1989) Thixotropic composition containing smectite clays for personal care products, EP 1989-301065, 5 pp.
- Theng BKG (1970) Interactions of Clay Minerals with Organic Polymers - Some Practical Applications. Clays and Clay Minerals 18(6): 357-&.
- Trappe V and Weitz DA (2000) Scaling of the viscoelasticity of weakly attractive particles. Physical Review Letters 85(2): 449-452.
- van Olphen H, An introduction to clay colloid chemistry, Wiley, New York (1977):
Welty JR, Wicks CE and Wilson RE, Fundamentals of Momentum, Heat and Mass Transfer 3rd ed., Wiley, New York (1984): 772-773
- Willenbacher N (1996) Unusual thixotropic properties of aqueous dispersions of Laponite RD. Journal of Colloid and Interface Science 182(2): 501-510.
- Winter HH and Mours M (2004) <http://rheology.tripod.com/>
- Wong D (2004) Novel pharmaceutical formulations containing polymer clay composites. U.S. Pat. Appl. Publ., US 20044101559, May 27, 2004, USA: 4pp.
- Zebrowski J, Prasad V, Zhang W, Walker LM and Weitz DA (2003) Shake-gels: shear-induced gelation of laponite-PEO mixtures. Colloids and Surfaces a-Physicochemical and Engineering Aspects 213(2-3): 189-197.

Chapter 3

ELECTROSPINNING OF NEAT AND LAPONITE FILLED AQUEOUS POLY(ETHYLENE OXIDE) SOLUTIONS

3.1 Introduction

Electrospinning has received significant research interest because it is a fast, direct and simple method to produce polymeric nanofibers (Buer *et al.*, 2001; Hohman *et al.*, 2001a; Hohman *et al.*, 2001b; Huang *et al.*, 2003; Jayaraman *et al.*, 2004; Reneker, 2003) of which a variety of potential novel applications are emerging (Caruso *et al.*, 2001; Doshi and Reneker, 1995; Guan *et al.*, 2004; Jia *et al.*, 2002; Kataphinan *et al.*, 2003; Khil *et al.*, 2005; Krauthauser *et al.*, 2003; Shields *et al.*, 2004; Viswanathamurthi *et al.*, 2004; Zhang *et al.*, 2005). Electrospinning results in nonwoven, porous mats of fibers of diameter of a few nanometers to a few micrometers. The fiber morphology depends on the rheological and electrical properties of the solutions being spun and the operating conditions as was shown earlier for several polymer solutions (Casper *et al.*, 2004; Deitzel *et al.*, 2001a; Deitzel *et al.*, 2001b; Fridrikh *et al.*, 2003; Megelski *et al.*, 2002).

In electrospinning, an applied electric field pulls a polymer solution into a jet. The jet becomes unstable by “whipping” (Deitzel *et al.*, 2001a; Hohman *et al.*, 2001b; Shin *et al.*, 2001a; Shin *et al.*, 2001b; Yarin *et al.*, 2001) and “splaying” (Deitzel *et al.*, 2001a; Yarin *et al.*, 2001). In addition, a capillary instability can lead to the formation of beads for less viscous spinning solutions (Fong *et al.*, 1999). A

varicose instability has also been shown to produce beaded fibers (Fong *et al.*, 1999a; Hohman *et al.*, 2001a; Hohman *et al.*, 2001b). The electrospun jet dries rapidly but may reach the collector in a partially or completely dried state depending upon the volatility of the solvent used, which can lead to coalescence of fibers to produce a mechanically connected, nonwoven mat.

Successful electrospinning occurs in an identifiable range of electrical and rheological properties of the polymer solution or melt (Hohman *et al.*, 2001b; Shin *et al.*, 2001a) and processing conditions. Firstly, the material must be electroactive so that electric field, the primary driving force for jet formation, can act on the polymer solution. Secondly, the material's viscoelasticity must be sufficient such that fibers can be drawn without breaking up into droplets (*i.e.*, electrospaying) (Shenoy *et al.*, 2005). There is significant interest in quantifying the relationships connecting the resultant fiber mat properties, such as fiber diameter and morphology, to the solution's rheology, electrical properties, surface tension and the process variables such as spinning voltage and the working distance (*i.e.* the distance of the needle tip from the collector). For example, McKee *et al.* (2004) correlate the final diameter of polyester fibers and the spinning solution's zero-shear viscosity, $D = 13000(\eta_0)^{0.8}$ where D is expressed in *nm* and η_0 is in *Pa.s*. It is unknown, however, if such correlations hold for other polymer-solvent systems, or whether the shear viscosity is sufficient to truly correlate final fiber diameter.

Recently, there has also been interest in incorporating nanoparticles into the electrospun fiber matrix in order to enhance or impart some desired properties to

the fiber, to obtain a one dimensional array of nanoparticles, or to obtain a high surface area of nanoparticles within the fiber matrix (Drew *et al.*, 2003; Krikorian *et al.*, 2004; Salalha *et al.*, 2004; Ye *et al.*, 2004). Electrospinning investigations of aqueous poly(ethylene oxide) (PEO) solutions by Drew *et al.* (Drew *et al.*, 2003) suggest that the addition of titanium oxide particles also enables electrospinning at lower polymer concentrations than normally possible. Particle addition leads to similar fiber diameters when the spinning solutions have comparable shear viscosities. Here again, whether this observation is general and whether similar quantitative relationships hold between fiber morphology and size and spinning solution properties in the presence of nanoparticles has not been established.

In Chapter 2, it was demonstrated for a model system of laponite (a synthetic nanoclay) dispersed in aqueous poly(ethylene oxide) (PEO) solutions that over a range of concentrations relevant for electrospinning, the linear viscoelasticity of neat and laponite-filled aqueous PEO solutions can be superimposed in the form of a master rheological curve (Figure 2.20). Thus it was shown that these aqueous neat and laponite filled PEO-water solutions constitute a model system of rheologically similar fluids.

The goals of the work reported here are to determine if the correlation between zero shear viscosity and electrospun fiber diameter and morphology also holds for an aqueous polymer solution, and whether this can be extended to the electrospinning of solutions containing dispersed nanoparticles. In contrast to the polyester solutions examined by McKee *et al.* (2004), here we study model,

viscoelastic, aqueous solutions of PEO (Devanand and Selser, 1991; Hammouda *et al.*, 2002; Hammouda *et al.*, 2004; Ho *et al.*, 2003). In addition, the solvent used here (water) is less volatile than the 70/30 w/w mixture of chloroform/dimethyl formamide used by McKee *et al.* (2004), which may also be a factor in setting fiber morphology. Finally, we exploit the established rheological simplicity of the model system of aqueous PEO-laponite (Chapter 2) to examine the influence of the addition of nanoclay on the electrospun fiber properties.

The five PW base solutions, namely, PW3, PW5, PW8, PW10 and PW12 (Table 2.1), and all the PWL mixtures (Table 2.5) for which the rheology was shown in Chapter 2 were sheared and electrospun at room temperature within 1 to 2 days after preparation. Thus, the differences in the electrospun fiber morphology can be understood as a consequence of difference in the composition and not due to sample ageing.

3.2 Results

SEM micrographs of fibers formed from the electrospun PW and PWL solutions are shown in Figure 3.1. Although only one representative micrograph is shown here for fibers formed from PWL solutions, multiple micrographs were imaged and are included separately as Appendix 3.1 at the end of this chapter. Solution PW3, with a PEO concentration slightly below the transition to the concentrated regime (c^{**}) (as shown in Figure 2.6), exhibited bead formation along the axis of the fibers. The addition of laponite reduced beading, in qualitative agreement with the observations of Drew *et al.* (2003). All other samples were in the concentrated regime

and formed fibers without beading. Laponite addition at higher polymer concentration leads to a broader distribution in fiber diameters.

The average diameter of the PW and PWL electrospun fibers and the zero shear viscosity (Chapter 2) of the spun solutions are shown in Table 3.1. Figure 3.2 shows that the average diameter of PEO fibers correlates well with the zero shear viscosity as,

$$D (nm) = (126.7 \pm 5.7) \eta_0^{(0.164 \pm 0.022)}$$

where, η_0 is in *Pa.s*. Although this result is qualitatively similar to a previous report for polyester solutions by McKee *et al.* (McKee *et al.*, 2004), the power law dependence of fiber diameter on viscosity is much weaker. The former correlation (for polyester fibers) is also shown in Figure 3.2 for comparison, demonstrating that such correlations are not transferable across materials and electrospinning parameters.

The average (number) diameter of the PWL electrospun fibers *vs.* their zero-shear viscosities (Chapter 2) are plotted in Figure 3.3 along with the standard deviation. Large variations in the measured fiber diameters are evident for the laponite containing systems. As Figure 3.3 shows, the average fiber diameter for the PWL solutions are generally higher than PW solutions with similar viscosities, and the diameters for the laponite containing systems do not correlate with the zero shear viscosities.

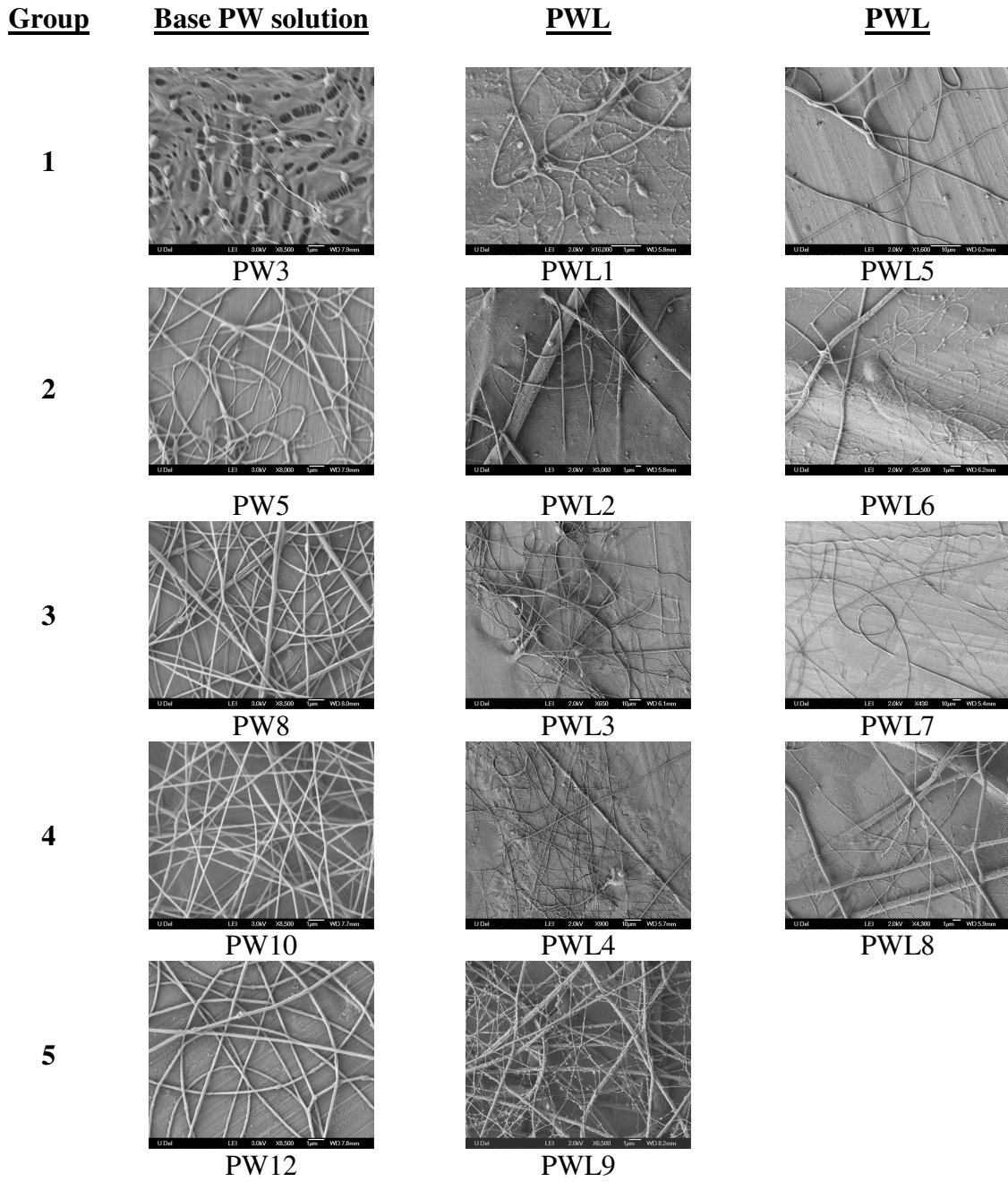


Figure 3.1: SEM micrographs of neat and laponite containing aqueous poly(ethylene oxide) solutions.

Table 3.1: Diameter and viscosity of neat and laponite-filled poly(ethylene oxide) fibers.

| Solution | Zero shear Viscosity [<i>Pa.s</i>] | Average Diameter [<i>nm</i>] | Standard deviation in diameter [<i>nm</i>] |
|----------|---|-----------------------------------|--|
| PW3 | 0.18 | 84 | 24 |
| PW5 | 0.91 | 133 | 32 |
| PW8 | 2.65 | 153 | 24 |
| PW10 | 6.44 | 178 | 52 |
| PW12 | 15.6 | 191 | 28 |
| PWL1 | 0.86 | 116 | 151 |
| PWL2 | 1.9 | 800 | 720 |
| PWL3 | 3.0 | 680 | 495 |
| PWL4 | 7.4 | 375 | 284 |
| PWL5 | 4.5 | 432 | 503 |
| PWL6 | 4.5 | 519 | 488 |
| PWL7 | 5.7 | 1166 | 621 |
| PWL8 | 10.0 | 168 | 273 |
| PWL9 | 17.5 | 144 | 140 |

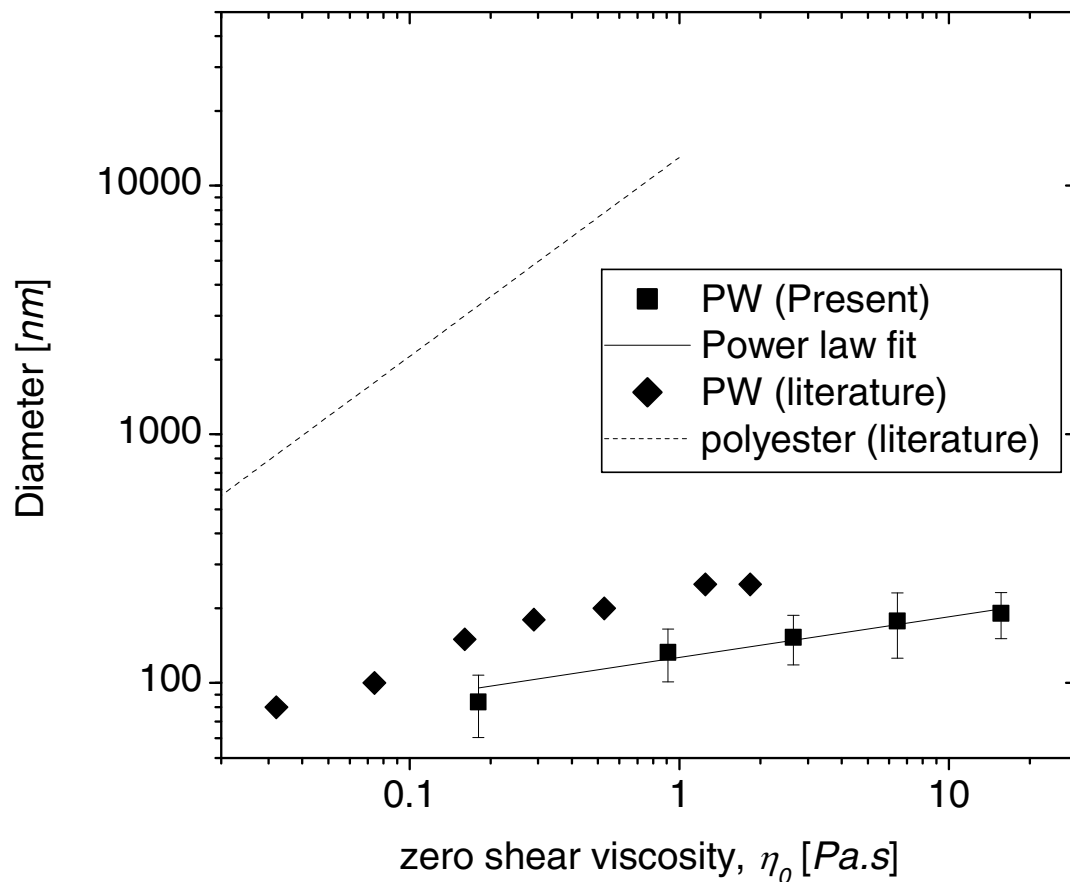


Figure 3.2: Dependence of the diameter of electrospun fibers of neat polymer solutions with the zero shear viscosity of the spun solutions: (-■-) PW solutions (present work) with electric field, $E=1.54$ kV/cm (◆) PW solutions at $E=0.7$ kV/cm (Fong *et al.*, 1999a), (- - -) the diameter correlation obtained for polyesters at $E=0.75$ kV/cm (McKee *et al.*, 2004).

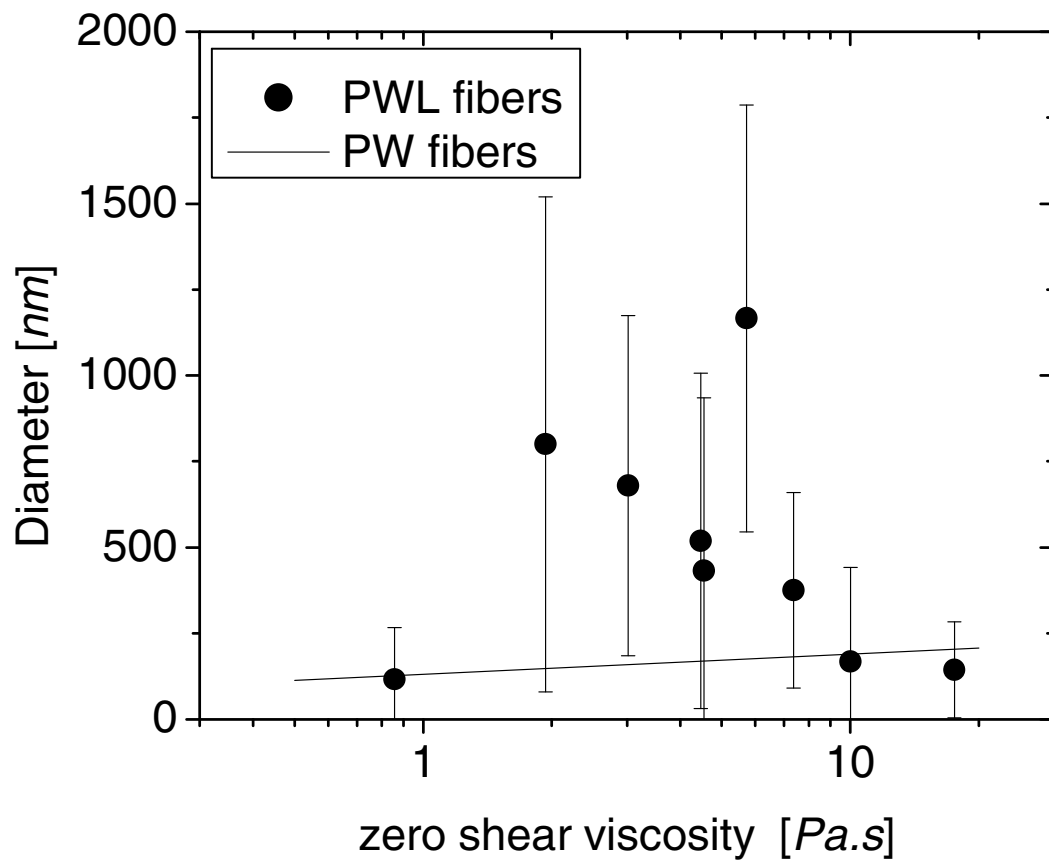


Figure 3.3: Diameter of electrospun fibers of laponite-filled aqueous poly(ethylene oxide) solutions compared to that for PW solutions.

Normalized cumulative diameter frequencies have been plotted in Figures 3.4 and 3.5. Figure 3.4 shows the data for mixtures belonging to groups 1 and 3 and Figure 3.5 shows the same for groups 2, 4 and 5. In all cases, as laponite was added or increased, the zero shear viscosity in these groups increased (Chapter 2). However, the change in the distribution of diameter was different in groups 1 and 3 from groups 2, 4 and 5. In the case of groups 1 and 3, as the laponite content increased, the distribution shifted towards larger diameter values *i.e.* almost all the fibers formed had a larger diameter than the sample(s) in the same group having lesser laponite content. This is consistent with the observation that the fiber diameter increases with the zero shear viscosity of the spinning solution. However, in the case of groups 2, 4 and 5, increasing the laponite concentration results in the formation of fibers with both greater and smaller diameters than the corresponding PW solutions. For example, PWL2 and PWL6 belong to group 2 with PWL6 containing a higher laponite content and yet a majority of fibers formed are of lesser diameters than that formed from PWL2, despite the increasing spinning solution viscosity with laponite addition. Similarly, for group 4, the addition of laponite results in many fibers smaller than those observed in the corresponding PW solutions.

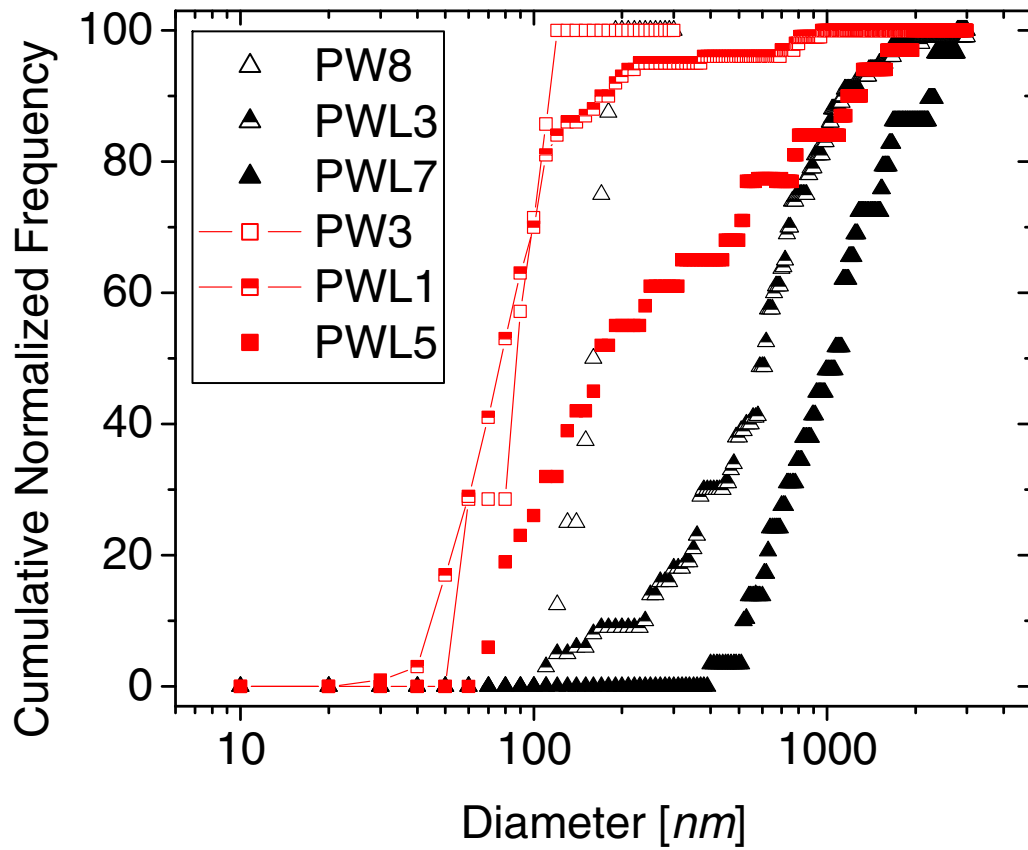


Figure 3.4: Diameter distribution of electrospun fibers belonging to groups 1 and 3 (The line+symbol representation of PW3 and PWL1 is to indicate the formation of beads on their electrospun fibers.).

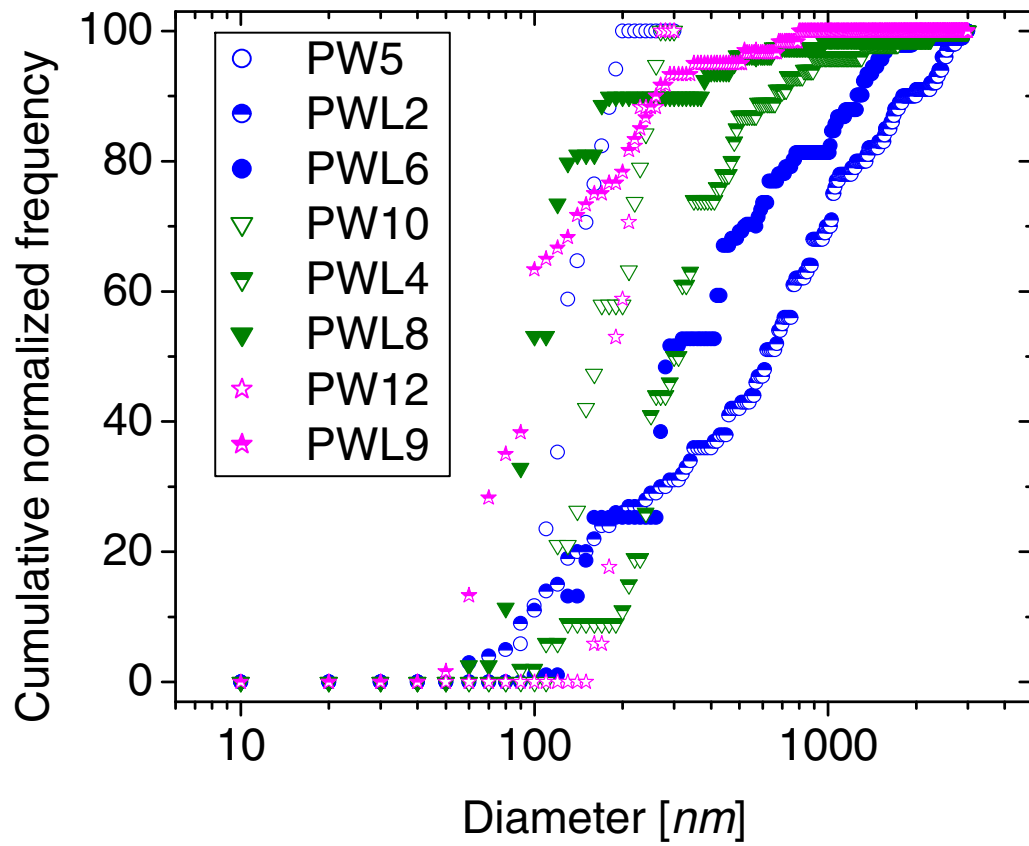


Figure 3.5: Diameter distribution of electrospun fibers belonging to groups 2, 4 and 5.

3.3. Discussion

It has been shown that for a given polymer-solvent pair regardless of their very different properties (PW solution vs. polyester solutions of McKee *et al.* (2004)) the diameter of electrospun fibers correlates with the zero shear viscosity as shown by the power law relations in Figure 3.2. Figure 3.2 also compares the electrospun fiber diameters for neat PEO fibers vs. spinning solution zero shear viscosity at two different electric fields ($E=0.7$ kV/cm for Fong *et al.* (Fong *et al.*, 1999b) versus 1.54 kV/cm (present work)) to the polyester fibers spun by McKee *et al.* (2004). As seen, at fixed solution viscosity, the diameter of the polyester fibers spun at $E=0.75$ kV/cm are significantly larger than those spun from PEO at comparable field strength. Further, comparing the PEO fibers spun from solutions with the same viscosity shows a dependence on electric field strength. These results show that fiber diameter is not simply a function of spinning solution zero shear viscosity.

Consequently, although shear viscosity can be correlated to electrospinning performance for a single spinning solution containing only polymer, other solution properties and processing conditions, such as dielectric constant, surface tension, extensional properties, and solvent volatility may have a significant impact on final fiber size and fiber size distributions. Helgeson and Wagner (2005) demonstrate a universal correlation between two parameters derived from dimensional analysis of electrospinning

$$\text{Bh} = \frac{2\bar{\epsilon}^2\Phi_0^2}{K\eta_0L^2} \quad \text{Oh} = \frac{\eta_0}{(\rho\gamma R)^{1/2}}$$

where Bh is a ratio of electrostatic and electroviscous stresses, and Oh, the Ohnesorge number, relates viscous to inertial and surface forces. The Ohnesorge number has been shown (Lopez-Herrera and Ganan-Calvo, 2004) to govern capillary stability in free surface flows of electrified jets. These two dimensionless groups depend on the dielectric permittivity of air ($\bar{\epsilon}=8.85 \times 10^{-12} \text{ C}^2/\text{N}\cdot\text{m}$), the applied voltage (Φ_0), the collector to tip distance (L), and the bead-free fiber diameter (R), as well as the spinning solution's conductivity (K), density (ρ), zero-shear viscosity (η_0), and surface tension (γ). Upon reducing electrospinning data for neat polymer-solvent systems from multiple sources using the dimensionless groups, an inverse correlation between Oh and Bh was observed by Helgeson and Wagner, such that $\text{Oh} \sim 1/\text{Bh}$, suggesting that the fiber size does not depend on the zero-shear viscosity to a first order approximation. Additionally, deviations from this scaling at low Oh can be explained in terms of capillary breakup of the electrospinning jet resulting in beaded fibers (Helgeson and Wagner, 2005). Calculations of Bh and Oh for the neat PEO fibers presented here and the results presented by McKee *et al.* (2004) and Fong *et al.* (1999) are shown in Figure 3.6. The agreement between the three data sets when represented in this dimensionless form is very good even though the systems were spun in different laboratories with significant variations in PEO concentrations and spinning conditions. This analysis also demonstrates that shear viscosity is not a primary variable for correlating final fiber diameter.

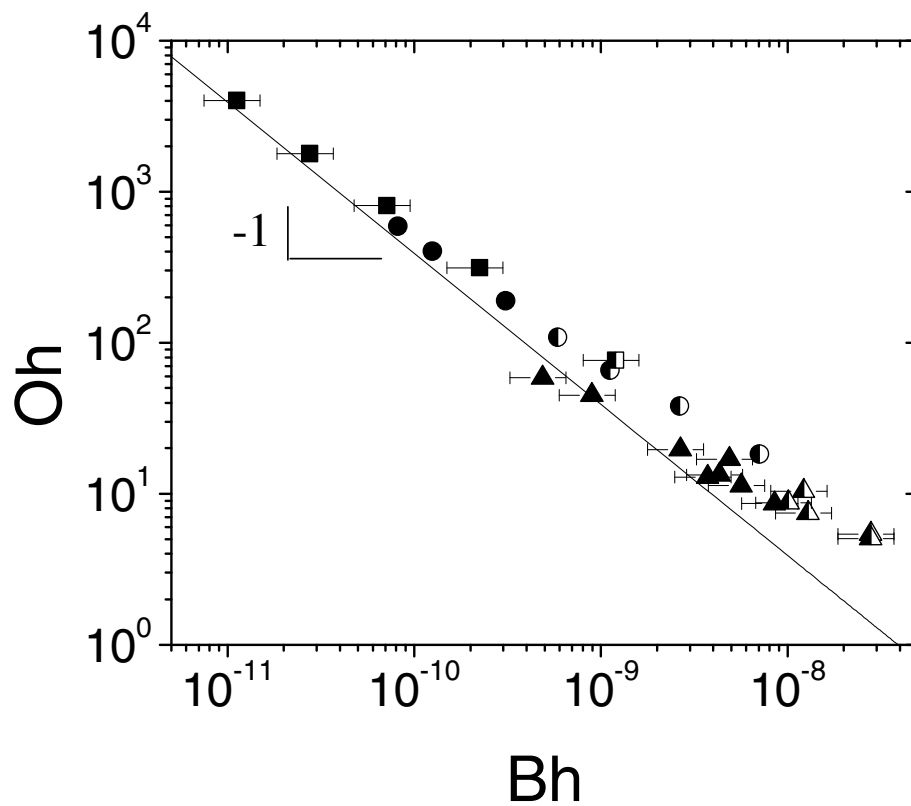


Figure 3.6: Correlation of electrospinning data using dimensional analysis (Helgeson and Wagner, 2005) for neat PEO solutions presented in this (■) and other work (Fong *et al.*, 1999) (●), and for fibers spun from polyester solutions¹ (▲). Half-filled points represent fibers in which significant beading was reported.

If shear viscosity is not directly relevant in determining the final fiber diameter, the question remains as to why an apparent correlation can be obtained over limited and specific experimental results. As jet formation in electrospinning is primarily an elongational flow, the fiber diameter may be more fundamentally related to the elongational viscosity. For aqueous PEO solutions comparable to those explored here, it is known that the Trouton ratio, which is the ratio of elongational to shear viscosities, remains almost constant for solutions of 1 to 2 wt % PEO of $\sim 1 \times 10^6$ g/mol at elongational rates of 10^2 s⁻¹ or less (Gauri and Koelling, 1997), which is in the range of elongational rates imposed on the jet during electrospinning (Feng, 2003). Thus, correlations with zero shear viscosity may simply reflect an underlying correlation with elongational viscosity as the Trouton ratio is nearly constant.

Shenoy *et al.* (2005) review the concept that there is a transition from polymer beads to continuous fibers upon reaching a sufficient polymer chain entanglement density. However, as shown here, once this entanglement density has been reached and there is sufficient viscoelasticity and/or elongational viscosity to prevent bead formation, the final fiber diameter is nearly independent of the spinning solution's viscosity. As seen in Chapter 2, the PEO solutions studied here and by others were well above the critical entanglement concentration and exhibited measurable viscoelasticity. This might help explain the significantly stronger dependence on viscosity reported for the polyester system by McKee *et al.* (2004), as their solutions were viscous, but Newtonian and without measurable viscoelasticity. It is plausible that the dependence of fiber size on solution viscosity reported by McKee *et al.* (2004) is a consequence of sensitivity to another solution property, such as

surface tension and/or electrical conductivity, which varies systematically along with solution viscosity. This has been the subject of further investigation (Helgeson and Wagner).

Turning to the main topic of the effects of added nanoparticles on the fiber morphology and electrospinning process, the study by Drew *et al.* (2003) of the effects of added TiO₂ particles on the properties of electrospun PEO fibers (Mw = 3x10⁵ g/mol) concluded that particle addition to the spinning solution in order to build viscosity was effective in producing electrospun fibers. Further, they report that above a minimum concentration, the presence of particles no longer affects fiber diameter. These conclusions are not supported by the work reported here on aqueous PEO-laponite solutions, suggesting that particle addition has influences on the solution's electrical properties and surface tension that are more significant than effects on the shear viscosity. As discussed in Chapter 2 and shown in Figure 2.14, the addition of laponite builds viscosity through polymer adsorption and bridging. The interactions of PEO and laponite in water are rich and, in different compositions, lead to a variety of highly nonlinear materials (Feller *et al.*, 2004; Pozzo and Walker, 2004; Zebrowski *et al.*, 2003), which can also exhibit significant strain hardening. Model calculations (Feng, 2003) demonstrate that strain hardening leads to thicker fibers. Thus, the addition of dispersed nanoparticles may significantly affect the elongational viscosity, and hence, the fiber diameters, and the effect will be specific to details of the polymer-particle interactions. Further exploration of this requires accurate, reliable measurements of the transient elongational viscosities at rates comparable to those observed during electrospinning.

Note that addition of nanoclay particles to a PEO solution leads to a significant broadening in the fiber size distribution. A key factor in rationalizing some of the differences between the two studies may be the state of dispersion of the nanoparticles in the PEO solutions. In particular, Drew *et al.* (2003) report significant beading in the presence of the TiO₂ particles, which they attribute to particle aggregation in the spinning solution. The dimensional analysis in Fig. 8 shows that the results of Drew *et al.* (2003) were for solutions at low Ohnesorge number, such that beading may have been due to capillary breakup rather than particle aggregation. The particles used by Drew *et al.* (2003) were 21 nm in diameter, which compare well in size with the disc-shaped laponite particles, which are 30 nm in diameter and 1-5 nm in thickness. Here, however, the nanoclay dispersions are well dispersed and do not show evidence of aggregation in fibers or significant bead formation. Further, the laponite-PEO solutions exhibit sufficient viscoelasticity, and sufficiently high Ohnesorge number, to avoid beading.

There are additional factors that might contribute to the increase in standard deviation in fiber diameter for the solutions containing nanoclay. A large degree of splaying (Deitzel *et al.*, 2001b, Yarin *et al.* 2001) is evident in the SEM micrographs of electrospun PWL solutions an example of which is shown in Figure 3.7. The addition of nanoclay (which is charged) and its counterions (Willenbacher *et al.*, 1997) increases the surface charge density of the solution, which is known to result in splaying through electrohydrodynamic instabilities that are alleviated by lowering the surface charge density through surface generation (Deitzel *et al.*, 2001a).

In conclusion, we observe a weak increase of fiber diameter with the spinning solution's zero shear viscosity for concentrated PEO-water solutions, but view this as an artifact of more a more fundamental dependence of the electrospun fiber morphology on the spinning solutions elongational viscosity and electrical properties. Comparison to the literature (McKee *et al.*, 2004) shows that such simplistic correlations with viscosity are at best, specific to the polymer solution. Rather, a dimensionless scaling proposed by Helgeson and Wagner is shown to provide a unifying description of the results for neat spinning solutions. Further, we find that although the addition of dispersed, model nanoclay particles to model PEO-water solutions leads to solutions with comparable linear viscoelastic properties (Chapter 2), the fibers formed show much broader distributions in diameter than expected based on the spinning solution's zero shear viscosity. Splaying is evident for the nanoclay containing solutions, which is attributed to the increase in charge density due to the nanoclay and associated counterions. Comparison to reports in the literature suggests that good particle dispersion and stability in solutions are important in producing fibers without beading. The nontrivial consequences of nanoparticle addition on fiber stability and final morphology warrant further investigation in order to control composite fiber mat formation by electrospinning.

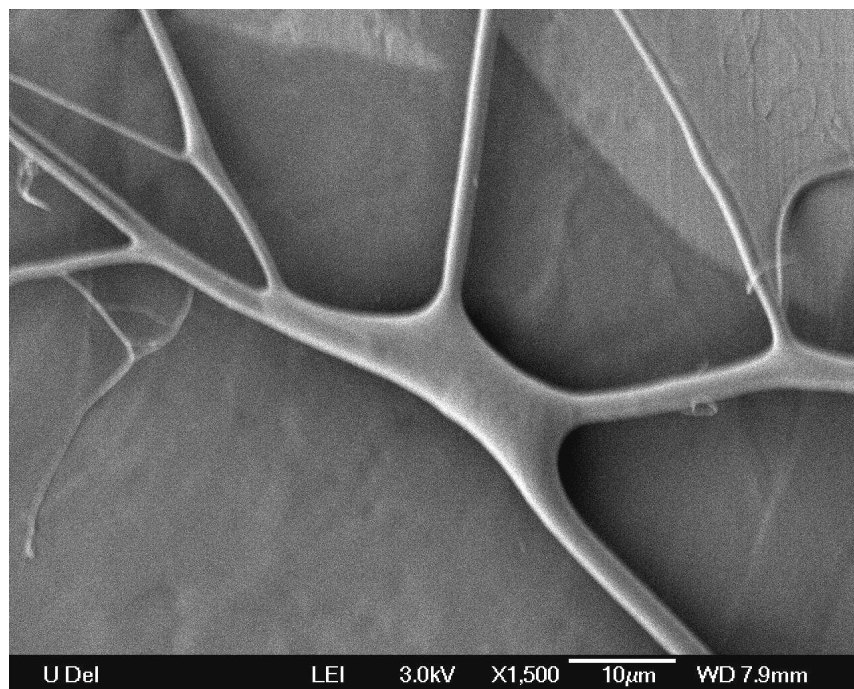


Figure 3.7: Evidence of splaying for the case of PWL6 fibers.

APPENDIX 3.1

PWL fibers showed a large dispersity in diameter and therefore several SEM micrographs as shown in Figures 3.8 to 3.14 were imaged of which the ones shown in Figure 3.1 are representatives. Since PWL7 and PWL9 showed little spread in the fiber size, only one image was taken as already shown in Figure 3.1.

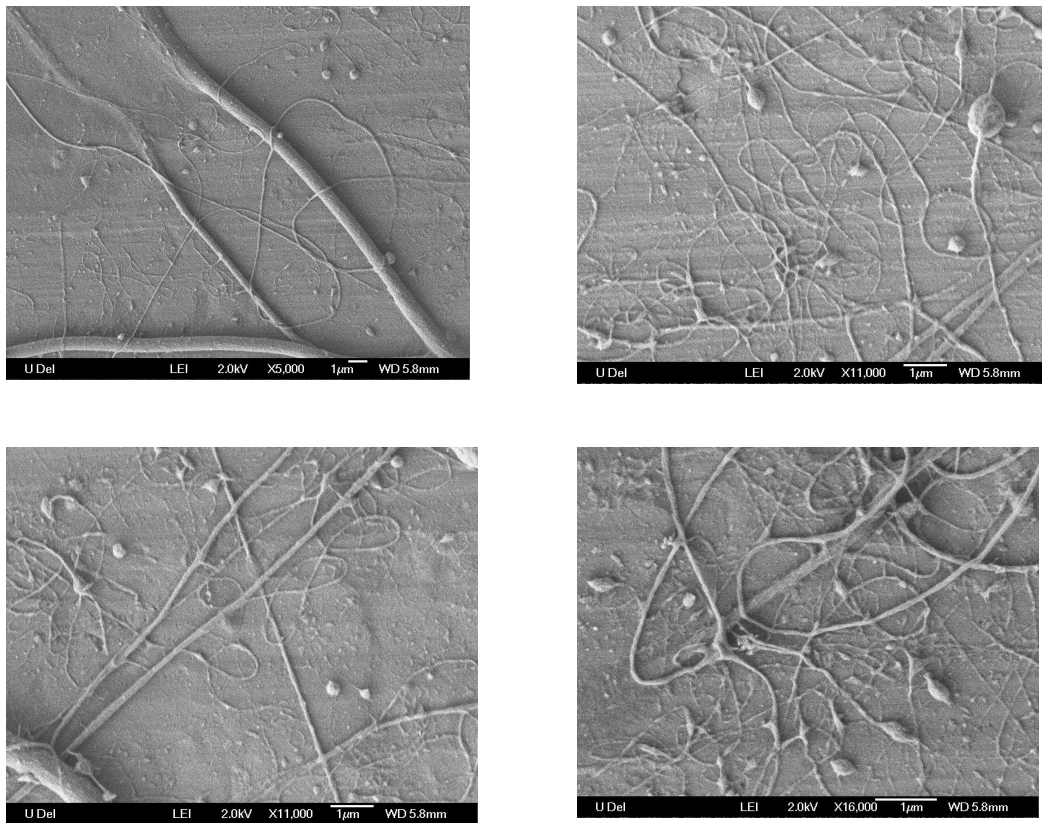


Figure 3.8: All SEM images of PWL1 fibers.

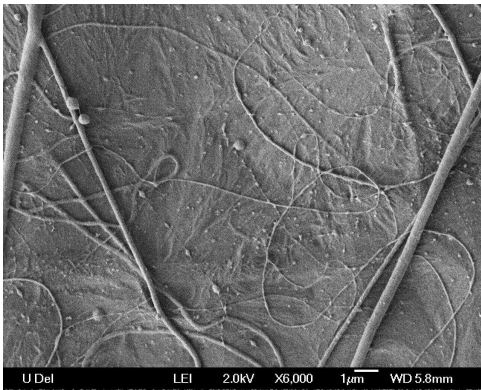
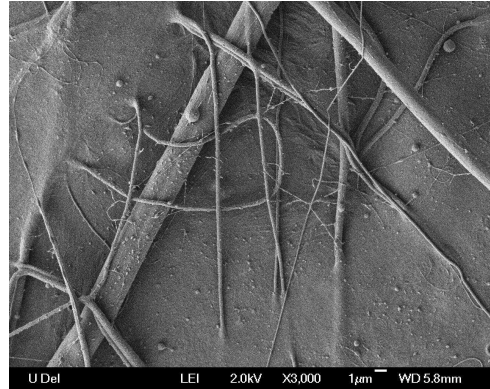
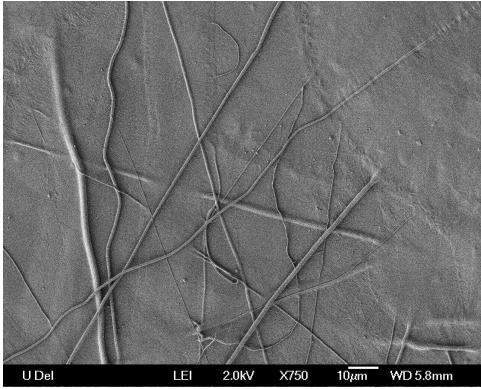


Figure 3.9: All SEM images of PWL2 fibers.

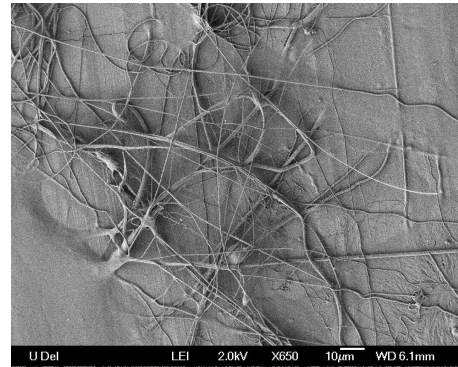
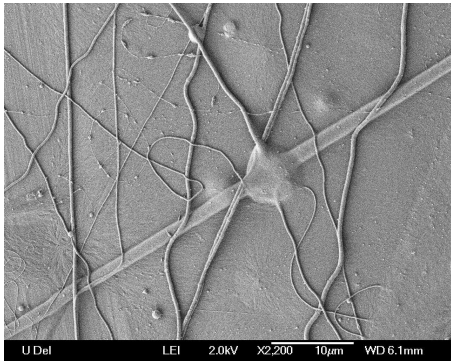


Figure 3.10: All SEM images of PWL3 fibers.

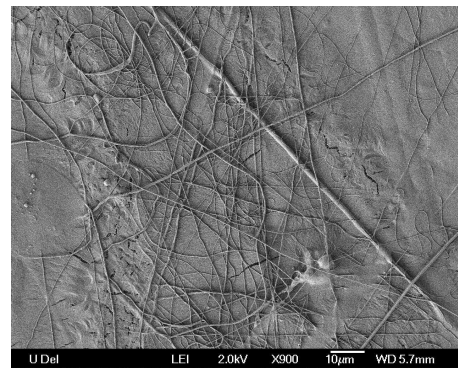
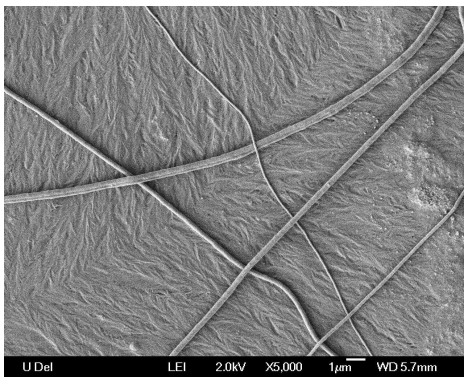


Figure 3.11: All SEM images of PWL4 fibers.

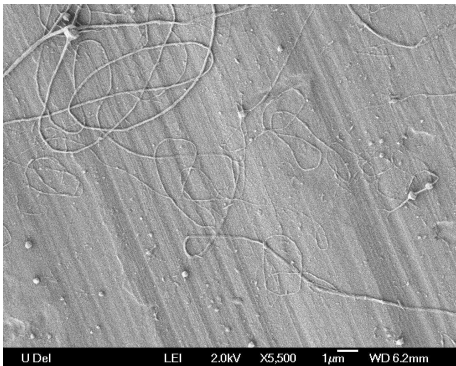
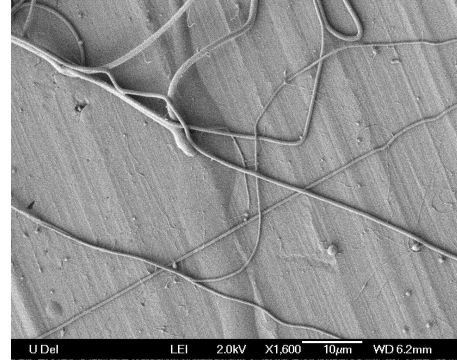
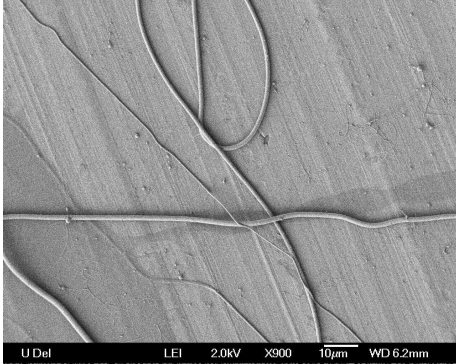


Figure 3.12: All SEM images of PWL5 fibers.

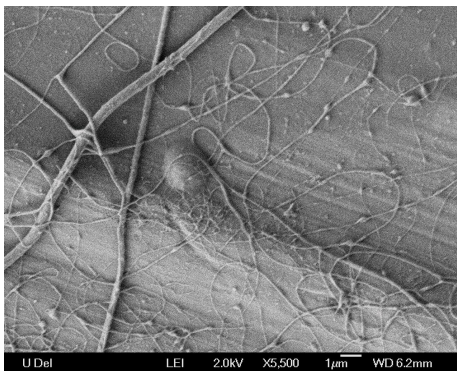
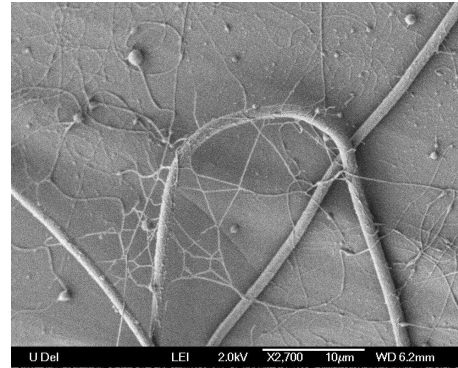
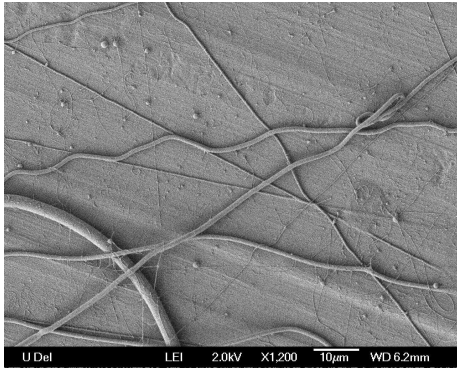


Figure 3.13: All SEM images of PWL6 fibers.

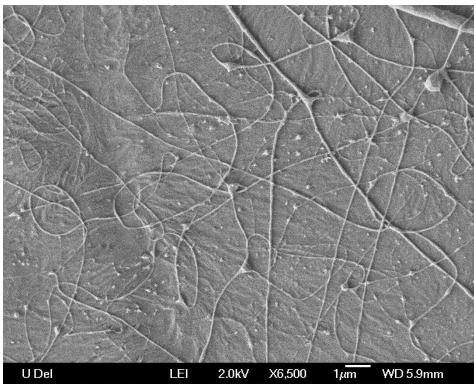
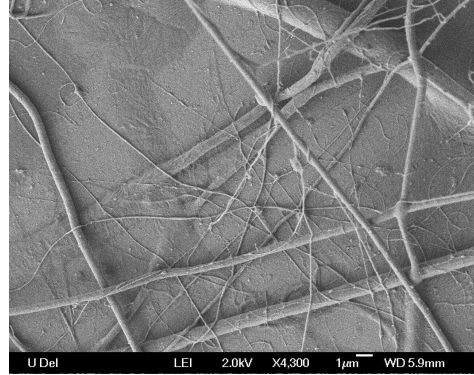
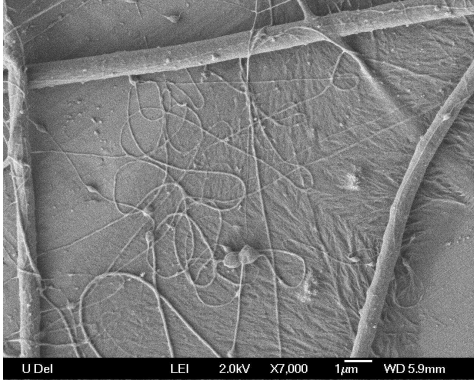


Figure 3.14: All SEM images of PWL8 fibers.

REFERENCES

- Buer A, Ugbolue SC and Warner SB (2001) Electrospinning and properties of some nanofibers. *Textile Research Journal* 71(4): 323-328.
- Caruso RA, Schattka JH and Greiner A (2001) Titanium dioxide tubes from sol-gel coating of electrospun polymer fibers. *Advanced Materials* 13(20): 1577.
- Casper CL, Stephens JS, Tassi NG, Chase DB and Rabolt JF (2004) Controlling surface morphology of electrospun polystyrene fibers: Effect of humidity and molecular weight in the electrospinning process. *Macromolecules* 37(2): 573-578.
- Deitzel JM, Kleinmeyer J, Harris D and Tan NCB (2001a) The effect of processing variables on the morphology of electrospun nanofibers and textiles. *Polymer* 42(1): 261-272.
- Deitzel JM, Kleinmeyer JD, Hirvonen JK and Tan NCB (2001b) Controlled deposition of electrospun poly(ethylene oxide) fibers. *Polymer* 42(19): 8163-8170.
- Devanand K and Selser JC (1991) Asymptotic-Behavior and Long-Range Interactions in Aqueous-Solutions of Poly(Ethylene Oxide). *Macromolecules* 24(22): 5943-5947.
- Doshi J and Reneker DH (1995) Electrospinning Process and Applications of Electrospun Fibers. *Journal of Electrostatics* 35(2-3): 151-160.
- Drew C, Wang XY, Samuelson LA and Kumar J (2003) The effect of viscosity and filler on electrospun fiber morphology. *Journal of Macromolecular Science-Pure and Applied Chemistry* A40(12): 1415-1422.
- Feng JJ (2003) Stretching of a straight electrically charged viscoelastic jet. *Journal of Non-Newtonian Fluid Mechanics* 116(1): 55-70.
- Fong H, Chun I and Reneker DH (1999) Beaded nanofibers formed during electrospinning. *Polymer* 40(16): 4585-4592.

- Fridrikh SV, Yu JH, Brenner MP and Rutledge GC (2003) Controlling the fiber diameter during electrospinning. *Physical Review Letters* 90(14).
- Gauri V, Koelling K. W. (1997) Extensional Rheology of PEO solutions. *Rheologica Acta* 36(5).
- Guan HY, Shao CL, Liu YC, Yu N and Yang XH (2004) Fabrication of NiCO₂O₄ nanofibers by electrospinning. *Solid State Communications* 131(2): 107-109.
- Hammouda B, Ho D and Kline S (2002) SANS from poly(ethylene oxide)/water systems. *Macromolecules* 35(22): 8578-8585.
- Hammouda B, Ho DL and Kline S (2004) Insight into clustering in poly(ethylene oxide) solutions. *Macromolecules* 37(18): 6932-6937.
- Helgeson, M. E.; Wagner, N. J. (2005) Nano Letters in preparation for submission (private communication).
- Ho DL, Hammouda B and Kline SR (2003) Clustering of poly(ethylene oxide) in water revisited. *Journal of Polymer Science Part B-Polymer Physics* 41(1): 135-138.
- Hohman MM, Shin M, Rutledge G and Brenner MP (2001a) Electrospinning and electrically forced jets. I. Stability theory. *Physics of Fluids* 13(8): 2201-2220.
- Hohman MM, Shin M, Rutledge G and Brenner MP (2001b) Electrospinning and electrically forced jets. II. Applications. *Physics of Fluids* 13(8): 2221-2236.
- Huang ZM, Zhang YZ, Kotaki M and Ramakrishna S (2003) A review on polymer nanofibers by electrospinning and their applications in nanocomposites. *Composites Science and Technology* 63(15): 2223-2253.
- Jayaraman K, Kotaki M, Zhang YZ, Mo XM and Ramakrishna S (2004) Recent advances in polymer nanofibers. *Journal of Nanoscience and Nanotechnology* 4(1-2): 52-65.
- Jia HF, Zhu GY, Vugrinovich B, Kataphinan W, Reneker DH and Wang P (2002) Enzyme-carrying polymeric nanofibers prepared via electrospinning for use as unique biocatalysts. *Biotechnology Progress* 18(5): 1027-1032.
- Kataphinan W, Teye-Mensah R, Evans EA, Ramsier RD, Reneker DH and Smith DJ (2003) High-temperature fiber matrices: Electrospinning and rare-earth modification. *Journal of Vacuum Science & Technology A* 21(4): 1574-1578.

- Khil MS, Bhattarai SR, Kim HY, Kim SZ and Lee KH (2005) Novel fabricated matrix via electrospinning for tissue engineering. *Journal of Biomedical Materials Research Part B-Applied Biomaterials* 72B(1): 117-124.
- Krauthauser C, Deitzel JM, Wetzel ED and O'Brien D (2003) Durable transparent materials: Electrospun nanofibers infused with transparent resin. *Abstracts of Papers of the American Chemical Society* 226: U442-U442.
- Krikorian V, Casper C, J. R and Pochan D (2004) Electrospinning of nanocomposite fibers based on poly(L-lactic acid) and organoclays. *Polymeric Materials Science and Engineering* 90(51).
- Lopez-Herrera, J. M.; Ganan-Calvo, A. M. *Journal of Fluid Mechanics* 2004, 501, 303-326.
- McKee MG, Wilkes GL, Colby RH and Long TE (2004) Correlations of solution rheology with electrospun fiber formation of linear and branched polyesters. *Macromolecules* 37(5): 1760-1767.
- Megelski S, Stephens JS, Chase DB and Rabolt JF (2002) Micro- and nanostructured surface morphology on electrospun polymer fibers. *Macromolecules* 35(22): 8456-8466.
- Mongondry P, Nicolai T and Tassin JF (2004) Influence of pyrophosphate or polyethylene oxide on the aggregation and gelation of aqueous laponite dispersions. *Journal of Colloid and Interface Science* 275(1): 191-196.
- Pozzo DC and Walker LM (2004) Reversible shear gelation of polymer-clay dispersions. *Colloids and Surfaces a-Physicochemical and Engineering Aspects* 240(1-3): 187-198.
- Reneker DH (2003) Electrospinning. *Abstracts of Papers of the American Chemical Society* 225: U282-U282.
- Salalha W, Dror Y, Khalfin RL, Cohen Y, Yarin AL and Zussman E (2004) Single-walled carbon nanotubes embedded in oriented polymeric nanofibers by electrospinning. *Langmuir* 20(22): 9852-9855.
- Shenoy, S. L.; Bates, W. D.; Frisch, H. L.; Wnek, G. E. *Polymer* 2005, 46, 3372-3384.

- Shields KJ, Beckman MJ, Bowlin GL and Wayne JS (2004) Mechanical properties and cellular proliferation of electrospun collagen type II. *Tissue Engineering* 10(9-10): 1510-1517.
- Shin YM, Hohman MM, Brenner MP and Rutledge GC (2001a) Electrospinning: A whipping fluid jet generates submicron polymer fibers. *Applied Physics Letters* 78(8): 1149-1151.
- Shin YM, Hohman MM, Brenner MP and Rutledge GC (2001b) Experimental characterization of electrospinning: the electrically forced jet and instabilities. *Polymer* 42(25): 9955-9967.
- Viswanathamurthi P, Bhattarai N, Kim HY, Khil MS, Lee DR and Suh EK (2004) GeO₂ fibers: Preparation, morphology and photoluminescence property. *Journal of Chemical Physics* 121(1): 441-445.
- Willenbacher N (1996) Unusual thixotropic properties of aqueous dispersions of Laponite RD. *Journal of Colloid and Interface Science* 182(2): 501-510.
- Willenbacher, N.; Hanciogullari, H.; Wagner, H. G. *Chemical Engineering & Technology* 1997, 20, 557-563.
- Yarin AL, Koombhongse S and Reneker DH (2001) Bending instability in electrospinning of nanofibers. *Journal of Applied Physics* 89(5): 3018-3026.
- Ye HH, Lam H, Titchenal N, Gogotsi Y and Ko F (2004) Reinforcement and rupture behavior of carbon nanotubes-polymer nanofibers. *Applied Physics Letters* 85(10): 1775-1777.
- Zebrowski J, Prasad V, Zhang W, Walker LM and Weitz DA (2003) Shake-gels: shear-induced gelation of laponite-PEO mixtures. *Colloids and Surfaces a-Physicochemical and Engineering Aspects* 213(2-3): 189-197.
- Zhang YZ, Ouyang HW, Lim CT, Ramakrishna S and Huang ZM (2005) Electrospinning of gelatin fibers and gelatin/PCL composite fibrous scaffolds. *Journal of Biomedical Materials Research Part B-Applied Biomaterials* 72B(1): 156-165.

Chapter 4

CONCLUSIONS AND FUTURE WORK

4.1 Conclusions

It was found that the diameter of nanofibers that result from the electrospinning of PW solutions follow a power law correlation with the zero shear viscosity of the spun solutions, qualitatively similar to an earlier observation for polyester fibers (McKee *et al.*, 2004b). However, the properties of the two solutions are very different and so the correlations are quantitatively different. The value of the correlations is that only a few experiments are required to predict the diameter of fibers that would form from at different concentrations. The zero shear viscosity could be easily and accurately measured or predicted using the time-concentration shift factors and the analysis shown in Chapter 2 in section 2.5. However, the work presented in this thesis shows that the connection between fiber diameter and spinning solution composition is specific to the polymer-solvent pair and hence, is not fundamental nor universal.

Findings indicate that to avoid bead formation, the polymer solutions should be in the concentrated regime. The occurrence of beads along the fibers that resulted from PW solution (PW3) in the semi dilute regime close to the concentrated regime indicates that the transition from semi dilute to concentrated regime is closely linked with the transition from beaded to non beaded fibers. This confirms previously

published results linking stable electrospinning with entangled solution (Shenoy *et al.*, 2005).

Through a series rheological measurement on neat and laponite-filled aqueous PEO solutions, it was observed that the rheology of the later is superimposable on that of the former. In this manner it was concluded that the viscoelasticity in both the systems arose as a result of polymer-polymer entanglements in the bulk and not due to colloidal-colloidal interactions. To capture the change in rheology as laponite is added or increased, a systematic design of compositions was employed. The procedure used here provides a layout in which the rheology of other attracting polymer-particle systems may be characterized to yield shift factors and master curves. The advantages of this procedure are that it:

- a) could be used to predict the rheology of the system at hand at temperature and concentration states at which no measurements were performed. One limitation of course is that the temperature and concentration at which the prediction is to be made must be in the range of values at which the measurements are carried out.
- b) could provide insights into the molecular microstructure of the polymer-particle system
- c) results in significant data size reduction in a manner which retains all the information of a larger data set

As laponite was introduced in neat PW solutions, the polymer-polymer entanglements varied systematically. The polymer-polymer entanglements are understood to be a prime reason for formation of continuous fibers and is also understood to affect the diameter (McKee *et al.*, 2004a). However, for the case of PWL spinning, a systematic variation in the polymer-polymer entanglements did not result in a corresponding systematic variation in the fiber diameter. The reason for the lack of a trend with the zero-shear viscosity was explained in terms of the possible lack in trend of the electrical properties and/or elongational properties of PWL systems. The PWL fibers showed a large scatter in the diameters ranging from a few nanometers to a few microns unlike the PW fibers which formed nearly monodisperse fibers.

4.2 Other preliminary investigation: formation of pits

When the polymer fibers are electrospun in a sufficiently high humid environment and the solvent is volatile enough, the electrospun polymer fibers are formed with a pitted surface (Casper *et al.*, 2004; Megelski *et al.*, 2002).

A reasonable hypothesis to explain the formation of pits is that as the jet issues the volatile solvent evaporates and results in cooling at the surface of the jet from where it derives its latent heat of evaporation much like the breadth figures observed by Srinivasarao *et al.* (2001). If the evaporation rate is fast enough, *i.e.*, if the solvent is volatile enough, the temperature of the jet surface might drop to a temperature lower than the dew point of the water vapor in the atmosphere thereby causing the condensation of water vapor on the surface of the electrospinning jet. If

the condensed water does not dissolve into the polymer solution on the surface of the jet, it will retain its identity as droplets that form due to interfacial tension effects much like the droplet condensation on a cold glass plate. The interfacial tension between water and air being high, the water droplets would then sink into the surface of the liquid polymer solution of the jet to reduce the interfacial area with air. Finally, as the jet dries it solidifies and the water evaporates to leave behind pits on the surface.

To establish this hypothesis, it must be proven that water condenses on the surface of the jet and that the amount of water condensed acts as a nonsolvent for polymer solutions on the surface of the jet so that it would not dissolve. This has been briefly explored through phase diagram modeling of polymer-solvent-nonsolvent system and heat and mass transfer modeling.

4.2.1 Polymer-solvent-nonsolvent phase diagram

Flory-Huggins model was used to calculate the phase diagrams using the Nelder-Mead simplex direct search method in MATLAB. In the discussions that follow the nomenclature used is as follows:

| | |
|------------------|---|
| NS | Nonsolvent |
| S | Solvent |
| P | Polymer |
| ΔG_{mix} | Free energy change upon formation of a mixture from pure components |
| n | Amount in moles |

| | |
|---------------------|---|
| φ | Volume fraction |
| g | Concentration dependent binary interaction parameters |
| χ | Concentration independent binary interaction parameters |
| R | Universal gas constant |
| T | Temperature |
| \underline{V} | Molar volume of the components |
| x | Mole fraction |
| m | Ratio of molar volume of the components with the molar lattice volume (\underline{V}_L) |
| f | Degrees of freedom |
| P | Number of phases |
| C | Number of components |
| a | Polymer volume fraction in the polymer lean phase |
| x, y, z | Variables used for binodal calculations. A particular known set along with known a corresponds to concentration of two phases |
| q, r, s | Functions of x, y and z |
| F | Objective function matrix |
| <u>Superscripts</u> | |
| a, b | Polymer rich and polymer lean phases respectively |
| <u>Subscripts</u> | |
| i, j | Components nonsolvent (1), solvent (2) and polymer (3) |

For the case of ternary systems, when the three binary interaction parameters are dependent on concentration the Flory-Huggins model expands to (Yilmaz and McHugh, 1986),

$$\frac{\Delta G_{mix}}{RT} = n_1 \ln \varphi_1 + n_2 \ln \varphi_2 + n_3 \ln \varphi_3 + g_{12}(u_2)n_1\varphi_2 + g_{13}(\varphi_3)n_1\varphi_3 + g_{23}(\varphi_3)n_2\varphi_3 \quad (4.1)$$

where, the nonsolvent (NS), solvent (S) and polymer (S) are denoted by 1, 2 and 3 respectively. In the above equation ΔG_{mix} denotes the change in the Gibbs free energy due to the formation of mixture from pure components. R and T denote the universal gas constant and temperature respectively. Among the terms on the RHS, n_i denotes the number of moles of component i ($= 1, 2, 3$) in the mixture, φ_i denotes the volume fraction of each of the three components and g_{ij} denotes the concentration dependent binary interaction parameters between the components. The variable u_2 is a concentration dependent parameter (Yilmaz and McHugh, 1986) and denotes the ratio of volume fraction of component 2 to the sum of volume fractions of component 1 and component 2. Thus,

$$u_2 = \frac{\varphi_2}{\varphi_1 + \varphi_2} \quad (4.2)$$

$$u_1 = 1 - u_2$$

The volume fractions, φ_i in terms of mole fractions are given by,

$$\varphi_i = \frac{\underline{V}_i x_i}{\underline{V}_1 x_1 + \underline{V}_2 x_2 + \underline{V}_3 x_3} \quad i = 1, 2, 3 \quad (4.3)$$

The difference between the chemical potentials of a component i in a mixture at a particular temperature and pressure and the chemical potential of the same component in pure state at the same temperature and pressure is given by (Koningsveld, 2001),

$$\frac{\Delta\mu_i}{RT} = \left(\frac{\partial(\Delta G_{mix}/RT)}{\partial n_i} \right)_{T,P,n_j \neq i} \quad (4.4)$$

The value of m_1 , m_2 and m_3 , which are the ratio of the molar volume of the components with the lattice molar volume, \underline{V}_L (Koningsveld, 2001) denote the relative size of the molecules of the three components. The molar volume of the nonsolvent can be assumed to be equal to the molar lattice volume (Koningsveld, 2001). Furthermore the since only ratios of molar volumes affect the final solution, the molar volume of the nonsolvent, \underline{V}_1 , can be assumed to be unity. Thus,

$$\begin{aligned} m_1 &= \frac{\underline{V}_1}{\underline{V}_L} = \frac{\underline{V}_1}{\underline{V}_1} = 1 \\ m_2 &= \frac{\underline{V}_2}{\underline{V}_L} = \frac{\underline{V}_2}{\underline{V}_1} = \underline{V}_2 \\ m_3 &= \frac{\underline{V}_3}{\underline{V}_L} = \frac{\underline{V}_3}{\underline{V}_1} = \underline{V}_3 \end{aligned} \quad (4.5)$$

Using expression 4.4, three analytical expressions were derived for the difference in chemical potentials in the mixture and in pure state for the three components (Yilmaz and McHugh, 1986). Those three expressions have been modified to expressions 4.6, 4.7 and 4.8 by dividing them by m_1 , m_2 and m_3 respectively. For NS-S-P mixtures considered here, since the segment length of the nonsolvent is taken as unity, the

equation corresponding to nonsolvent is not divided by m_i as it is unity. The modification of dividing the expressions derived by Yilmaz and McHugh (1986) leads to a better scaling and hence easier numerical convergence to solutions (Koningsveld, 2001).

$$\begin{aligned} \Delta\mu_1/RT = \ln \varphi_1 + 1 - \varphi_1 - \frac{\varphi_2}{m_2} - \frac{\varphi_3}{m_3} + (g_{12}\varphi_2 + g_{13}\varphi_3)(\varphi_2 + \varphi_3) \\ - \frac{1}{m_2} g_{23}\varphi_2\varphi_3 - u_1u_2\varphi_2 \left(\frac{dg_{12}}{du_2} \right) - \varphi_1\varphi_3^2 \left(\frac{dg_{13}}{d\varphi_3} \right) - \frac{\varphi_2\varphi_3^2}{m_2} \left(\frac{dg_{23}}{d\varphi_3} \right) \end{aligned} \quad (4.6)$$

$$\begin{aligned} \frac{\Delta\mu_2}{RT} = \frac{\ln \varphi_2}{m_2} + \frac{1}{m_2} - \varphi_1 - \frac{\varphi_2}{m_2} - \frac{\varphi_3}{m_3} + \left(g_{12}\varphi_1 + g_{23} \frac{\varphi_3}{m_2} \right) (\varphi_1 + \varphi_3) \\ - g_{13}\varphi_1\varphi_3 + u_1u_2\varphi_1 \left(\frac{dg_{12}}{du_2} \right) - \varphi_1\varphi_3^2 \left(\frac{dg_{13}}{d\varphi_3} \right) - \frac{\varphi_2\varphi_3^2}{m_2} \left(\frac{dg_{23}}{d\varphi_3} \right) \end{aligned} \quad (4.7)$$

$$\begin{aligned} \frac{\Delta\mu_3}{RT} = \frac{\ln \varphi_3}{m_3} + \frac{1}{m_3} - \varphi_1 - \frac{\varphi_2}{m_2} - \frac{\varphi_3}{m_3} + \left(g_{13}\varphi_1 + g_{23} \frac{\varphi_2}{m_2} \right) (\varphi_1 + \varphi_2) \\ - g_{12}\varphi_1\varphi_2 + \left\{ \varphi_1 \left(\frac{dg_{13}}{d\varphi_3} \right) + \frac{\varphi_2}{m_2} \left(\frac{dg_{23}}{d\varphi_3} \right) \right\} \varphi_3 (\varphi_1 + \varphi_2) \end{aligned} \quad (4.8)$$

The phase equilibrium equations are given by the following expressions (Koningsveld, 2001):

$$\Delta\mu_1^a = \Delta\mu_1^b \quad \Rightarrow \quad \Delta\mu_1^a / RT = \Delta\mu_1^b / RT \quad (4.9)$$

$$\Delta\mu_2^a = \Delta\mu_2^b \quad \Rightarrow \quad \frac{\Delta\mu_2^a / RT}{m_2} = \frac{\Delta\mu_2^b / RT}{m_2} \quad (4.10)$$

$$\Delta\mu_3^a = \Delta\mu_3^b \quad \Rightarrow \quad \frac{\Delta\mu_3^a / RT}{m_3} = \frac{\Delta\mu_3^b / RT}{m_3} \quad (4.11)$$

$$\varphi_1^a + \varphi_2^a + \varphi_3^a = 1 \quad (4.12)$$

$$\varphi_1^b + \varphi_2^b + \varphi_3^b = 1 \quad (4.13)$$

For the liquid-liquid phase equilibrium the two liquid phases expected to form are the polymer rich phase and the polymer lean phase which are denoted here by superscript “a” and “b” respectively. The degree of freedom, f , for this system with the number of components (C) equal to 3 and number of phases (p) equal to 2 becomes,

$$\begin{aligned} f &= C + 2 - p \\ &= 3 + 2 - 2 \\ &= 3 \end{aligned} \quad (4.14)$$

Two out of these three degrees of freedoms are used up by fixing the temperature at 298.15 K and pressure at 1 atm. As suggested in the literature (Yilmaz and McHugh, 2001), the polymer volume fraction in the polymer lean phase was set to a value ($\varphi_3^b = a$) to make the numerical solutions unique. Making the following substitutions,

$$\varphi_1^a = x, \quad \varphi_2^a = y, \quad \varphi_1^b = z \quad (4.15)$$

the remaining variables in terms of x, y and z become,

$$\begin{aligned}\varphi_2^b &= 1 - a - z \\ \varphi_3^a &= 1 - x - y\end{aligned}\tag{4.16}$$

When the binary interaction parameters , g_{ij} , do not depend upon concentration, they are put equal to χ_{ij} . In addition, the terms containing derivatives of the concentration dependent interaction parameters become zero. For example, if g_{23} does not depend upon concentration then,

$$g_{23}^a = g_{23}^b = \chi_{23} \text{ (a rational number)}$$

$$\left(\frac{dg_{23}}{d\varphi_3}\right)^a = \left(\frac{dg_{23}}{d\varphi_3}\right)^b = 0$$

Equations 4.9, 4.10 and 4.11 when expanded using equations 4.6, 4.7 and 4.8 under conditions of concentration independent interaction parameter become,

$$\begin{aligned}& \left[\ln \varphi_1^a + 1 - \varphi_1^a - \frac{\varphi_2^a}{m_2} - \frac{\varphi_3^a}{m_3} + (\chi_{12}\varphi_2^a + \chi_{13}\varphi_3^a)(\varphi_2^a + \varphi_3^a) - \frac{1}{m_2} \chi_{23}\varphi_2^a \varphi_3^a \right] \\ & - \left[\ln \varphi_1^b + 1 - \varphi_1^b - \frac{\varphi_2^b}{m_2} - \frac{\varphi_3^b}{m_3} + (\chi_{12}\varphi_2^b + \chi_{13}\varphi_3^b)(\varphi_2^b + \varphi_3^b) - \frac{1}{m_2} \chi_{23}\varphi_2^b \varphi_3^b \right] \\ & = 0 \equiv q \text{ (say)}\end{aligned}\tag{4.17}$$

$$\begin{aligned}
& \left[\frac{\ln \varphi_3^a}{m_3} + \frac{1}{m_3} - \varphi_1^a - \frac{\varphi_2^a}{m_2} - \frac{\varphi_3^a}{m_3} + \left(\chi_{13} \varphi_1^a + \chi_{23} \frac{\varphi_2^a}{m_2} \right) (\varphi_1^a + \varphi_2^a) - \chi_{12} \varphi_1^a \varphi_2^a \right] \\
& - \left[\frac{\ln \varphi_3^b}{m_3} + \frac{1}{m_3} - \varphi_1^b - \frac{\varphi_2^b}{m_2} - \frac{\varphi_3^b}{m_3} + \left(\chi_{13} \varphi_1^b + \chi_{23} \frac{\varphi_2^b}{m_2} \right) (\varphi_1^b + \varphi_2^b) - \chi_{12} \varphi_1^b \varphi_2^b \right] \quad (4.18) \\
& = 0 \equiv r \text{ (say)}
\end{aligned}$$

$$\begin{aligned}
& \left[\frac{\ln \varphi_2^a}{m_2} + \frac{1}{m_2} - \varphi_1^a - \frac{\varphi_2^a}{m_2} - \frac{\varphi_3^a}{m_3} + \left(\chi_{12} \varphi_1^a + \chi_{23} \frac{\varphi_3^a}{m_2} \right) (\varphi_1^a + \varphi_3^a) - \chi_{13} \varphi_1^a \varphi_3^a \right] \\
& - \left[\frac{\ln \varphi_2^b}{m_2} + \frac{1}{m_2} - \varphi_1^b - \frac{\varphi_2^b}{m_2} - \frac{\varphi_3^b}{m_3} + \left(\chi_{12} \varphi_1^b + \chi_{23} \frac{\varphi_3^b}{m_2} \right) (\varphi_1^b + \varphi_3^b) - \chi_{13} \varphi_1^b \varphi_3^b \right] \quad (4.19) \\
& = 0 \equiv s \text{ (say)}
\end{aligned}$$

The solutions to equations 4.17, 4.18 and 4.19 were found using 4.15 and 4.16 by minimizing the objective function,

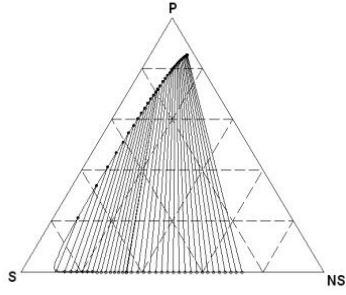
$$F = q^2 + r^2 + s^2 \quad (4.20)$$

for $a = 10^{-30}$ and $\chi_{12} = 0$, $\chi_{13} = 1.5$, $\chi_{23} = 0.5$, $m_2 = 5$ and $m_3 = 500$. The nontrivial solutions found in terms of x , y and z are,

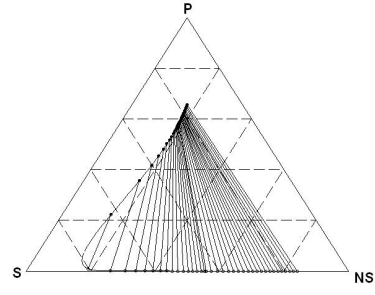
$$\begin{aligned}
x &= 0.06848444763964 \\
y &= 0.16311585633456 \\
z &= 0.27092182230898
\end{aligned}$$

The values of the five unknown volume fractions for these values of x , y and z can be obtained from expressions 4.15 and 4.16. These values represent the binodal solutions

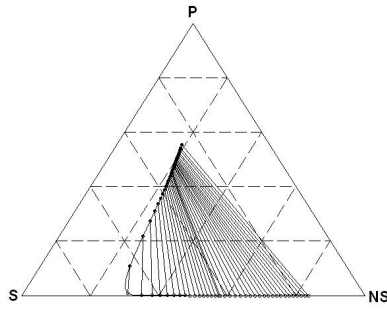
at $\phi_3^b = a = 10^{-30}$, $\chi_{12} = 0$, $\chi_{13} = 1.5$, $\chi_{23} = 0.5$, $m_2 = 5$ and $m_3 = 500$ and can be used to calculate the binodals for all NS-S-P systems with constant interaction parameters. The entire binodal curve was calculated by changing the value of a in small steps and optimizing the objective function F to obtain values of x , y and z and hence the corresponding volume fractions. Likewise, the interaction parameters and m values were varied in small steps to calculate the binodal curves for a variety of values as shown in Figure 4.1.



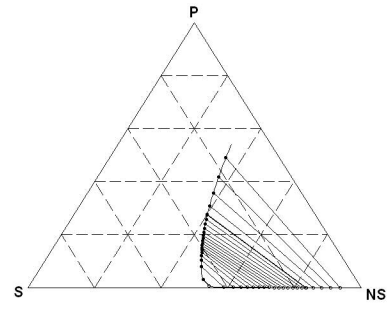
(a) $\chi_{12} = 0, \chi_{13} = 1.5, \chi_{23} = 0, m_2 = 5, m_3 = 500$



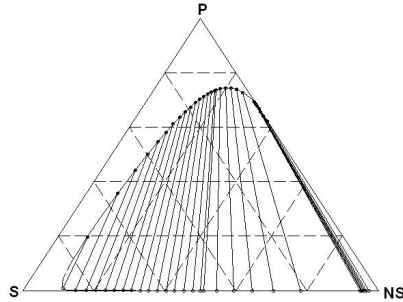
(b) $\chi_{12} = 1, \chi_{13} = 1.5, \chi_{23} = 0.5, m_2 = 5, m_3 = 500$



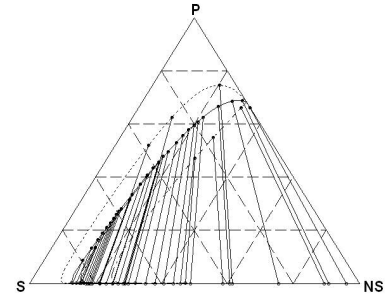
(c) $\chi_{12} = 1, \chi_{13} = 1.5, \chi_{23} = 0, m_2=5, m_3=500$



(d) $\chi_{12} = 1, \chi_{13} = 1, \chi_{23} = 0, m_2 = 5, m_3 = 500$



(e) $\chi_{12} = -0.3, \chi_{13} = 1, \chi_{23} = 0.2, m_2 = 5, m_3 = 500$



(f) See captions for parameter values

Figure 4.1: Phase diagrams for different parameter values obtained using a single known initial guess, (f): Dotted curve, $\chi_{12} = -0.3, \chi_{13} = 1, \chi_{23} = 0.2, m_2 = 5, m_3 = 1000$, Solid outer curve: $\chi_{12} = 0.03, \chi_{13} = 1, \chi_{23}=0.2, m_2 = 5, m_3 = 10000$, Solid inner curve: $\chi_{12} = 0.03, \chi_{13} = 1, \chi_{23} = 0.2, m_2 = 5, m_3 = 1000$, Dash-dot curve: $\chi_{12} = 0.3, \chi_{13} = 1, \chi_{23} = 0.2, m_2 = 5, m_3 = 1000$

Figure 4.1 shows that the results of the codes developed agrees with the results of calculations presented in the literature (Yilmaz and McHugh, 1986; Smoulders, 1982).

Choosing polystyrene (PS) solution in tetrahydrofuran (THF), the hypothesis of formation of pits was explored. Figure 4.2 shows the phase behavior studies carried out experimentally as well as using the above model at 25 °C and 1 atm for PS (3)-tetrahydrofuran (2)-water (3) system with the molecular weight of polystyrene equal to 190000 g/mol (used by Megelski et al. (2002)). The binodal was calculated with constant binary interaction parameters: $\chi_{12}=0.927$, $\chi_{13}=3.2$, $\chi_{23}=0.2$. The values of interaction parameter between water and THF were obtained by fitting Flory-Huggins model to the liquid-liquid equilibrium (T-x-x) data available in the literature (Rosso and Carbonell) to the Flory-Huggins model. The values of the other two interaction parameters were adjusted by trial and error within the range of values provided in the Polymer Handbook, edition 2 so that the binodal coincided with the experimentally measured binodal. The theoretical binodal does not coincide with the experimental binodal in all the regions except in the low water region. This is the limitation of constant interaction parameters chosen which actually should be concentration dependent. However, coincidence in the low water region suggests that roughly water in excess of about 2 % by volume is sufficient to cause phase separation.

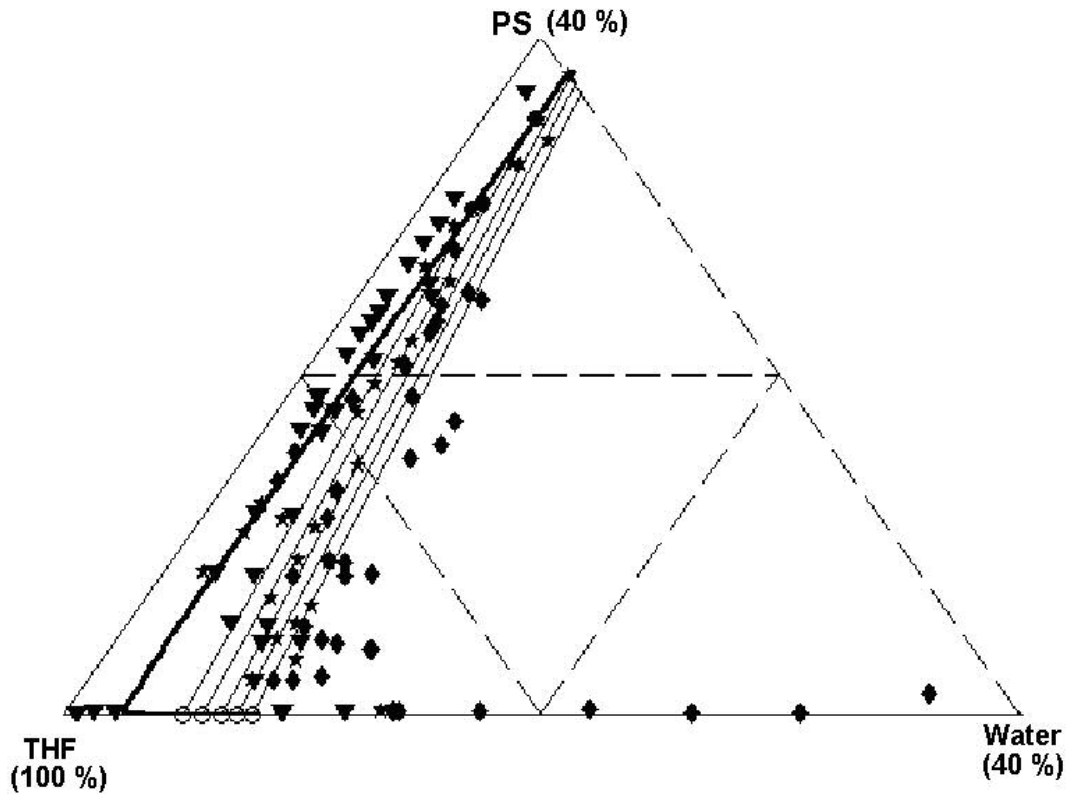


Figure 4.2: Phase diagram of water – THF – PS (190000 g/mol). Black thick line: calculated binodal for $\chi_{12}=0.927$, $\chi_{13}=3.2$ and $\chi_{23}=0.2$. Black filled circles: concentration of the polymer rich phase as predicted, black empty circles: concentration of the polymer lean phase as predicted, lines connecting black circles: tie lines. Diamond, star and inverted triangles represent experimental data points. Diamonds: distinct phase separation with gel-like bottom phase, star: phase separation with cloudy bottom phase and a clear upper phase, inverted triangle: no phase separation. Dashed lined represent constant concentration lines with a distance between two such consecutive lines equivalent to a difference of 0.2 volume fraction.

4.2.2 Model for the formation of pits

The heat and mass transfer modeling of the PS-THF jet was carried out to find out the amount of water that is expected to condense on the jet surface. Figure 4.3 shows a schematic diagram of the traveling jet in which an element of the jet is shown. THF evaporates and diffuses in the environment and at the same time water vapor from the environment diffuses towards the jet and condenses on it. Assuming, no temperature and concentration gradient across the cross-section, straight trajectory, constant velocity (v_z) and linear variation in the diameter of the jet, the following differential equations were derived for the temperature of the jet and concentration of water and THF in the jet:

$$\frac{dC_2}{dz} = -\frac{4N_2}{D_{jet}v_z} \quad (4.1)$$

$$\frac{dC_1}{dz} = -\frac{4N_1}{D_{jet}v_z} \quad (4.2)$$

$$\frac{dT}{dz} = \frac{4}{\rho_{jet}C_{p, jet}D_{jet}v_z} \left[(-N_1H_1^{vap} - N_2H_2^{vap}) + h(T_{environment} - T) \right] \quad (4.3)$$

where, ρ_{jet} , $c_{p, jet}$ and D_{jet} are the density, heat capacity and diameter of the polymer jet, z is the distance from the starting point, i.e., the tip of the needle where the jet originated, C_i , N_i and H_i^{vap} are the concentrations, fluxes and latent heats of THF (2) and water (1). The fluxes were calculated based upon laminar flow regime over a flat plate. The NRTL model was used to calculate the concentration of THF and water in the gaseous phase just near the surface of the jet. To calculate N_1 and N_2 the required

mass transfer coefficient and concentration near the surface were estimated as shown in Appendix 4.1. The convective heat transfer coefficient, h , was calculated using the mass transfer coefficients by Chilton-Colburn analogy.

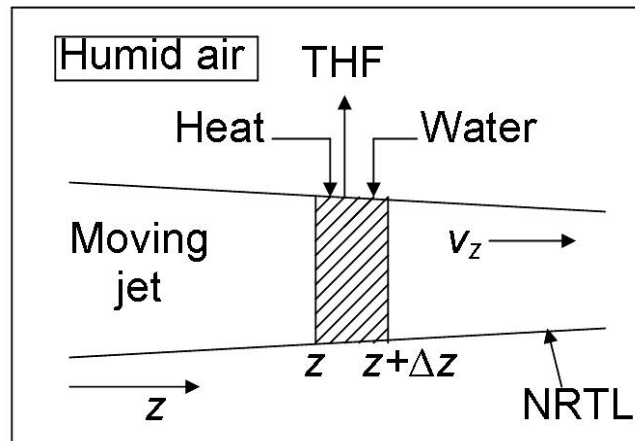


Figure 4.3: Schematic diagram of an element of the moving jet.

Upon solving the coupled differential equations, the profiles for the temperature of the jet and the amount of water condensed obtained are shown in Figures 4.4 and 4.5. Figure 4.4 shows a monotonic decrease in the jet temperature as it travels towards the collector (in z direction). Figure 4.5 shows that at a relative humidity of 70%, the concentration of water builds up to about 4 % during the same distance, which is sufficient to cause phase separation, thus validating the hypothesis.

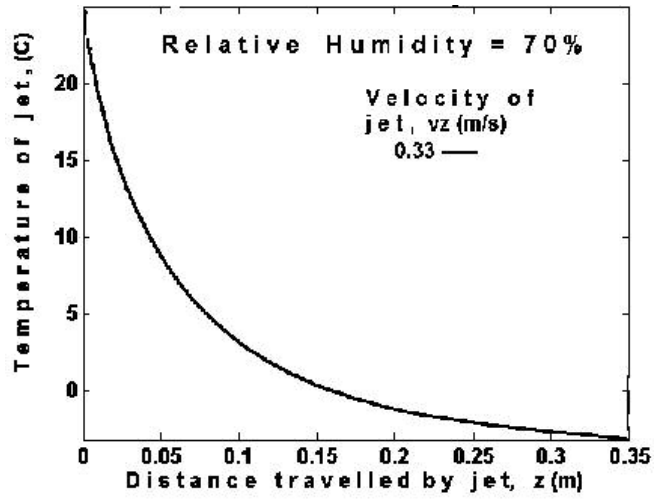


Figure 4.4: Temperature of the jet as it moves starting from the needle tip.

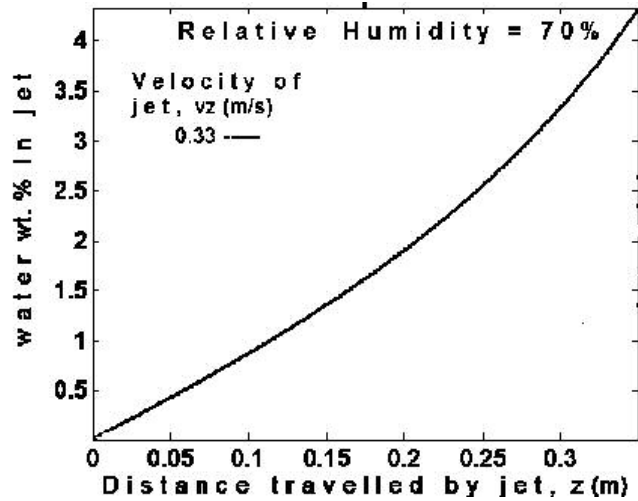


Figure 4.5: Water content in the jet as it moves starting from the needle tip.

4.3 Future work

Electrospinning primarily being an elongational flow, the elongational viscosity should determine the stretching of the spinning jet. For simple non-associating polymer solutions both the shear viscosity and the elongational viscosity is expected to increase with concentration. However, with even a little laponite added to the neat PW solutions, elongational strain hardening might occur, which might explain partly why the average diameter of PWL fibers was not found to follow a trend with the zero shear viscosity.

In addition, a large degree of splaying is evident in the case of PWL electrospinning. It is known that splaying occurs when the surface charge density becomes excessive such that new surface area is created by splaying of smaller fibers from the main jet (Deitzel *et al.*, 2001; Yarin *et al.*, 2001). Higher degree of splaying may result in the case of PWL electrospinning because the laponite is known to release sodium ions into the solution (Willenbacher, 1996) making it more electroactive. Hence, to better understand and control the electrospinning process a precise measurement and control of electrical properties (that lead to charging of the polymer solutions and consequent splaying) and the elongational viscosity (that opposes the stretching of the jet) is required.

APPENDIX 4.1

Calculation of mass transfer coefficient, K_z and the concentration near the surface of the jet

Calculating mass transfer coefficient, K_z

Assuming fluid (air) flow over a flat surface, the local Reynolds number is given by,

$$Re_z = \frac{\rho_{air} v_z z}{\mu_{air}}$$

where ρ_{air} , μ_{air} , v_z and z are the density and viscosity of air and the velocity of the jet in z direction and z is the distance from the tip. The j factor for laminar boundary layer along a flat plate is expressed in terms of Re_z as,

$$j_{D_{local}} = 0.332(Re_z)^{-0.5}$$

From the value of j factor the value of local mass transfer coefficient, K_z , can be found by using the relation below,

$$j_{D_{local}} = \frac{K_z}{C v_z} \left(\frac{\mu_{air}}{\rho_{air} D_{SA}} \right)^{2/3}$$

Where C is the concentration of any species (THF and water) and D_{SA} is the diffusivity of the species in air.

The expression of K_z thus obtained becomes,

$$Kz = 0.332Cv_z \left(\frac{\mu_{air}}{\rho_{air}D_{SA}} \right)^{-2/3} \left(\frac{\rho_{air}v_z}{\mu_{air}} \right)^{-0.5} z^{-0.5}$$

Calculating concentration of THF near the jet surface

Assuming that PS just lies in the PS-THF without any interaction, the vapor pressure of THF near the surface of the jet can be taken equal to its vapor pressure. In addition, since the pressure equals 1 atm, the air-THF vapor mixture can be approximated an ideal gas and the ideal gas equation of state can be applied to get an estimate of C ,

$$C_A = \frac{P^{sat}}{RT} \quad (\text{Ideal gas law})$$

where P^{sat} is the vapor pressure given by Antoine equation.

Calculating concentration of water near the jet surface

Assuming that the water condensed forms a homogeneous mixture with the THF, NRTL model was applied to find the vapor pressure of water near the surface of the jet.

Verifying laminar regime

Note that the expression of K_z obtained above is valid for laminar flow because j_D was valid for laminar boundary layer. Therefore before using this expression of K_z , it must be verified that the flow of air outside the jet is in the laminar regime. For a flat plate profile the transition of flow from laminar to turbulent regime occurs at $Re_z = 3 \times 10^5$.

From the expression of Re_z given above,

$$z = \frac{Re_z \mu_{air}}{\rho_{air}v_z}$$

Putting $Re_z=3 \times 10^5$, the value of z at which transition occurs can be got as a function of v_z as,

$$z_{transition} = \frac{3.997}{v_z} m$$

Here v_z is in m/s. Putting $v_z= 1$ m/s, $z_{transition} =3.997$ m. Since the working distance during electrospinning is an order of magnitude lower, laminar flow assumption holds good.

Thus, the regime of airflow outside the jet is generally laminar under the assumptions of non-whipping trajectory and the expression of K_z as derived above is applicable. It is, however, approximate since airflow was assumed to be over flat plate geometry instead of cylindrical which however is not expected to be a significant deviation as the air would flow tangential to the surface just as it does over flat plate. Due to this geometry of the flow, there is no form drag associated with the flow of air past the jet as is the case in flow over flat surfaces.

REFERENCES

- Casper CL, Stephens JS, Tassi NG, Chase DB and Rabolt JF (2004) Controlling surface morphology of electrospun polystyrene fibers: Effect of humidity and molecular weight in the electrospinning process. *Macromolecules* 37(2): 573-578.
- Deitzel JM, Kleinmeyer JD, Hirvonen JK and Tan NCB (2001) Controlled deposition of electrospun poly(ethylene oxide) fibers. *Polymer* 42(19): 8163-8170.
- Koningsveld R., *Polymer Phase Diagrams*. 2001: Oxford University Press.
- McKee MG, Elkins CL and Long TE (2004a) Influence of self-complementary hydrogen bonding on solution rheology/electrospinning relationships. *Polymer* 45(26): 8705-8715.
- McKee MG, Wilkes GL, Colby RH and Long TE (2004b) Correlations of solution rheology with electrospun fiber formation of linear and branched polyesters. *Macromolecules* 37(5): 1760-1767.
- Megelski S, Stephens JS, Chase DB and Rabolt JF (2002) Micro- and nanostructured surface morphology on electrospun polymer fibers. *Macromolecules* 35(22): 8456-8466.
- Pozzo DC and Walker LM (2004) Reversible shear gelation of polymer-clay dispersions. *Colloids and Surfaces a-Physicochemical and Engineering Aspects* 240(1-3): 187-198.
- Rosso and Carbonell, *Chimie Physique*
- Smolders, F. (1982) Calculation of Liquid-Liquid Phase Separation in a Ternary System of a Polymer in a mixture of a Solvent and a Nonsolvent. *Macromolecules*, 1982. **15**: p. 1491-1497.
- Srinivasarao M, Alan Philips D.C., Patel S., Three-dimensionally ordered array of air bubbles in a polymer film. *Science*, 2001. **292**: p. 79-83.
- Shenoy, S. L.; Bates, W. D.; Frisch, H. L.; Wnek, G. E. *Polymer* 2005, 46, 3372-3384.

- Willenbacher N (1996) Unusual thixotropic properties of aqueous dispersions of Laponite RD. *Journal of Colloid and Interface Science* 182(2): 501-510.
- Yarin AL, Koombhongse S and Reneker DH (2001) Bending instability in electrospinning of nanofibers. *Journal of Applied Physics* 89(5): 3018-3026.
- Yilmaz L and McHugh A (1986) Analysis of Nonsolvent-Solvent-Polymer Phase Diagrams and Their Relevance to Membrane Formation Modeling. *Journal of applied Polymer Science* 31: 997-1018.
- Zebrowski J, Prasad V, Zhang W, Walker LM and Weitz DA (2003) Shake-gels: shear-induced gelation of laponite-PEO mixtures. *Colloids and Surfaces a-Physicochemical and Engineering Aspects* 213(2-3): 189-197.